^{197}Au Mössbauer Study of Au/M (M = Fe, Co, Ni) Multilayers

Yasuhiro KOBAYASHI

Department of Material Physics,
Faculty of Engineering Science,
Osaka University
January, 1997

Abstract

^{197}Au Mössbauer measurements have been performed for Au/*M* (*M* = Fe, Co, Ni) multilayers. In order to discuss the magnetic properties of the Au layers, thickness of the Au layer has been changed and thickness of magnetic layers has been fixed. ^{197}Au Mössbauer spectra obtained from Au/*M* multilayers mainly consist of two components. One component is the magnetic component, which is strongly perturbed by adjacent magnetic layers. Another component is a nonmagnetic component having zero isomer shift, which is due to the Au atoms existing far from the magnetic layers. From the area ratio of these components, it is determined that the strongly perturbed Au atoms exist within 0.2 ~ 0.4 nm from the interface with magnetic layer. Similar values have been obtained for all of the multilayers investigated. In order to clarify the elastic properties of multilayers, we compared the recoil-free fraction of ^{197}Au Mössbauer resonance, which relates with the mean square displacement of the Mössbauer probe atom. In Au(1.0 nm)/Ni(1.0 nm) multilayer, Au atom ratio in multilayer and buffer layer has been prepared to be 2:1, however, the area ratio in ^{197}Au Mössbauer spectrum has been determined to be 3.2:1 in a thin-foil approximation at 11 K. This result suggests a large recoil-free fraction of ^{197}Au in multilayer than that in Au buffer layer. Temperature dependence of the area ratio has been analyzed using a Debye model and the Debye temperature of ^{197}Au in this multilayer has been determined to be 235 K, which is much higher than 164 K of bulk Au metal, suggesting the existence of the supermodulus effect in this multilayer. The Debye temperatures of Au(1.0 nm)/Fe(0.8 nm) and Au(1.0 nm)/Co(2.0 nm) multilayer are 175 K and 185 K, respectively. These values do not so

differ from that of pure Au bulk. Au layers in these multilayers could not show the supermodulus effect.

Contents

1. Introduction

1.1 Introduction

A metallic multilayer, which is alternately stacked two or more different kinds of metals using evaporation or sputtering technique, is new material and does not exist in nature [1, 2]. Metallic multilayers have been interested not only in science but also in their application in practical use; for example, a magnetic censor, a recording media and so on. The "Giant Magneto-Resistance (GMR)" is one of the unique properties of the multilayers [3]. GMR implies the large decrease of the electrical resistance by applying the external magnetic field. This phenomenon has been already applied to the industrial materials for a magnetic censor and a magnetic reading head. The "supermodulus effect" is also an unique phenomenon of the multilayers [4]. This is due to the enhancement of the elastic modulus by constructing their multilayer comparing with bulk metals.

Mössbauer spectroscopy is one of the most powerful technique to analyse the microscopic properties of multilayers. Using the nuclear methods like Mössbauer spectroscopy, the information from probe element can be extracted for the complex material like multilayers. For the Mössbauer spectroscopy, ^{57}Fe nuclei is the most common probe, and already there are reports to study multilayers using ^{57}Fe Mössbauer effects [2]. They have been studying about structure, magnetic structure, magnetic anisotropy and so on. The magnetic properties of nonmagnetic layer should be interested from the relation with adjacent magnetic layers [5]. There are not so many techniques to investigate the nonmagnetic layers in magnetic multilayers. Mössbauer

spectroscopy using nonmagnetic probe atom is a useful method to investigate the nonmagnetic layers. ^{197}Au Mössbauer spectroscopy has a difficulty in preparation of the γ-ray source using a nuclear reactor because of its short life-time. Au is the one of the most popular metallic element for preparation of multilayers, and its property is also important.

Since the supermodulus effect has been reported in some multilayers including Au layers [6], it is important to study on the elastic properties of Au layers selectively. When the supermodulus effect exists, the Debye temperature of Au layers should be changed. This change can be measured by a recoil-free fraction of Mössbauer spectroscopy.

We performed ^{197}Au Mössbauer measurements of Au/*M* (*M* = Fe, Co, Ni) multilayers to elucidate the magnetic and elastic properties of Au layers. In this study, we have obtained following results [7 ~ 10].

1) The Au atoms that affected by magnetic layers exist in 0.2 ~ 0.4 nm from the interface with the magnetic layers. These values are not so different in Au/Fe, Au/Co and Au/Ni multilayers and are much shorter than the distance of the inter-layer coupling of magnetic layers across the nonmagnetic layers. The influence to the ^{197}Au Mössbauer spectra from the inter-layer coupling is so small that it is not shown in ^{197}Au Mössbauer spectra.

2) The Debye temperature of Au(1.0 nm)/Ni(1.0 nm) multilayer is 235 K and this value is higher than that of bulk Au (164 K). This result suggests the existence of the supermodulus effect in this multilayer. However the Debye temperatures of Au(1.0 nm)/Fe(0.8 nm) and Au(1.0 nm)/Co(2.0 nm) multilayers are not so different from that of bulk Au.

In Chapter 1, I introduce about Mössbauer spectroscopy and hyperfine interaction parameters obtained from this spectroscopy.

Experimental method and preparation of multilayers have been described in Chapter 2. Discussion of the results obtained are given in Chapter 3. In Chapter 4, conclusion of the present investigation has been described.

1.2 Mössbauer Spectroscopy [11 ~ 13]

1.2.1 Mössbauer Effect

Considering two same atoms that are in ground state and in excited state, the excited atom will decay with emitting photon whose energy is the difference between excited state and ground state and then the atom in ground state can absorb this photon and can be excited. This phenomenon was reported by Wood *et al.* in 1904 using sodium atoms and the sodium D lines [14]. This phenomenon called "resonant absorption".

Same experiment using nuclear γ-ray was tried, but the observation of "nuclear resonant absorption" was difficult. The energy of γ-ray is 10^3 ~ 10^5 times larger than that of photon emitting by the decay of electronic states in atoms. The nucleus is recoilied by the emission of γ-ray and the γ-ray lose the energy by the energy conservation in the process of the recoil. In the case of "nuclear resonant absorption", this loss is not negligible, so the absorption would be not observed.

In the emission and absorption process of photon by nucleus, from the energy conservation law, the energy of excited state ΔE. is given by

$$\Delta E = \frac{1}{2}Mv^2 + E_\gamma, \tag{1.1}$$

where E_γ, is the energy of γ-ray, mass and velocity of the nucleus are M and v.

From the momentum conservation law,

$$0 = -Mv + \frac{E_\gamma}{C}, \tag{1.2}$$

$$v = \frac{E_\gamma}{Mc}. \tag{1.3}$$

The energy of the recoil E_R is given by

$$E_R = \Delta E - E_\gamma = \frac{1}{2} M v^2 \qquad (1.4)$$

$$E_R = \frac{E_\gamma^{\,2}}{2Mc^2}. \qquad (1.5)$$

In the case of ^{197}Au nucleus, the recoil energy E_R is 1.629 × 10^{-2} eV from E_γ = 77.345 keV [15]. Since the recoil occurs at both of the emission and absorption processes, additional energy $2E_R$ is necessary for the nuclear resonant absorption.

From the uncertainly principle between energy and time, the level width of the excited state Γ and lifetime τ. are ralated

$$\tau\Gamma \geq h \qquad (1.6)$$

$$\tau_{1/2}\Gamma = \ln 2\, \hbar \qquad (1.7)$$

where $\tau_{1/2}$ is he half-life of excited state. In ^{197}Au, τ = 1.91 ns [15] and the level width Γ is given as

$$\Gamma \geq 2.39\times10^{-7}\text{eV}. \qquad (1.8)$$

In the photon emission from the de-excitation of electron orbits, the recoil energy ($2E_R$) is much less than the level width and then the resonant absorption can be observed. In the case of γ-ray emission, the recoil energy is larger than the level width and then the resonant absorption is not observed. (Fig. 1-1) To compensate the recoil energy, two techniques were developed. The first is to add the Doppler energy by a mechanical motion (10^2 ~ 10^3 m/s). The second is using the thermal vibration of atoms at high temperature.

In 1957, R. L. Mössbauer was studying about the nuclear resonant absorption using the 129 keV γ-ray of ^{191}Ir nuclei at the Max Planck Institute for Medical Research in Heidelberg [16]. Since the experiment

at high temperature was difficult in his laboratory, he tried to observe the decrease of the resonance at low temperatures. However, the resonance increased with a decrease of the temperature. He explained this phenomenon as follows. In a solid, the recoil can create or annihilate the phonons. When the recoil energy is less than the energy of one phonon, there is probability of zero phonon emission and absorption. By this zero phonon excitation (or absorption), the recoil free resonant absorption can be observed. This recoil free resonant absorption is called Mössbauer effect. In this case, recoil energy is shown by

$$E_R = (1 - f)\hbar\omega \tag{1.9}$$

where, $\hbar\omega$ is energy of phonon, f is the probability of recoil free emission or absorption, called recoil free fraction.

1.2.2 Mössbauer Spectrum

Using Mössbauer effect, we can measure the hyperfine structure of nuclear with very high resolution. The nuclei are surrounded by electron. Measuring the hyperfine structure of the nuclei is measuring the electronic state of atoms. Figure 1-2 shows the schematic drawings of hyperfine structures of ^{57}Fe. Energy shift of these hyperfine structures are $10^{-7} \sim 10^{-8}$ eV. We can adjust the energy of γ-ray by using a mechanical motion which offers the Doppler shift in photon energy. The energy of Mössbauer γ-ray is less than 100 keV. The first order Doppler shift δE is expressed by

$$\delta E = \frac{v}{c} E_\gamma \tag{1.10}$$

where c is velocity of the light, and v is the relative velocity of source and absorber. The velocity that needs to scan the energy for hyperfine structure measurement is 10^0 ~ 10^1 mm/s in cases of ^{57}Fe and ^{197}Au. The spectra whose x axis is velocity and y axis is relative transmission or emission are called Mössbauer spectra. When the absorber and source are same the material having unsplit nuclear level, the absorption spectrum shows a dip at 0 velocity. Usually the spectrum obtained shifts and splits by the existence of the hyperfine structure.

1.2.3 Isomer Shift

Since the radii of nuclei in excited and ground state are usually different, the magnitude of electrostatic interaction at the nucleus is different. When the densities of electron at the nucleus are different in source and absorber, the energy levels shift by the difference of the electrostatic interaction. Resultant Mössbauer absorption peak shifts from the position of 0 velocity. This shift is called isomer shift. The isomer shift reflect the electronic density at nucleus, which is affected also by the chemical state of atom. The magnitude of the isomer shift δ is given by

$$\begin{aligned}\delta &= \left\{(E_e)_A - (E_g)_A\right\} - \left\{(E_e)_S - (E_g)_S\right\} \\ &= \frac{4}{5}\pi Z e^2 R^2 \frac{\Delta R}{R}\left\{\left|\varphi(0)\right|_A^2 - \left|\varphi(0)\right|_S^2\right\} \qquad (1.11)\end{aligned}$$

where, $(E_e)_A$ and $(E_g)_A$ are the energies of excited and ground state of the absorber, $(E_e)_S$ and $(E_g)_S$ are the energies of the source, $\left|\varphi(0)\right|_A^2$ and $\left|\varphi(0)\right|_S^2$ are electronic density at nucleus, R is radius of nucleus, ΔR is difference of nuclear radius between excited and ground state.

Only s-electrons have charge density at nucleus. $|\varphi(0)|_A^2$ and $|\varphi(0)|_s^2$ are depend only on the number of s-electrons. However, other electrons, d-electrons and so on, contribute to isomer shift through s-electrons. For example, in the case of Fe, adding a $3d$-electron reduce the attractive Coulomb potential and causes the $3s$-electron wave function to extend, reducing its charge density at the nucleus. This phenomenon called "screening effect".

1.2.4 Quadrupole Splitting

When the nuclear spin quantum number I is larger than 1, the nucleus lost the spherical symmetry. In this case, the nucleus has electric quadrupole moment, nuclear energy level changes by the interaction between nuclear quadrupole moment and electric field gradient. For ^{57}Fe nuclei, I = 3/2 in excited state and I = 1/2 in ground state, thus the excited state split into $M = \pm 1/2$ and $M = \pm 3/2$ by the nuclear quadrupole interaction with the electric field gradient. The resultant spectrum shows two peaks. Since ^{197}Au nuclei are I = 1/2 in excited state, and I = 3/2 in ground state, the spectrum splits as same as the case of ^{57}Fe under the electric field gradient. The energy difference between the two peaks is called quadrupole splitting, and its magnitude ($Q.S.$) is given by

$$Q.S. = \frac{1}{2}e^2qQ\left(1+\frac{\eta^2}{3}\right)^{\frac{1}{2}} \qquad (1.12)$$

where Q is the quadrupole moment of the nucleus and V_{ZZ} is the magnitude of electronic field gradient when the principle axis of

electronic field gradient is set into z axis. η is called as an asymmetry parameter defined by

$$\eta = \frac{V_{XX} - V_{YY}}{V_{ZZ}}. \qquad (1.13)$$

Usually, the axis are chosen as $|V_{ZZ}| \geq |V_{YY}| \geq |V_{XX}|$, thus $0 \leq \eta \leq 1$.

From the quadrupole splitting, we can measure the electronic field gradient at the nucleus. This field gradient is caused by not only the configuration of ions or ligands, but also the distortion of atom's own core orbits.

1.2.5 Magnetic Splitting

In the case of $I \geq 1/2$, nucleus has magnetic moment, and show Zeeman splitting under magnetic field. The split level is shown this,

$$\begin{aligned} E_{IM} &= -g_N \beta_N HM \\ &= -\gamma_N \hbar HM \\ &= \frac{\mu_N}{I} HM \end{aligned} \qquad (1.14)$$

where, I is nuclear spin, M is magnetic quantum number, γ_N is nuclear giromagnetic ratio, μ_N is nuclear magnetic moment, β_N is nuclear magneton, g_N is g-factor of the nucleus.

In the case of ^{57}Fe, I = 3/2 for excited state and I = 1/2 for ground state, so these state split into 4 and 2 levels, respectively. From the selection rule of M1 transition, 6 transitions are allowed. In the case of ^{197}Au, I = 1/2 for excited state and I = 3/2 for ground state. Since transition of ^{197}Au nucleus include 10% E2 transition in addition to M1 transition, 8 transitions are allowed. If the direction of the magnetic moments of atoms is random, the intensity ratio of peaks is 2 : 9 : 16 :

23 on a ^{197}Au Mössbauer spectrum. The split-width of spectra shows the magnitude of hyperfine magnetic field.

1.2.6 Recoil-free Fraction

The following discussion is similar to the that of Debye-Waller factor in X-ray diffraction.

The equation of the electromagnetic wave at time t is

$$A(t) = A_0 e^{i\omega_0 t}. \tag{1.15}$$

The light source is moving in velocity $v(t)$ to x direction, the angler frequency is

$$\omega(t) = \omega_0 \left[1 + \frac{v(t)}{c} \right] \tag{1.16}$$

Thus the equation of emitted electromagnetic wave is

$$\begin{aligned} A(t) &= A_0 e^{i\int_0^t \omega_0 dt} e^{i\int_0^t \omega_0 \frac{v(t)}{c} dt} \\ &= A_0 e^{i\omega_0 t} e^{i\omega_0 \frac{x(t)}{c}} \end{aligned} \tag{1.17}$$

$$A = A_0 e^{i\omega_0 t} e^{i\frac{x(t)}{\lambda_0}}. \tag{1.18}$$

This nucleus moves by thermal vibration, the amplitude is x_0, angular frequency is Ω. The position of this atom is

$$x(t) = x_0 \sin \Omega t. \tag{1.19}$$

Substituting this into (1.18)

$$A = A_0 e^{i\omega_0 t} e^{i\frac{x_0}{\lambda_0} \sin \Omega t}. \tag{1.20}$$

We use following formula,

$$e^{iy\sin\theta} = \sum_{n=-\infty}^{\infty} J_n(y)e^{ni\theta}$$
$$= J_0(y) + 2\sum_{n=1}^{\infty} J_{2n}(y)\cos 2n\theta + 2i\sum_{n=0}^{\infty} J_{2n+1}(y)\sin(2n+1)\theta \quad (1.21)$$

where, J_n is Bessel function, and its 0th order is

$$J_0(y) = \sum_{k=1}^{\infty}(-1)^k\left(\frac{y}{2}\right)^{2k}\left(\frac{1}{k!}\right)^2$$
$$= 1 - \left(\frac{y}{2}\right)^2 + \left(\frac{1}{2!}\right)^2\left(\frac{y}{2}\right)^4 - \left(\frac{1}{3!}\right)^2\left(\frac{y}{2}\right)^6 + \cdots. \quad (1.22)$$

Using this formula, (1.20) become

$$A = A_0 e^{i\omega_0 t}\sum_{n=-\infty}^{\infty} J_n\left(\frac{x_0}{\lambda\!\!\!^{-}_0}\right)e^{in\Omega t}$$
$$= A_0\sum_{n=-\infty}^{\infty} J_n\left(\frac{x_0}{\lambda\!\!\!^{-}_0}\right)e^{i(\omega_0 + n\Omega)t} \quad (1.23)$$

This equation means that the electromagnetic wave, A, consists of many angular frequency, ω_0, $\omega_0 + \Omega$, $\omega_0 + 2\Omega$, ... , $\omega_0 + \infty\Omega$, and $\omega_0 - \Omega$, $\omega_0 - 2\Omega$, ... , $\omega_0 - \infty\Omega$. In these frequencies, there is the term whose frequency does not change. This term is recoil free emission and the ratio of this term is recoil free fraction, f.

$$f = |A_{n=0}|^2 = J_0^2\left(\frac{x_0}{\lambda\!\!\!^{-}_0}\right) \quad (1.24)$$

The lattice vibrations of real solids are not only one frequency, it have complex distributed frequency. In the solid composed by N atoms, the lattice vibration consist of $3N$ normal frequencies, Ω_m, whose amplitudes are x_m. Recoil free fraction is the product of these vibration,

$$f = \prod_{m=1}^{3N} J_0^2\left(\frac{x_m}{\lambda\!\!\!^{-}_0}\right). \quad (1.25)$$

Since $x_m << \lambda\!\!\!^{-}_0$, we can approximate eq. (1.22) to

$$J_0(y) \approx 1 - \frac{y^2}{4}. \quad (1.26)$$

Substituting eq. (1.26) to the logarithm of eq. (1.25)

$$\ln f = 2\sum_{m=1}^{3N} \ln\left\{1 - \frac{1}{4}\left(\frac{x_m}{\lambda\!\!\!^{-}_0}\right)^2\right\}. \tag{1.27}$$

Since $(x_m/\lambda\!\!\!^{-}_0)^2/4 << 1$, the logarithm of eq. (1.27) can expand to

$$\ln f \approx -\frac{1}{2}\sum_m \left(\frac{x_m}{\lambda\!\!\!^{-}_0}\right)^2. \tag{1.28}$$

The mean square amplitude of atoms are defined as

$$\langle u^2 \rangle = \frac{1}{2}\sum_m x_m{}^2. \tag{1.29}$$

Using this

$$f = \exp\left\{-\frac{\langle x^2 \rangle}{\lambda\!\!\!^{-}_0{}^2}\right\} = \exp\left\{-\frac{4\pi^2\langle u^2 \rangle}{\lambda_0{}^2}\right\}. \tag{1.30}$$

We consider the mean square amplitude using Debye model. The mean energy of jth harmonic oscillator is written using mean square of amplitude, r.

$$\begin{aligned}\langle \varepsilon_j \rangle &= \left(\frac{1}{2} + \langle n_j \rangle\right)\hbar\omega \\ &= M\omega_j{}^2\langle r_j{}^2 \rangle\end{aligned} \tag{1.31}$$

where, $\langle n_j \rangle$ is mean of vibrational quantum number. This value is given by Planck distribution function,

$$\langle n_j \rangle = \frac{1}{e^{\frac{\hbar\omega_j}{kT}} - 1}. \tag{1.32}$$

Thus the mean square amplitude is shown

$$\langle r^2 \rangle = \frac{\hbar}{MN}\sum_{3N} \frac{\frac{1}{2} + \langle n_j \rangle}{\omega_j}. \tag{1.33}$$

The summation is replaced with integration using the distribution function, $\rho(\omega)$,

$$\langle r^2 \rangle = \frac{\hbar}{MN} \int_0^{\omega_D} \left\{ \frac{1}{2} + \frac{1}{e^{\frac{\hbar\omega}{kT}} - 1} \right\} \frac{\rho(\omega)}{\omega} d\omega. \tag{1.34}$$

Assuming the distribution function $\rho(\omega)$ as Debye model,

$$\rho(\omega) = a\omega^2. \tag{1.35}$$

Normalizing to $3N$ oscillator.

$$\rho(\omega) = \frac{9N\omega^2}{\omega_D{}^3}. \tag{1.36}$$

Substitute to eq. (1.34),

$$\langle r^2 \rangle = \frac{9\hbar}{M\omega_D{}^3} \int_0^{\omega_D} \left\{ \frac{1}{2} + \frac{1}{e^{\frac{\hbar\omega}{kT}} - 1} \right\} \omega \, d\omega. \tag{1.37}$$

We define θ_D (Debye temperature) and u as

$$\theta_D = \frac{\hbar\omega_D}{k} \qquad u = \frac{\hbar\omega}{kT} \tag{1.38}$$

and substitute to eq. (1.37),

$$\langle r^2 \rangle = \frac{9\hbar}{4Mk\theta_D} \left\{ 1 + 4\left(\frac{T}{\theta_D}\right)^2 \int_0^{\theta_D/T} \frac{u \, du}{e^u - 1} \right\}. \tag{1.39}$$

The vibration is isotropic in x, y, z direction,

$$\langle u^2 \rangle = \frac{\langle r^2 \rangle}{3}. \tag{1.40}$$

So f is shown as,

$$f = \exp\left[-\frac{3E_R}{2k\theta_D}\left\{1 + 4\left(\frac{T}{\theta_D}\right)^2 \int_0^{\theta_D/T} \frac{u\,du}{e^u - 1}\right\}\right]. \qquad (1.41)$$

Figure 1-3 shows the recoil free fraction of ^{197}Au as a function of temperature assuming different three Debye temperature. In the case of ^{197}Au, the energy of γ-ray is rather high and recoil free fraction is small.

1.2.7 ^{197}Au Mössbauer Effect

In this study, we used ^{197}Pt as γ-ray source of ^{197}Au Mössbauer measurement. Its half-life is 18 hours and is not so long. However this source is easily prepared by reaction of ^{196}Pt(n,γ)^{197}Pt using a nuclear reactor. This source obtained from the reactor is used usually for the ^{197}Au Mössbauer measurements. Figure 1-4 shows the decay scheme of ^{197}Pt to ^{197}Au, and Figure 1-5 shows the schematic drawing of the ^{197}Au Mössbauer level and its hyperfine splitting [15]. Since Mössbauer transition of ^{197}Au include M1 transition and 10% E2 transition [15], 8 transitions exist. Figure 1-6 shows calculated ^{197}Au Mössbauer spectra. Since the lifetime of excited state is rather short, the line width of ^{197}Au Mössbauer spectra is broad, and estimated to 1.8 mm/s in experiments. The spectrum with small magnetic splitting looks like a single peak or a doublet. The natural abundance of ^{197}Au is 100%.

The effective thickness of Mössbauer measurement T is

$$T = f\,n\,\sigma_0 \qquad (1.42)$$

where f is recoil free fraction, n is the number of resonant atoms in unit area and σ_0 is resonant cross section. In the case of ^{197}Au nucleus, the

resonant cross section is 4.351×10^{-20} cm^2 [17]. This value is smaller than that of ^{57}Fe, which is 236.3×10^{-20} cm^2 [17]. The energy of ^{197}Au Mössbauer γ-ray is 77.345 keV. This is larger than ^{57}Fe, which is 14.39 keV. So recoil free fraction of ^{197}Au is small, too. ^{197}Au Mössbauer spectra are observed usually at low temperature, less than 20 K. In other hands, since the recoil free fraction rapidly changes with the small change of the temperature, the measurement of Debye temperature from the recoil free fraction is easy.

1.3 Multilayer

1.3.1 Metallic Multilayer

In this study, we are interested in the multilayer materials, which is one of so called new materials, because multilayer is an artificially constructed and new physical and chemical properties can be expected [1, 2]. Using the deposition technique to make thin films, we can make controlled material in stacking direction. The superlattice of semiconductors, for example GaAs/GaAsAl, are well known and practically used as a quantum well material. The history of metallic multilayer (superlattices) is older than that of superlattice of semiconductors. In 70's the metallic multilayers were made as X-ray mirror and were not studied on their physical property. In the case of metals, there are many kinds of lattice structures and lattice constants, the diffusion of atoms is also easy and rapid, thus it is considered that to making good metallic superlattice is difficult. However It was clarified that to make good metallic superlattice is not so difficult. That is owing to the progress of vacuum and evaporation techniques. In 80's, many properties of multilayers were studied, for example superconductivity [18], elastic properties [19], magnetism and magnetic anisotropy [20]. In 1988 the giant magneto-resistance was discovered in Fe/Cr multilayer [3], the number of studies was suddenly increase. In 1992, the first international symposium on metallic multilayers was held in Kyoto, and second symposium was held in Cambridge, 1995.

1.3.2 Giant Magneto-Resistance and Inter-Layer Coupling

One of the characteristic property of multilayer is giant magneto-resistance. The giant magneto-resistance (GMR) was reported by Baibich *et al.* on Fe/Cr multilayers in 1988 [3]. They reported maximum 40% reduction of the electric resistance by applying magnetic field. Till then, largest magneto-resistance, which was known, was only a few percentages.

This phenomenon was explained qualitatively by the following [21]. The magnetic moments of the magnetic layers, which separated by nonmagnetic layers, couple in anti-parallel. The conduction electrons that run in nonmagnetic layers scattered at interface. In this case, since the magnetic layers coupled in anti-parallel, up polarized and down polarized electrons are scattered by magnetic layers. When the magnetic moments of magnetic layers become parallel by external field, only up or down polarized electrons are scattered and opposite polarized electrons are not scattered. So the total resistance is decrease. In GMR, the anti-parallel coupling of magnetic layers is important. If the magnetic layers couple in parallel without external field, GMR is not observed. When the thickness of nonmagnetic layers increases, the magnitude of GMR changes oscillatory [22]. The example of oscillatory behavior of the GMR is shown in Fig. 1-7. This oscillation was reported in many kinds of multilayers and explained by RKKY type conduction electron polarization [23] or stable state in quantum well [24].

1.3.3 Supermodulus Effect

In 1977, Yang *et al.* reported "super-modulus effect" in Au/Ni multilayers [4]. This phenomenon is enhancement of hardness of multilayers. The biaxial elastic modulus enhance quickly on the multilayers whose periods of stacking are less than 3 nm, shown as Fig. 1-8. On this experiment, they used a bulge tester, but its precision is not so high. The measurement of elastic property of thin film is difficult. Especially, the substrates interfere the measurement. Thus "super-modulus effect" have been measured and discussed. However, its essence is not so clear. Now, the misfit at the interface is considered the most likely origin of the super-modulus effect, and Jankowski reported enhancement of the elastic modulus from the calculation based on the assumption of the misfit [25].

The Au/Ni multilayer specimen that was used this study was studied about the pressure dependence of the lattice constant using the X-ray diffraction technique and the diamond anvil cell by Konishi *et al.* [6]. This study shows that the pressure dependent of lattice constant of multilayer is smaller than that of bulk metal. This result shows existence of super-modulus effect on this sample.

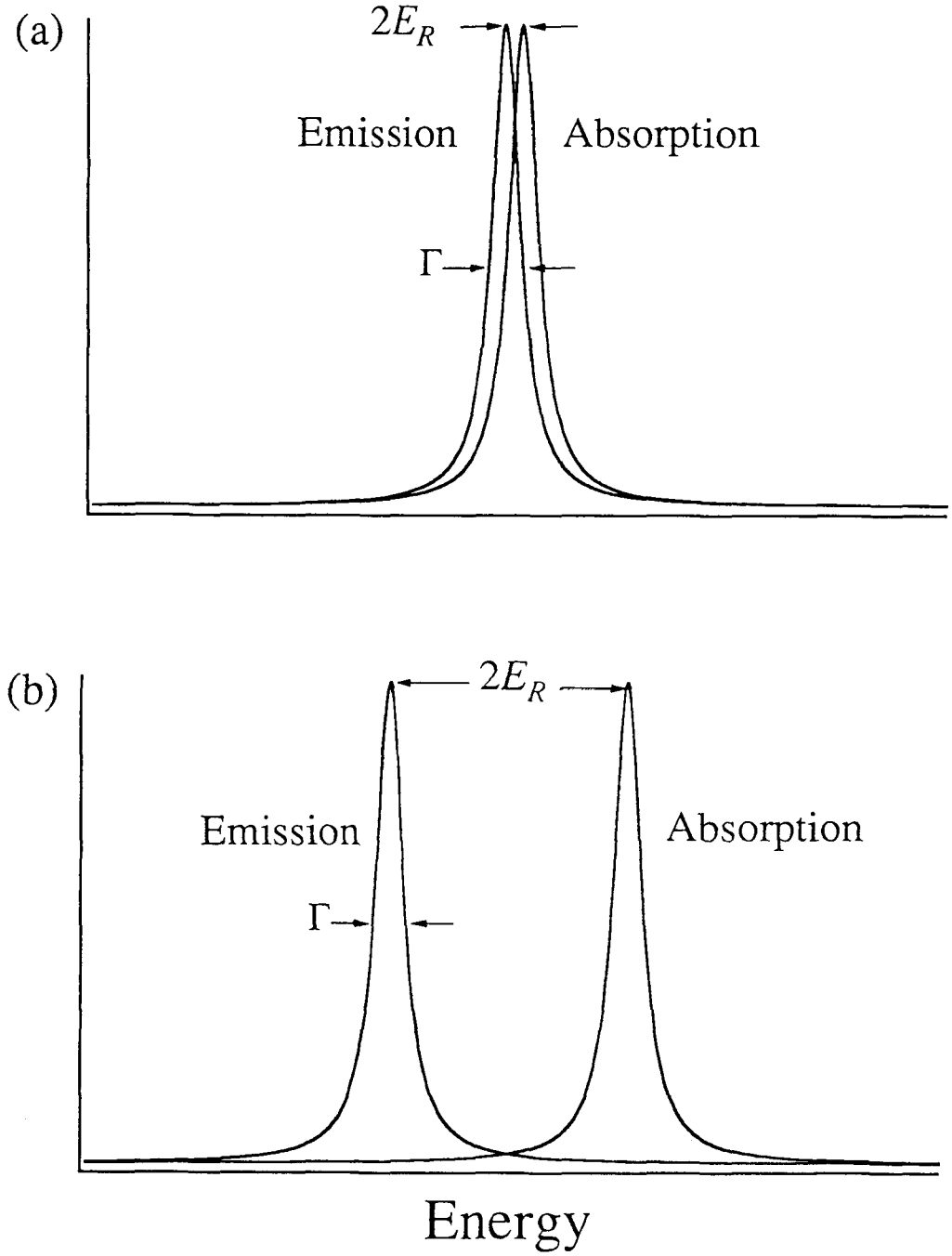

Fig. 1-1 Schematic drawing of resonant absorptions.
(a) Recoil-energy is small. Emmision and absorption lines overlap with each other within their linewidth.
(b) Recoil-energy exceeds the natural line width.

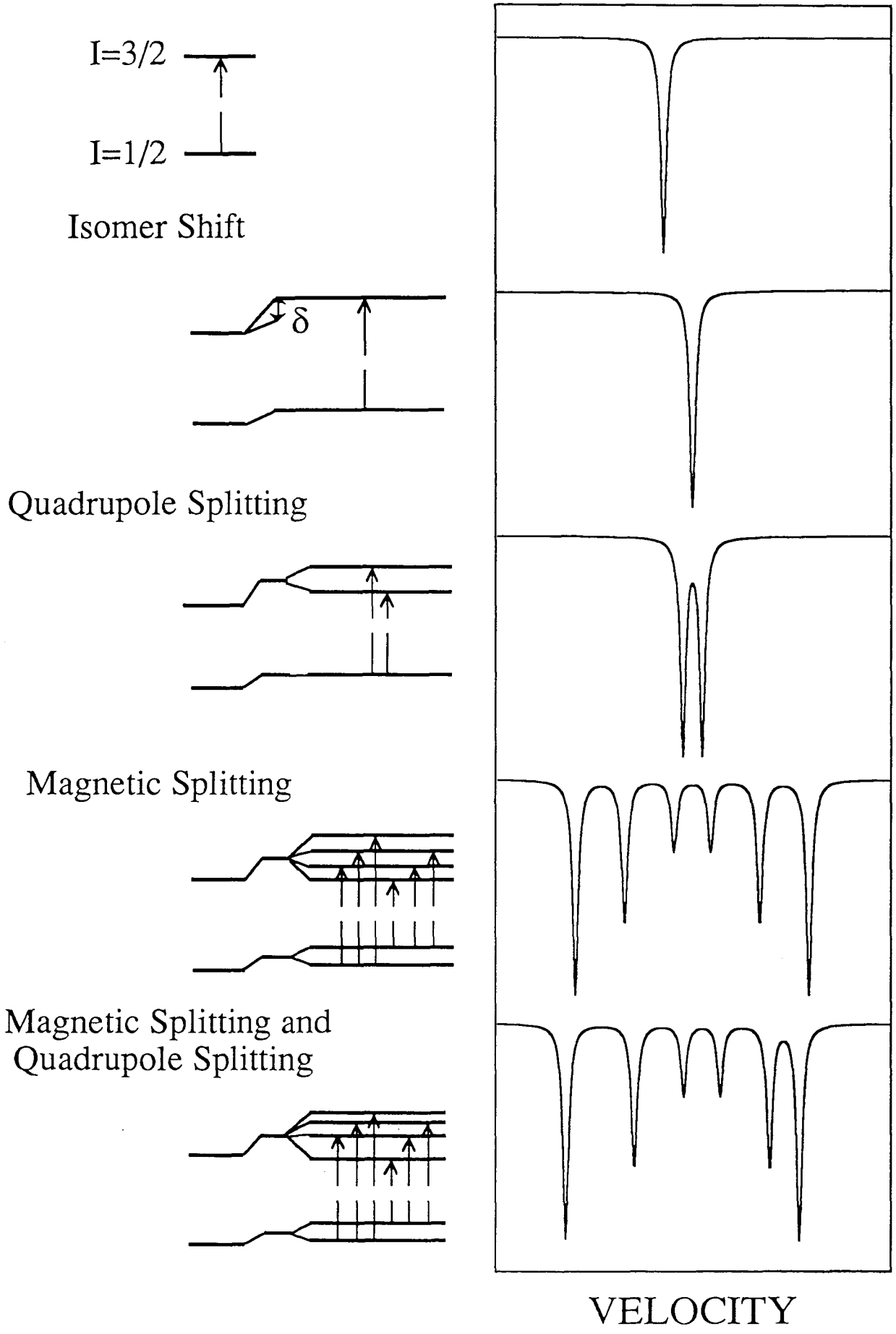

Fig. 1-2 Schematic drawing of hyperfine structure of ^{57}Fe and correspondent Mössbauer spectra.

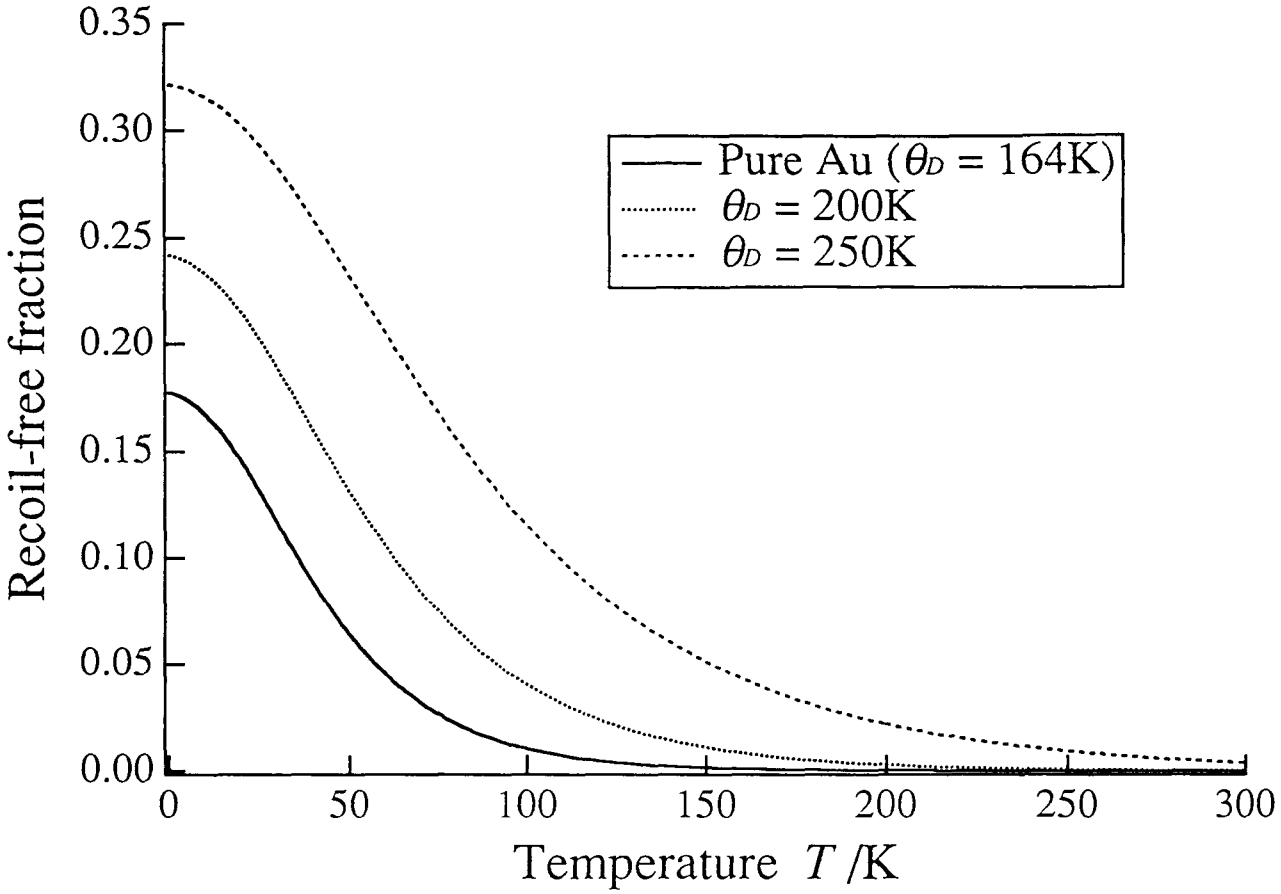

Fig. 1-3 Recoil-free fraction of ^{197}Au as a function of temperature. Three different Debye temperatures have been assumed.

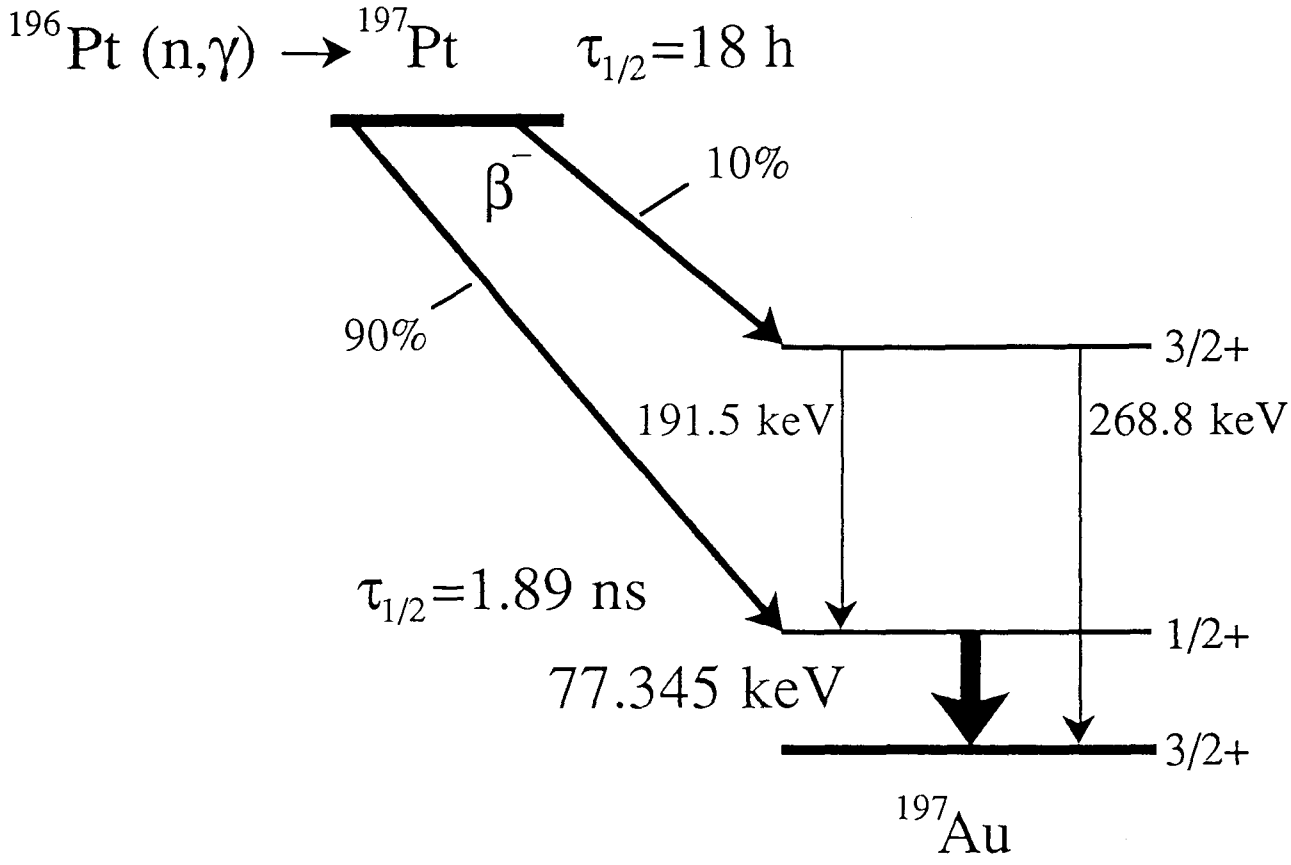

Fig 1-4 Decay scheme of ^{197}Pt to ^{197}Au [15].

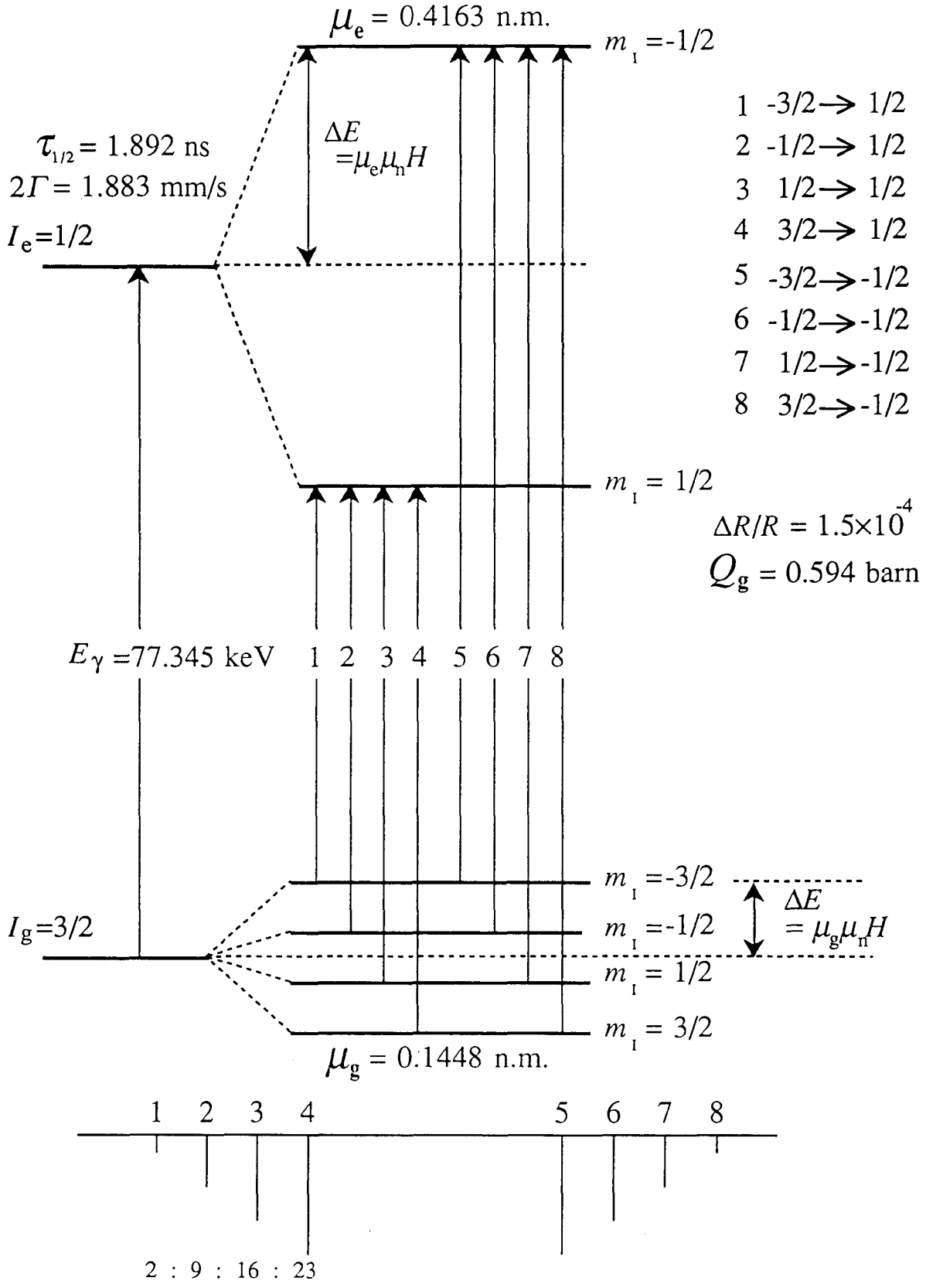

Fig. 1-5 Schematic drawing of the ^{197}Au Mössbauer level and its hyperfine splitting [15].

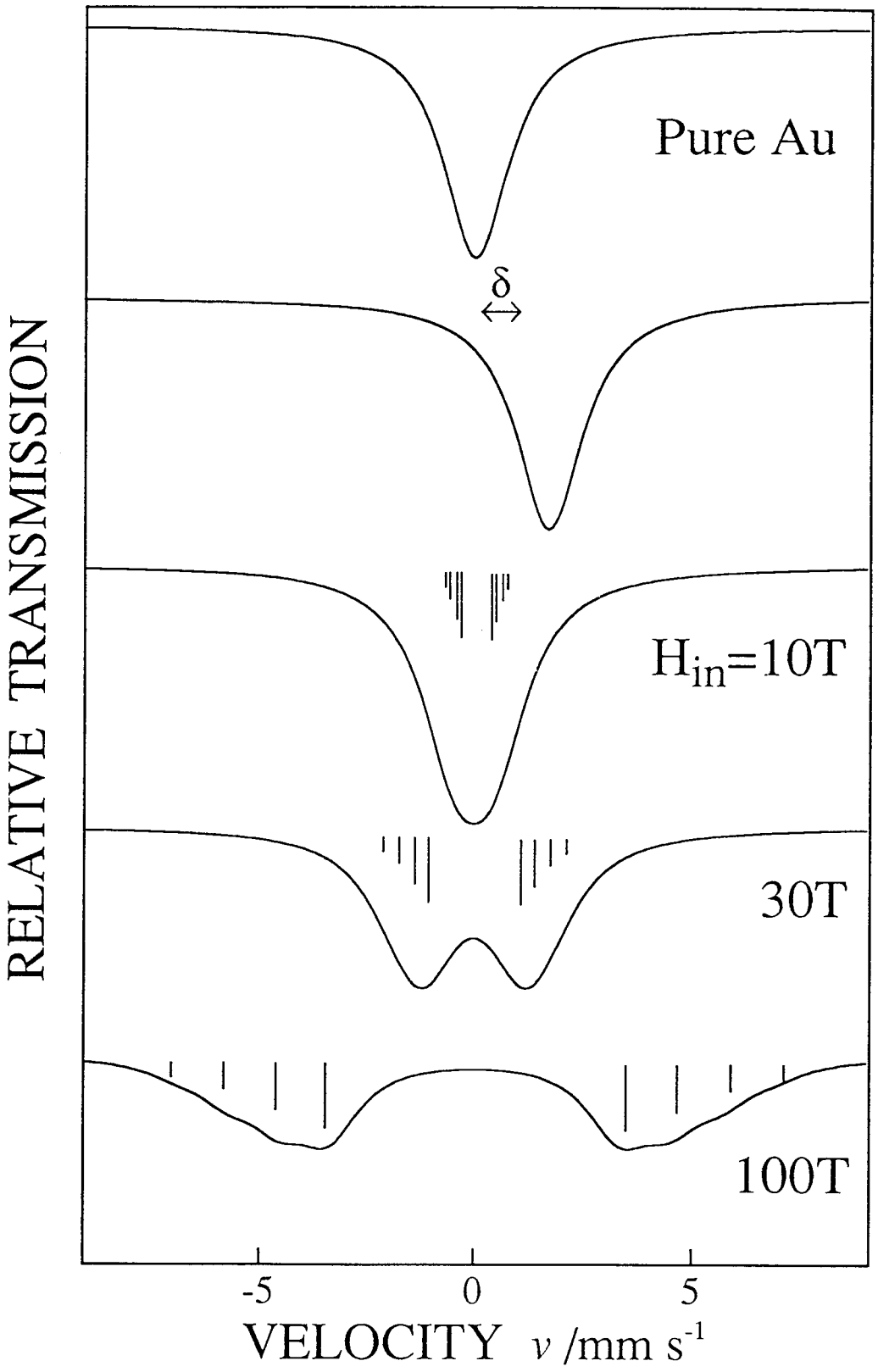

Fig. 1-6 The calculated ^{197}Au Mössbauer spectra showing the isomer shift and the hyperfine magnetic fields.

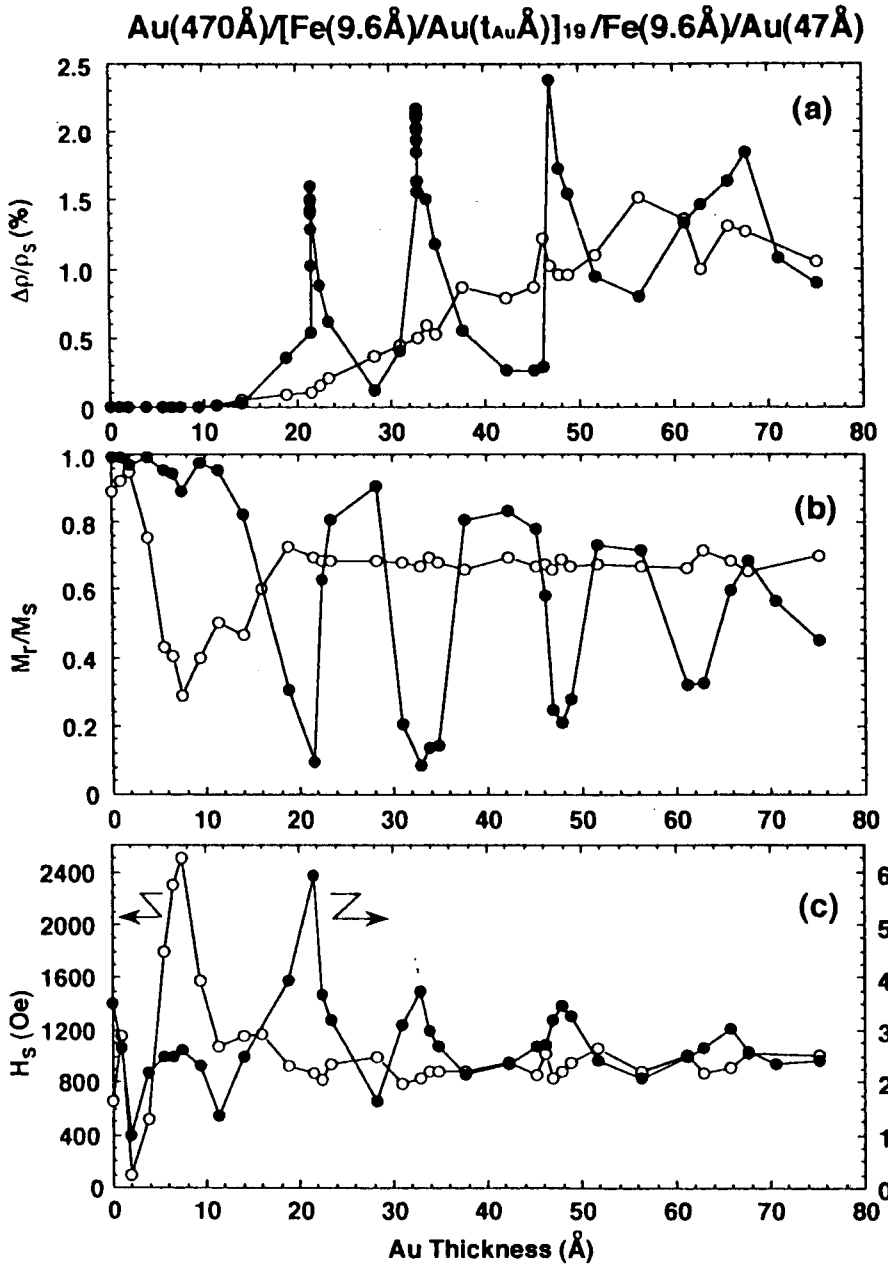

Fig. 1-7 Au-spacer-layer thickness dependence of the (a) MR ratio, (b) M_r/M_s, and (c) H_s of Au(470 Å)/[Fe(9.6 Å)/Au(t_{Au} Å)]$_{19}$/Fe(9.6 Å)/Au(47 Å) on GaAs substrates [closed circle, single-crystal-like Fe/Au(100) multilayers] and grass substrate [open circle, polycrystalline Au/Fe(111) multilayers] at RT. $\Delta\rho/\rho_s = [\rho(H) - \rho(H = H_s)]/\rho(H = H_s)$ [22].

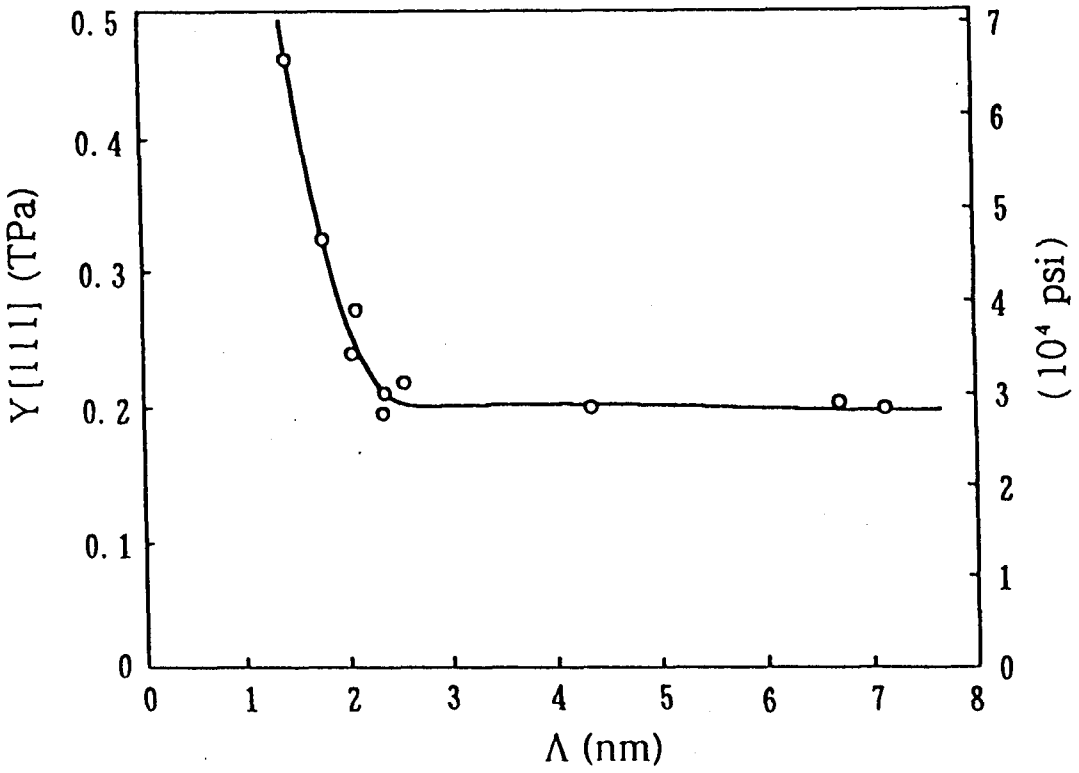

Fig. 1-8 The variation of $Y[111]$ with wavelength λ of the composition modulation for Au/Ni foils having an amplitude of 50at.% [4].

2. Experimental Procedure

2.1 Samples

Thickness and construction of each layer in Au/Fe, Au/Co and Au/Ni multilayers used in present investigation are tabulated in Table 2-1. These multilayer samples were prepared at Shinjo laboratory in Institute for Chemical Research in Kyoto University. The multilayers samples were prepared by evaporation technique in ultra-high vacuum chamber. The evaporation sources were heated by electron-gun (E-gun). First, the chamber was vacuumed by turbo-molecular pump and baked at 200°C in 20 ~ 30 hours. After the baking the pump was changed to cryo pump and the shroud was cooled by liquid nitrogen while the deposition. The pressure reached less than 1×10^{-8} Torr before the deposition. The thickness of the files was monitored by quartz-crystal oscillator thickness monitor and controlled by the shutter attached in front of the evaporation cell. The deposition rate was 0.02 ~ 0.03 nm/s and controlled by current of the E-gun. The thickness of films was controlled with the precision of less than 0.1 nm.

These samples are evaporated on polyimid film. Since the substrates do not have the orientation, the multilayers are poly-crystals in plane. All samples are deposited on Ag(100 nm) buffer layers not to disturb the ^{197}Au Mössbauer spectra. Ag(5.0 nm) layers are overlayer to protect from oxidation. Figure 2-1 shows lattice image of Au(3.0 nm)/Ni(3.0 nm) multilayer by the transmission electron microscope [26]. The arrow shows a domain boundary. The roughness at the interface seems to be exist, but the periodic structure is well shown. Lattice relationships of the Au/Ni multilayers were determined by X-ray

diffraction technique and electron microscope as $(111)_{Ni}//(111)_{Au}$ and $[2\bar{2}0]_{Ni}//[2\bar{2}0]_{Au}$ between Ni and Au layers [26]. Figure 2-2 shows X-ray diffraction pattern of the Au/Fe multilayers at middle angles. The reflection planes were in plane. In addition to the Ag(Au) 111 and Fe 110 peaks, the satellite peaks, which is due to the periodic structure, is shown. The period of the multilayers measured from the X-ray pattern were agree with the period of design. The relationship of the stacking plane is $(110)_{Fe}//(111)_{Au}$ between bcc Fe and Au layers. A structural analysis of these Au/Co multilayers has not yet been completed. Lee *et al.* reported lattice relationship of Au/Co multilayers as $(0001)_{hcp\ Co}//(111)_{Au}$ [27]. From this result, we consider the relationship of these Au/Co multilayers is same direction.

Figure 2-3 shows magnetization curves of the Au/Fe and Au/Co multilayers at 5 K [28]. The external magnetic field was applied in plane of the multilayers. The value of magnetizations were normalized by the saturated value. All samples show ferromagnetic hysteresis loops. The magnetization curve of Au(2.0 nm)/Fe(0.8 nm) multilayer shows soft magnetism and that of Au(0.5 nm)/Fe(0.8 nm) multilayer shows small anisotropy. The magnetization curves of Au/Co(2.0 nm) multilayers show large anisotropy.

We studied about Au-Fe, Au-Co and Au-Ni alloys to compare with the results of multilayers. All samples were solid solutions. The samples were prepared by melting using a high frequency induction furnace and an arc furnace. The samples were rolled at room temperature, annealed at the solid solution temperature and quenched into water. From the X-ray diffraction pattern, it was determined that the all samples as single phase.

2.2 Mössbauer measurement

The source for ^{197}Au Mössbauer measurement was ^{197}Pt in Pt metal, which was prepared by the ^{196}Pt(n,γ)^{197}Pt reaction. The half-life of the source is 18 hours. The neutron irradiation was performed by Kyoto University Reactor (KUR) in Research Reactor Institute of Kyoto University using the gas-pressure-transfer tube (Pn-1). The time of irradiation was one hour. The source was 200 mg disk, and enriched in 96.5% ^{196}Pt. After the irradiation, radioactivity of the source was 3.2 $\times$ 10^8 Bq. Using this source, we could measure the ^{197}Au Mössbauer spectra in about three days. In the source, the numbers of the reacted nuclei are negligible small, thus we can semipermanently use the source by repeatedly irradiation.

Figure 2-4 shows the construction of the cryostat that was used for ^{197}Au Mössbauer measurement [29]. This cryostat is in the Research Reactor Institute. The source and sample were cooled by the closed-cycle-helium refrigerator. The velocity transducer, the source and absorber (sample) were united. This unit was separated from the refrigerator and the vacuum pump that have big vibration. The sample's area was filled by helium gas at 1 atm.. The refrigerator of this cryostat was renewed in Sept. 1993. The coolest temperature of this cryostat is 16 K before the renewal, and 11 K after the renewal.

Figure 2-5 shows the construction of the sample and sample holder. The multilayer samples was evaporated in a circle area with diameter of 7 cm. Using only one piece of film, the total thickness of the Au layers was very thin for measurement of absorption. So we cut the films into 5 mm $\times$ 5 mm square and stacked up the pieces. The pieces were fixed by silicone grease. On Au/Ni multilayers, one film was cut into about

100 pieces and stacked up. On Au/Fe and Au/Co multilayers, two films were cut into 100 pieces respectively, the total is 200 pieces, and stacked up. The total thickness of Au layers is about 30 μm on Au/Ni multilayers and 100 ~ 200 μm on Au/Fe and Au/Co multilayers. On the measurement of thermal dependence, the samples were heated by the heater attached on the sample holder before the renewal of the refrigerator, or attached on the head of refrigerator after the renewal.

Figure 2-6 shows the schematic arrangement of the Mössbauer measurement. A conventional velocity transducer was operated in a constant acceleration mode. On ^{197}Au Mössbauer measurement, we used the internal clock of the multi channel analyzer. The detectors of the γ-ray were the scintillation counter with 5 mm thick NaI(Tl) crystal for ^{197}Au Mössbauer measurement, and proportional counter with Xe gas for ^{57}Fe Mössbauer measurement.

Figure 2-7 shows the energy spectrum of ^{197}Pt source. The biggest peak is regard as the peak of 77.345 keV Mössbauer γ-ray. However this peak includes another X-ray, for example Pt $K_{\beta 1}$ (75.6 keV) and Au $K_{\beta 1}$ (78.0 keV). If we use the solid state detector (SSD), we can separate these peaks and pick out the Mössbauer γ-ray. However the SSD has small detective area, and low detection efficiency. The scintillation counter is better than SSD for ^{197}Au Mössbauer measurement. For the ^{57}Fe Mössbauer measurements, we used the ^{57}Co diffused in Rh. The velocity scales were calibrated using the ^{57}Fe Mössbauer spectra of α-Fe at room temperature for ^{197}Au and ^{57}Fe measurement. The position of zero veracity is determined as the peacock position of pure Au metal for ^{197}Au measurement, and as the center of the spectrum of α-Fe for ^{57}Fe

measurement. The spectra were fitted by the least-mean-square method.

Table 2-1 Constructions of the multilayers' samples.

	Construction	Measurement
Au/Fe multilayers	Ag(100 nm)/[Fe(0.8 nm)/Au(0.5 nm)]$_{100}$/Fe(0.8 nm)/Ag(5.0 nm)	M
	Ag(100 nm)/[Fe(0.8 nm)/Au(1.0 nm)]$_{70}$/Fe(0.8 nm)/Ag(5.0 nm)	M, E
	Ag(100 nm)/[Fe(0.8 nm)/Au(2.0 nm)]$_{50}$/Fe(0.8 nm)/Ag(5.0 nm)	M
	Ag(100 nm)/[Fe(0.8 nm)/Au(3.0 nm)]$_{30}$/Fe(0.8 nm)/Ag(5.0 nm)	M
Au/Co multilayers	Ag(100 nm)/[Co(2.0 nm)/Au(0.5 nm)]$_{100}$/Co(2.0 nm)/Ag(5.0 nm)	M
	Ag(100 nm)/[Co(2.0 nm)/Au(1.0 nm)]$_{70}$/Co(2.0 nm)/Ag(5.0 nm)	M, E
	Ag(100 nm)/[Co(2.0 nm)/Au(2.0 nm)]$_{40}$/Co(2.0 nm)/Ag(5.0 nm)	M
Au/Ni multilayers	Au(0.5 nm)/[Ni(2.0 nm)/Au(0.5 nm)]$_{59}$	M
	Au(1.0 nm)/[Ni(2.0 nm)/Au(1.0 nm)]$_{29}$	M, E
	Au(2.0 nm)/[Ni(2.0 nm)/Au(2.0 nm)]$_{14}$	M
	Au(25 nm)/[Ni(1.0 nm)/Au(1.0 nm)]$_{50}$	E

M : Magnetic properties
E : Elastic properties

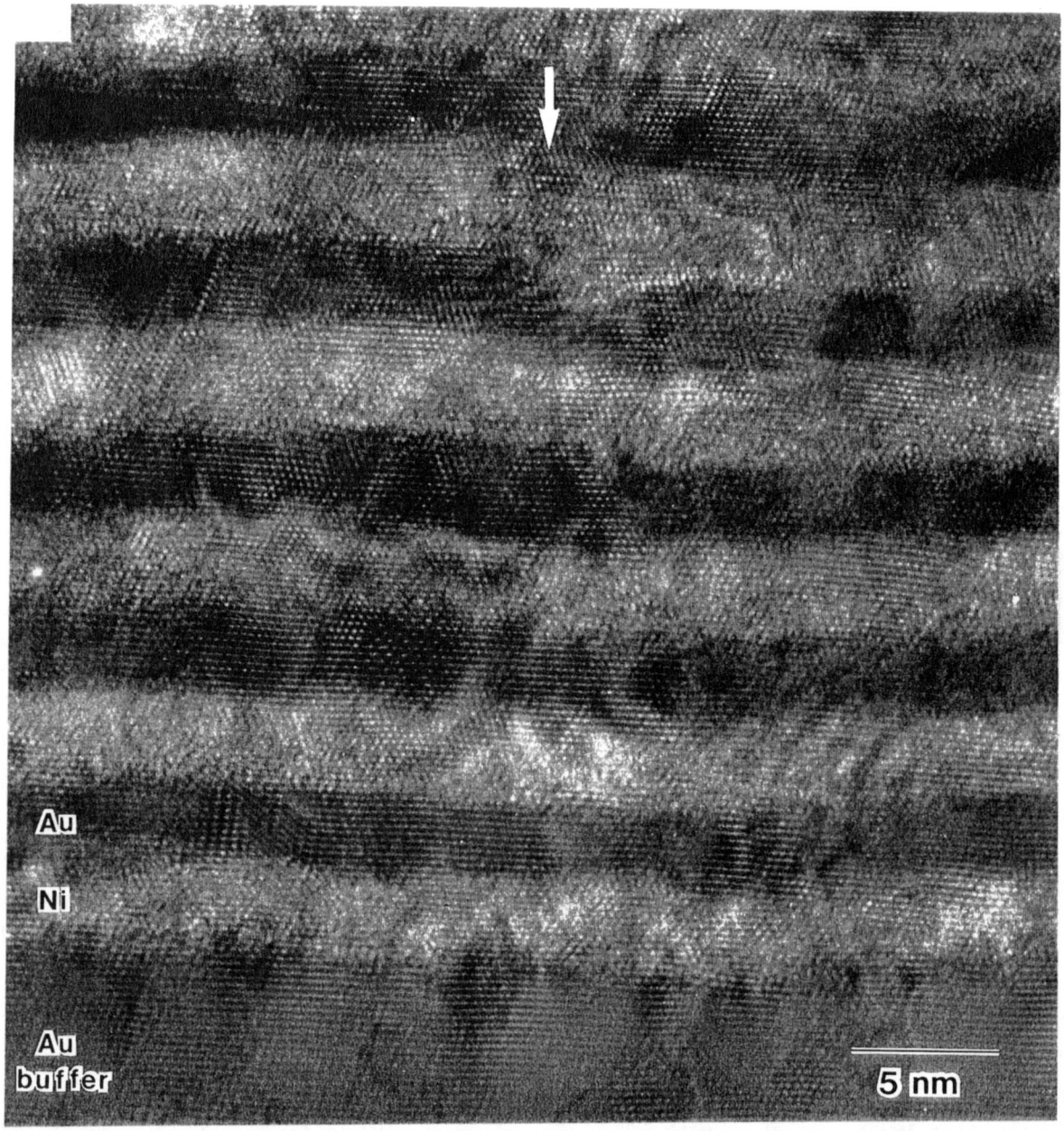

Fig. 2-1 Lattice image of the Au(3.0 nm)/Ni(3.0 nm) multilayer for regions near the buffer layers [26].

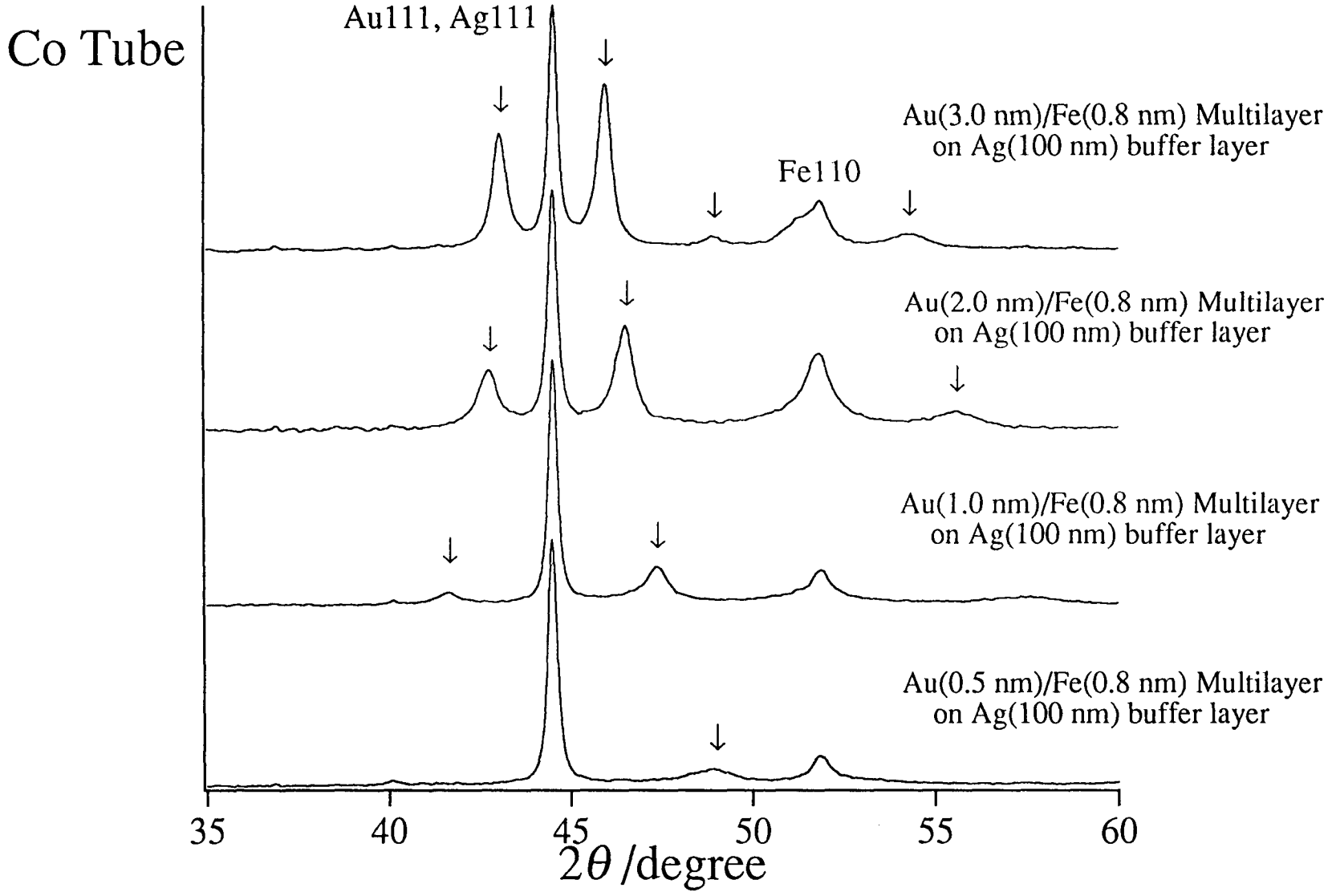

Fig. 2-2 X-ray diffraction patterns of Au/Fe multilayers.

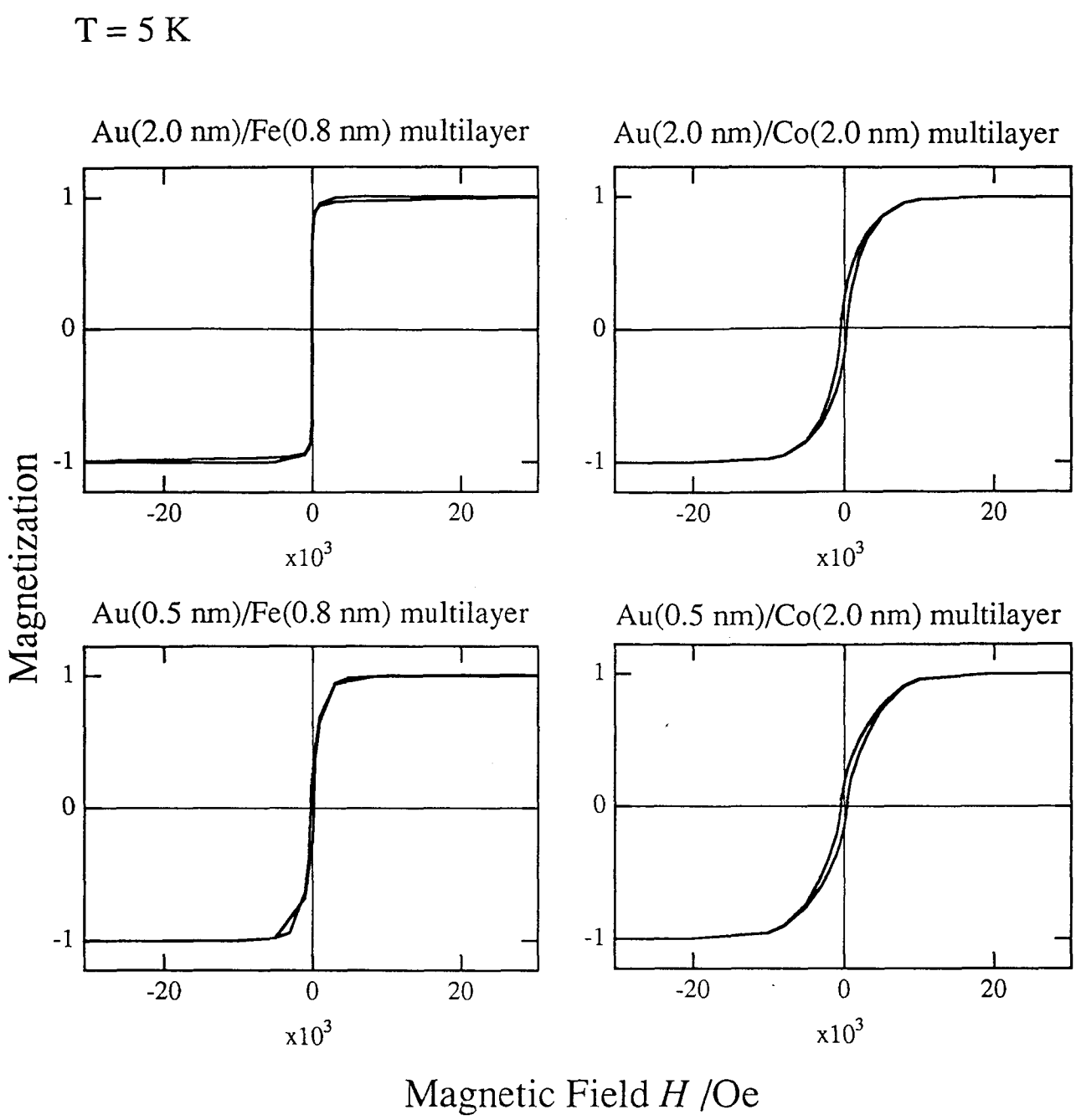

Fig. 2-3 Magnetization curves of Au/Fe and Au/Co multilayers at 5 K [28].

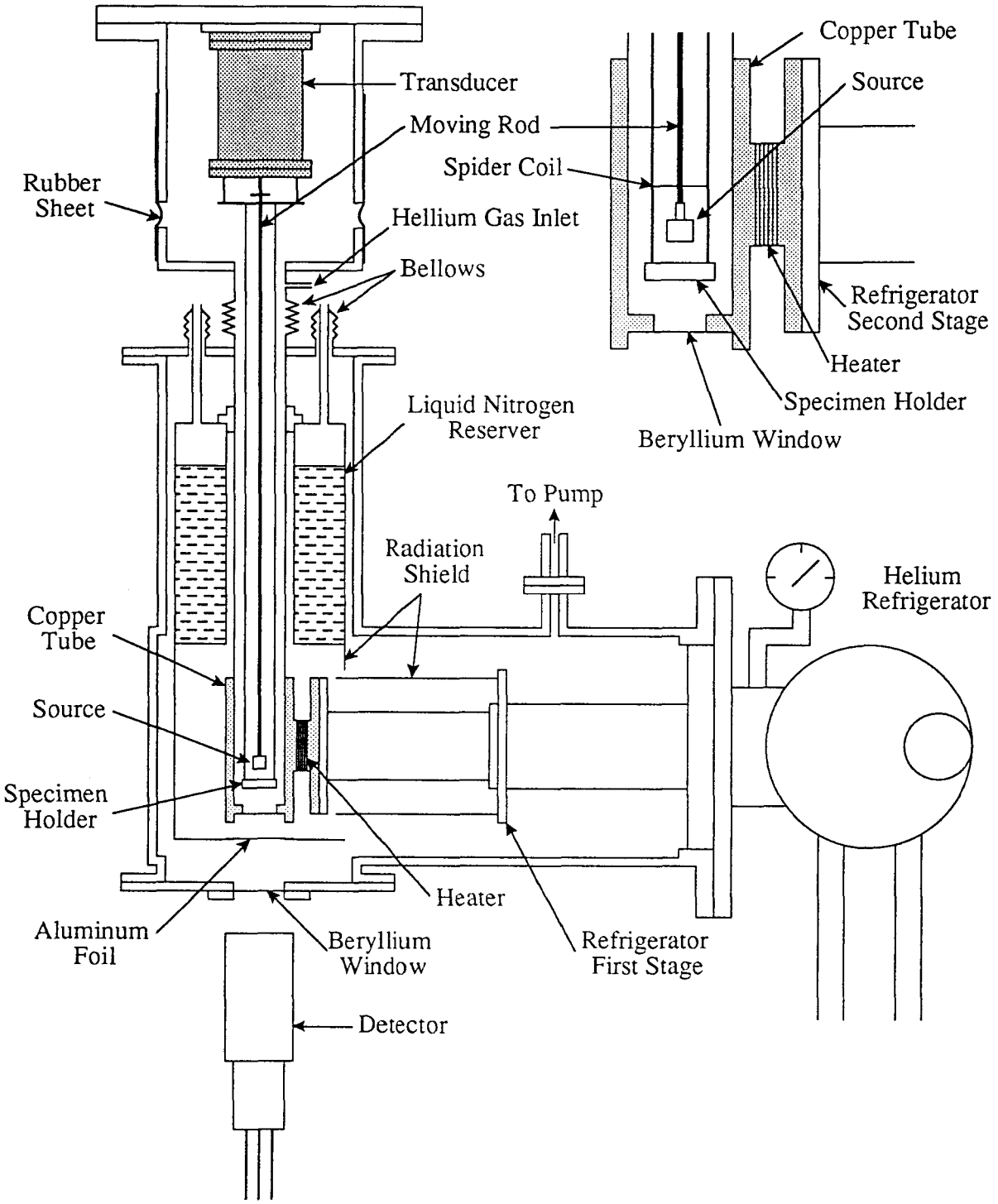

Fig. 2-4 The vertical section of the cryostat for ^{197}Au Mössbauer specroscopy [29].

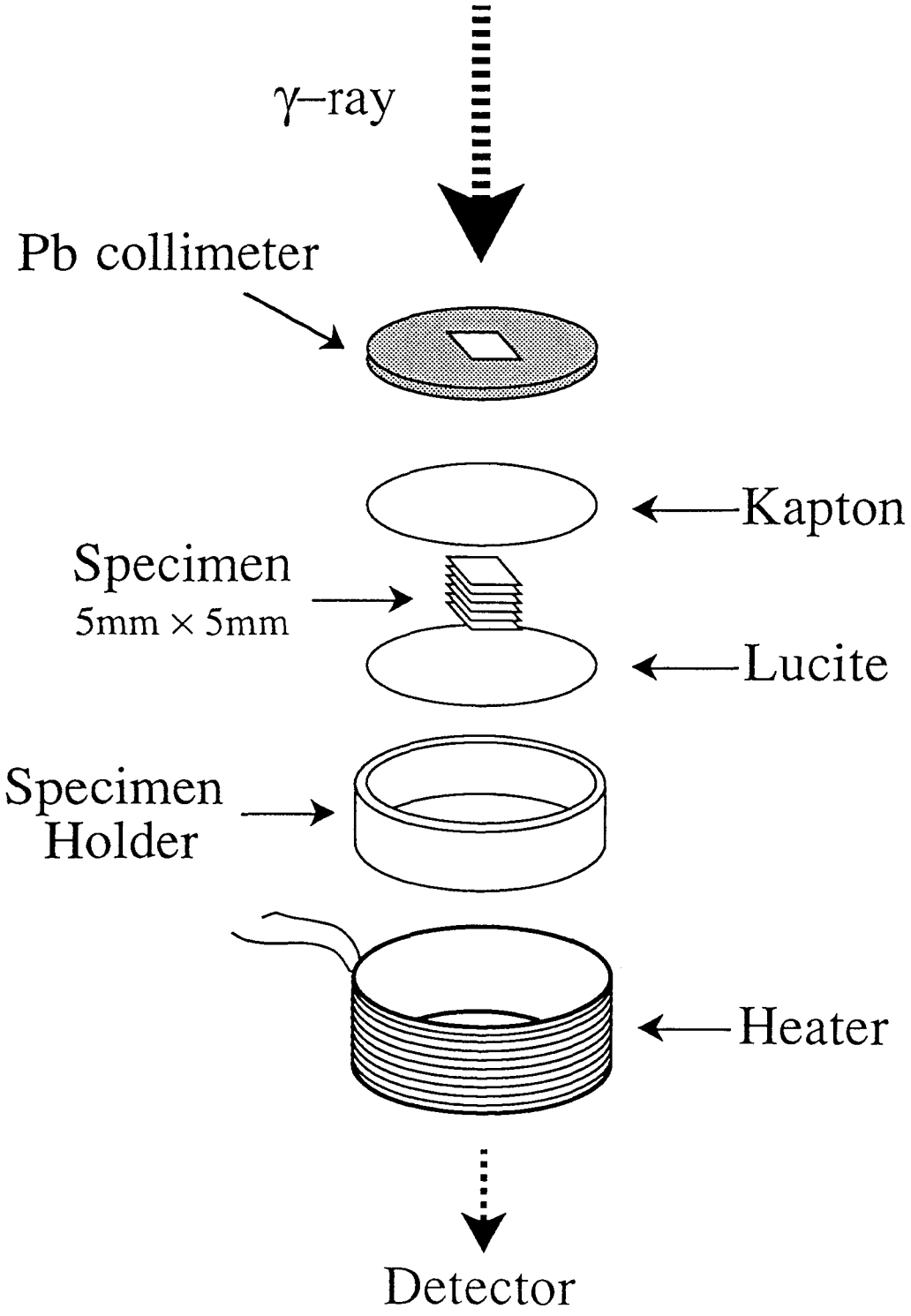

Fig. 2-5 The sketch of specimen and specimen holder.

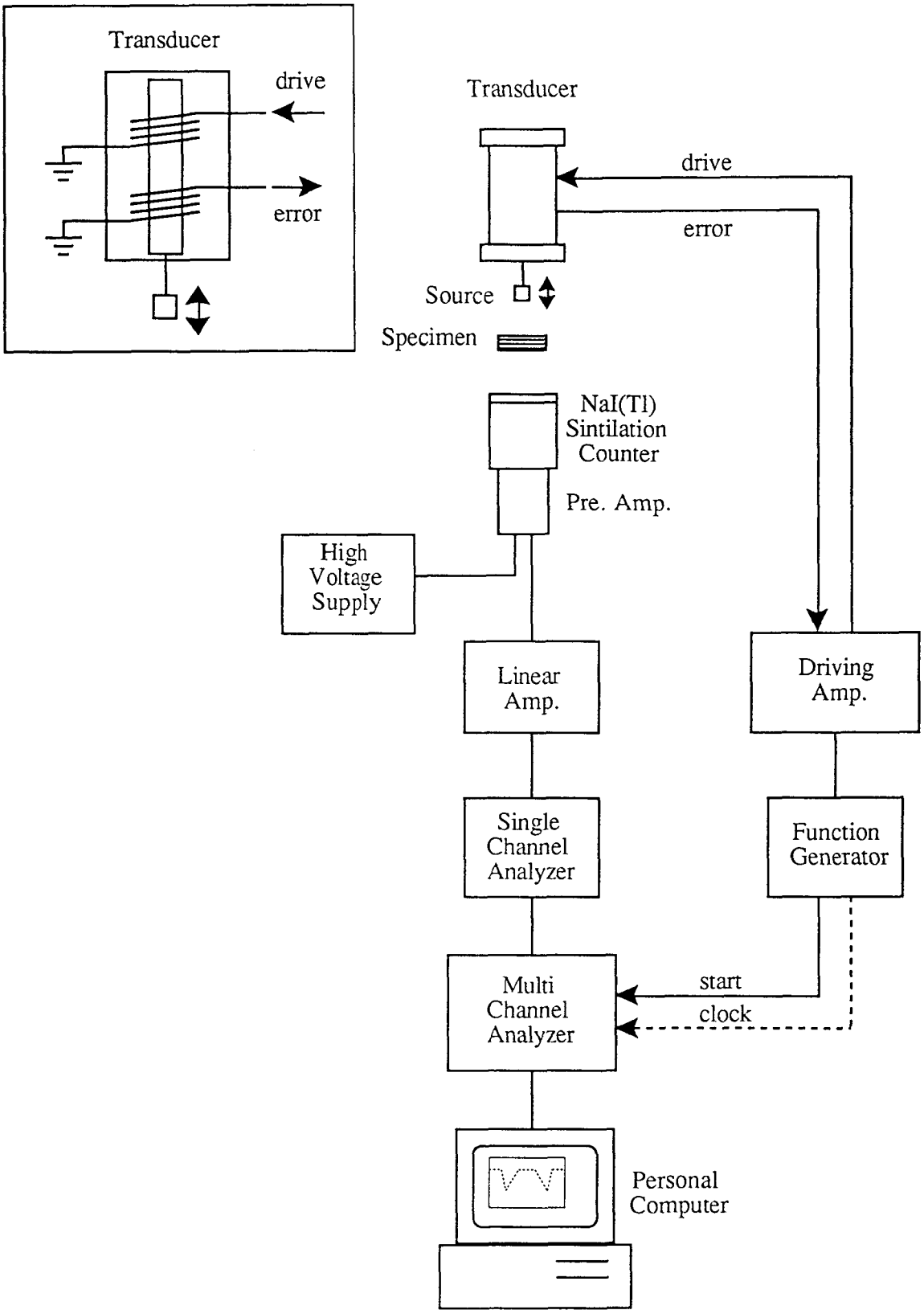

Fig. 2-6 Schemaitc arrangement for Mössbauer spectroscopy.

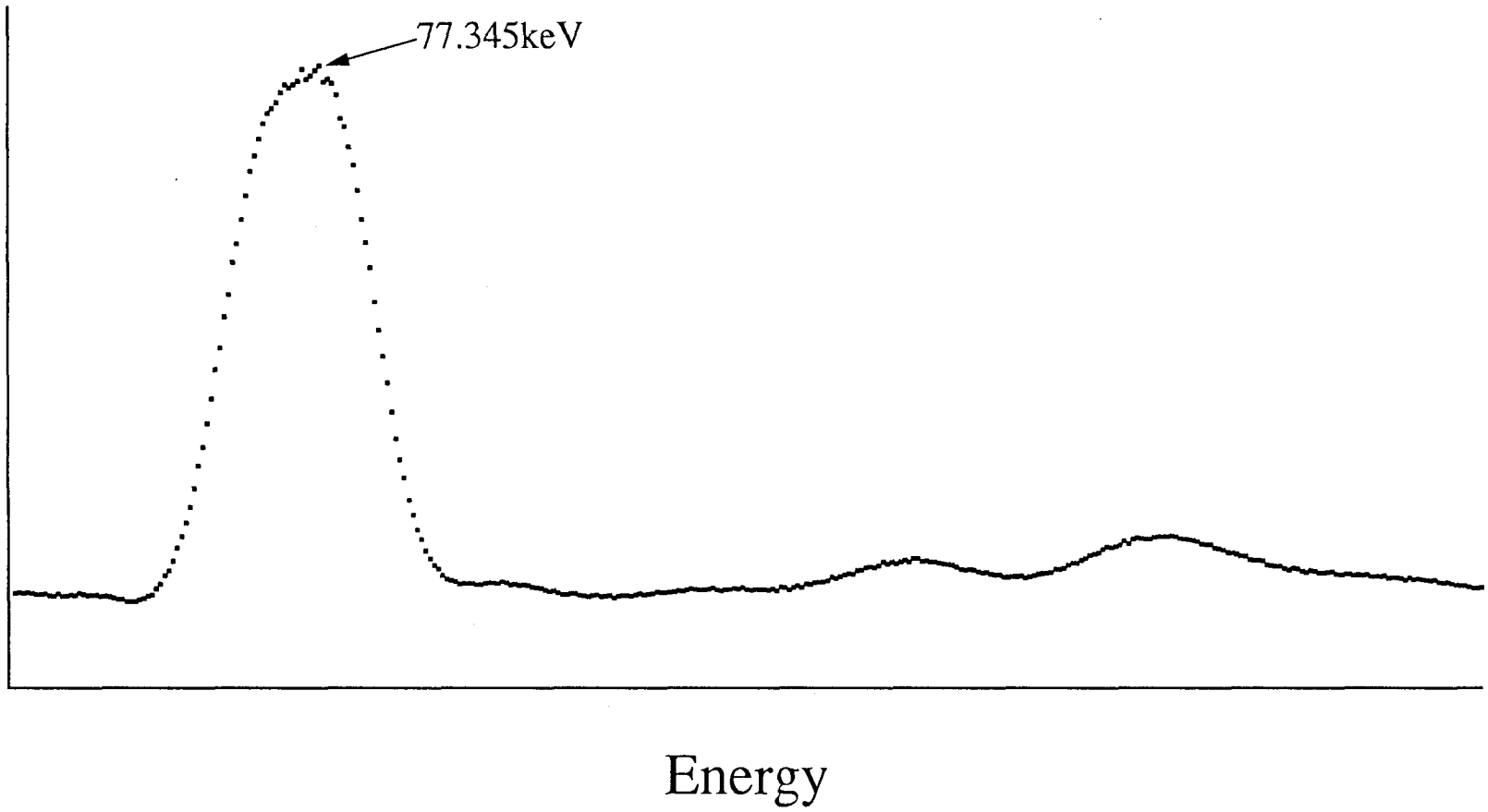

Fig. 2-7 Energy spectrum of ^{197}Pt source.

Results and Discussions

3.1 Alloys

We studied about the alloys that consist of the same metal-elements as multilayers to compare with the results from multilayers [30]. The Mössbauer parameters of the alloys are guides to the spectral analysis of the multilayers. The alloys consisted of Au and magnetic metals were studied since old time. For example, Au-Fe alloy is well known as spin glass material [31]. However almost these studies are measurements about magnetic elements. The study about nonmagnetic element was not so many.

Figure 3-1 shows the phase diagrams of Au-Fe, Au-Co and Au-Ni systems [32]. Au-Ni system has solid solution phase in all Ni content over 810.3°C. Au-Fe system has wide solid solution area. In Au-Co system, there is small area for solid solution. All the alloys have not intermetallic compounds in equilibrium state and this makes the spectral analysis of alloy and multilayers to be easy. We studied about single phase alloys, which are solid solutions.

Figure 3-2 shows ^{197}Au Mössbauer spectra of Au rich Au-Fe alloys at 11 K. The structures of all samples are determined to be fcc by X-ray diffraction measurements. The hyperfine magnetic field and the isomer shift increase with the increase of Fe content. The spectra of over 20at.%Fe alloy clearly show asymmetric shape. Usually the asymmetry of Mössbauer spectrum is due to the quadrupole splitting. However these samples are cubic and random solution alloys, so the large quadrupole splitting may not expect. On the other hand, the widths of the spectra are rather broad when we assumed that the spectrum

consists of only one magnetic component. We assumed the distribution of hyperfine magnetic field. When the magnetic field increases with an increase of the isomer shift, the 4 peaks on positive side in magnetically split spectrum shift to positive velocity side by the increase of the isomer shift and also by the increase of the magnetic splitting. So the widths of peaks in positive side become broad. On the other hand, the 4 peaks on negative side shift to positive velocity side by the increase of the isomer shift and shift to negative velocity side by the increase of the magnetic splitting. So the peaks in negative side become not so broad and look like sharper than the peaks in positive side by the compensation effect of the positive and negative shift. By this reason, the spectrum becomes asymmetric shape. Figure 3-3 shows the results of the spectral analysis by the distribution model. The spectra were fitted by the NORMOS DIST program developed by Brand [33] with a simple histogram method taking distributions of isomer shift into account. On this analysis, we assumed that the quadrupole splitting is zero. The isomer shift is linear to the hyperfine magnetic field. In Fig. 3-3, the experimental data and fitting curves show good agreement. So the asymmetries is due to the distribution of the hyperfine magnetic field, not due to a quadrupole splitting.

Figure 3-4 shows the ^{197}Au Mössbauer spectra of Au-95at.%Fe and 99at.%Fe alloys. These samples have bcc structure. The spectra show large hyperfine magnetic field. The magnitudes of hyperfine magnetic fields are 121 T for 95at.%Fe alloy and 126 T for 99at.%Fe alloy. These spectra show rather symmetrical shapes, so the distributions of the hyperfine magnetic fields are not so large. Figure 3-5 shows the Fe content dependence of isomer shifts, hyperfine magnetic fields and the

lattice constants of Au-Fe alloys. The lattice constants were measured by the X-ray diffraction technique. The values of the isomer shifts and the hyperfine magnetic fields of Au-10 ~ 50at.%Fe alloys are averaged values obtained from the distributions. The isomer shift and the hyperfine magnetic field increase in linearly as an increase of the Fe content from 10% to 50%. The values for Au-95at.%Fe and 99at.%Fe alloys are deviated from the linear relation mentioned above. This is due to the difference of the lattice structure. In the case of ^{197}Au nucleus, a positive isomer shift means the increase of the charge density at the nuclei. So the charge density at the nucleus increases with an increase of the Fe content. It looks strange, because Fe atoms have less electron than Au atoms. The electrons of Au atoms must expand and charge density at nucleus must decrease with increase of Fe content. However, this is not true. The lattice constants of the alloys are decrease with the increase of Fe contents, and the volumes of the Au atoms are decrease. So the electrons of Au atoms are pushed into smaller area, and the charge densities at nuclei are increase.

The relationship between the Fe content and the isomer shift is

$$I.S.(\text{mm s}^{-1}) = 0.3127 + 0.0437\ C(\text{at.}\%) \quad (C < 50) \qquad (3.1)$$

and between the Fe content and hyperfine magnetic field is

$$H_{in}(\text{T}) = 10.804 + 1.467\ C(\text{at.}\%) \qquad (C < 50). \qquad (3.2)$$

This relationships are used as a guide for the spectral analysis of the Au/Fe multilayers.

Figure 3-6 shows ^{197}Au Mössbauer spectra of Au-Ni alloys. These spectra show positive isomer shift. With the increase of Ni content, the widths of the spectra become broad. The spectra of the alloys that

contains more than 90%Ni shows magnetic splitting, so we considered that this broadening is due to magnetic splitting. The magnitude of the hyperfine magnetic field is smaller than that of Au-Fe alloys. We analyzed these spectra assuming the magnetic split spectra without quadrupole splitting. Figure 3-7 shows the isomer shift and the hyperfine splitting of this analysis. The isomer shift increases in proportional to the Ni content, and the slope shows small change at 40%Ni. The hyperfine magnetic field increases in proportional to the Ni content over 60%Ni. However the behavior of the hyperfine magnetic field blow 50%Ni is quite deferent. The relationship between the Ni content and the isomer shift is

$$\begin{aligned} I.S.(\text{mm s}^{-1}) &= 0.0458\ C(\text{at.}\%) && (C < 40) \\ I.S.(\text{mm s}^{-1}) &= -0.3329 + 0.0539\ C(\text{at.}\%) && (40 < C) \end{aligned} \qquad (3.3)$$

and between the Ni content and hyperfine magnetic field is

$$H_{in}(\text{T}) = -0.722 + 0.348\ C(\text{at.}\%) \qquad (60 < C). \qquad (3.4)$$

The parameters of 97%Ni alloy stray off the line. This is due to the reduction of Ni contents in preparing process. From the rigid band model, the magnetic moments of Ni atoms lost in Au-Ni alloys below 40at.%Ni as Cu-Ni alloy system. The change of slope of isomer shift at 40%Ni and the deviation from the proportional relation of the hyperfine magnetic field below 60%Ni are probably caused by the loss of magnetic moment. Assuming the hyperfine magnetic fields of the Au-Ni alloys below 40% are not zero, the spectra of 10 ~ 40at.%Ni alloys have been analysed. However the spectra of 10 ~ 40%Ni alloys show only broadening and not magnetically splitting. In conclusion, we assumed that this broadening is due to the hyperfine magnetic field, but this is

not correct. These spectra show the positive isomer shift. If the distribution of isomer shift exists, the spectrum becomes broad. We analyzed these spectra by the distribution of isomer shift and results shown in Fig. 3-8. By the assumption of the distribution of isomer shift, the experimental data and fit lines show good agreement. Finally we concluded that this broadening is due to the distribution of isomer shift and not due to the hyperfine magnetic field.

Figure 3-9 shows ^{197}Au Mössbauer spectra of the Au atoms diluted in magnetic host metal, Fe, Co and Ni. The Au-1at.%Fe alloy was bcc, the Au-0.7at.%Co and Au-1at.%Ni alloys are fcc. The magnitudes of hyperfine magnetic fields are 126 T in the Au-Fe, the 86 T in the Au-Co and 29 T in Au-Ni alloys. These values are nearly proportional to the magnetic moments of host atoms. The hyperfine magnetic field is due to the not only the external field but also the electronic state of the resonant atom, so it is sometime difficult to discuss the magnetic influence using the hyperfine magnetic field. However, in this case, the magnitudes of the hyperfine magnetic field reflect the magnetic influence from magnetic atoms. In Chapter 3.2 and 3.3, we discuss the magnetic influence of the Au atoms from the magnetic atoms using the magnitude of the hyperfine magnetic field.

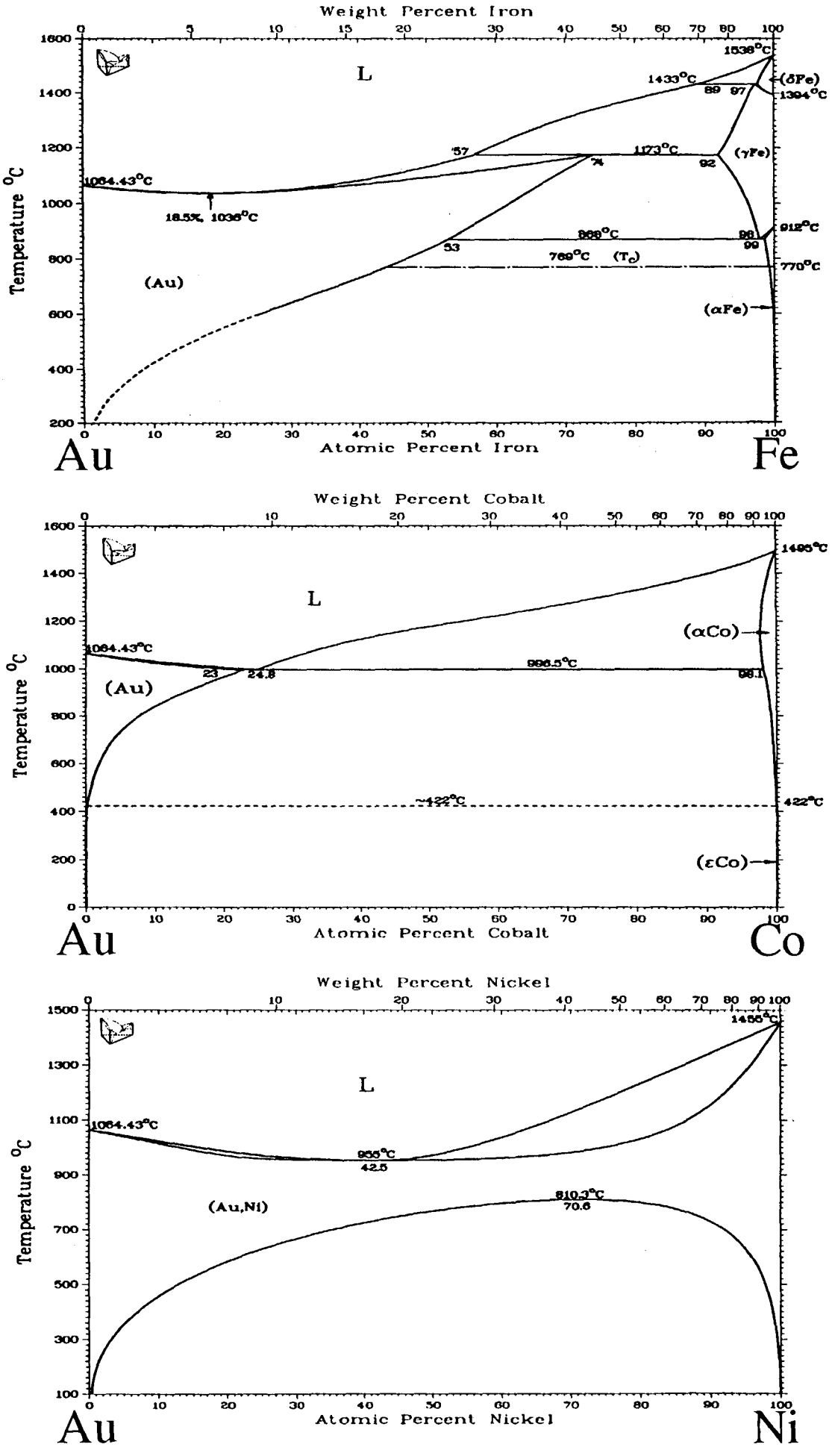

Fig. 3-1 Phase diagrams of Au-Fe, Au-Co and Au-Ni systems [32].

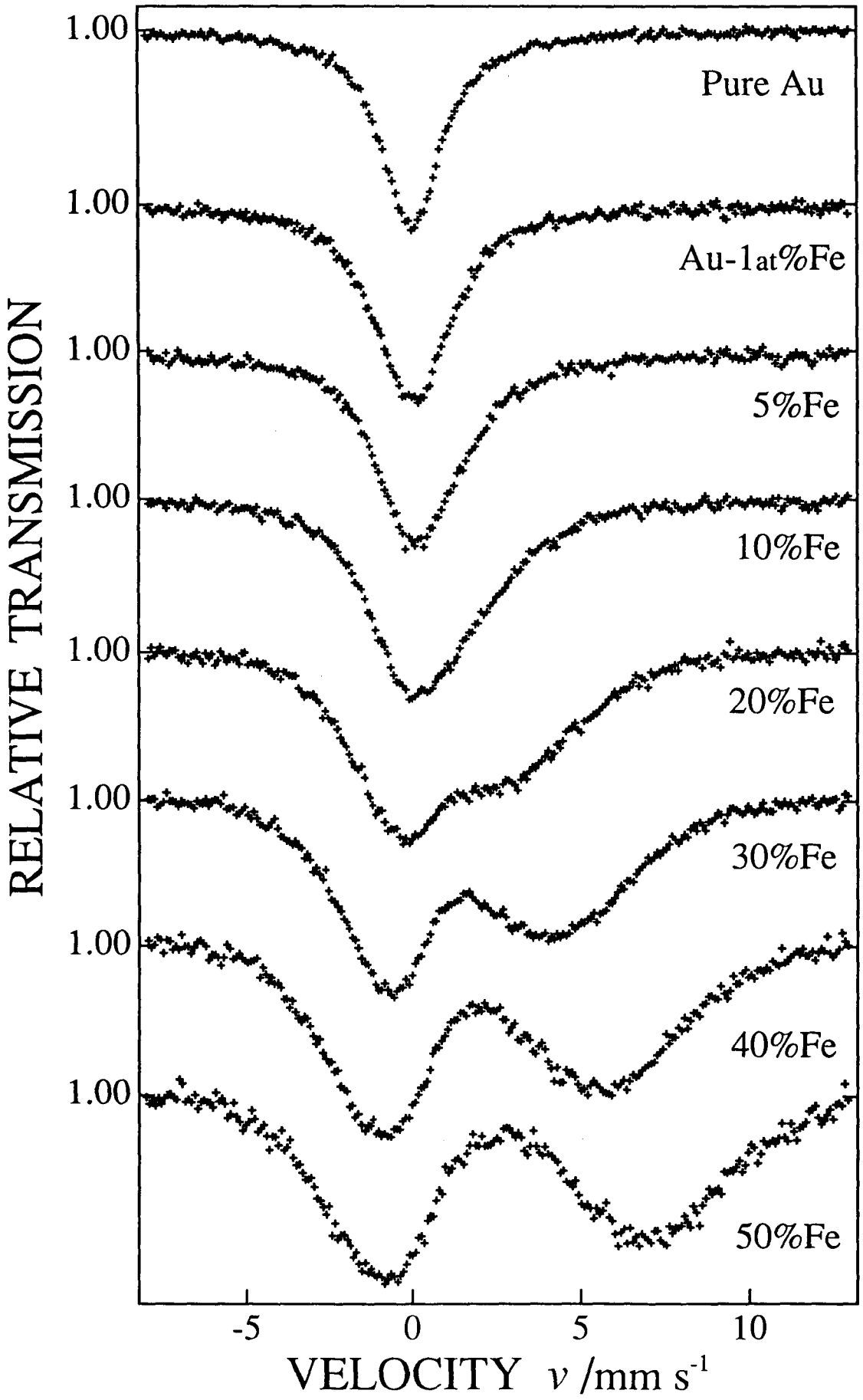

Fig. 3-2 ^{197}Au Mössbauer spectra of AuFe alloys (1at% - 50at%Fe) at 16K.

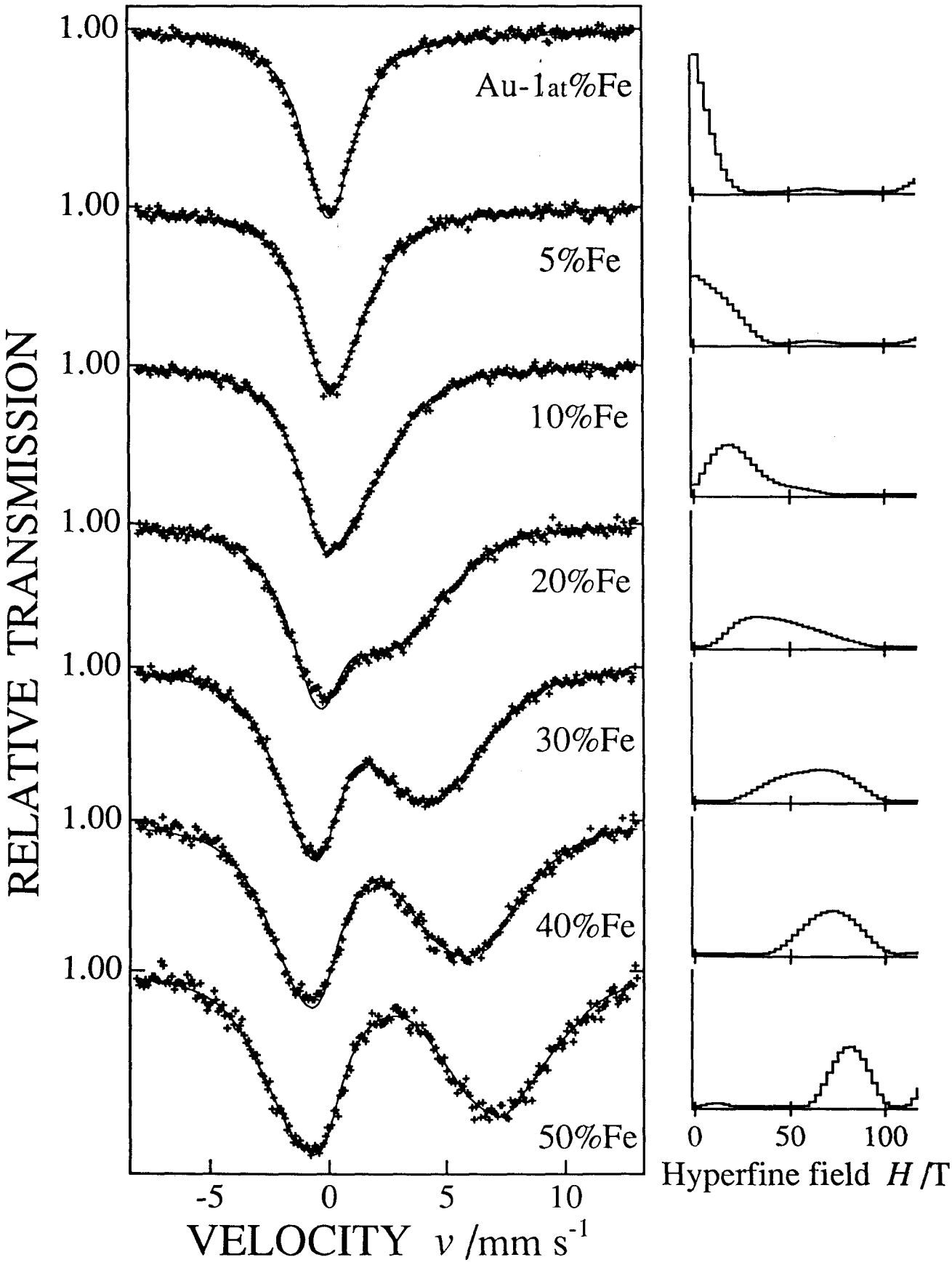

Fig. 3-3 ^{197}Au Mössbauer spectra of AuFe alloys fitted by the hyperfine field distribution model and the distribution of hyperfine field.

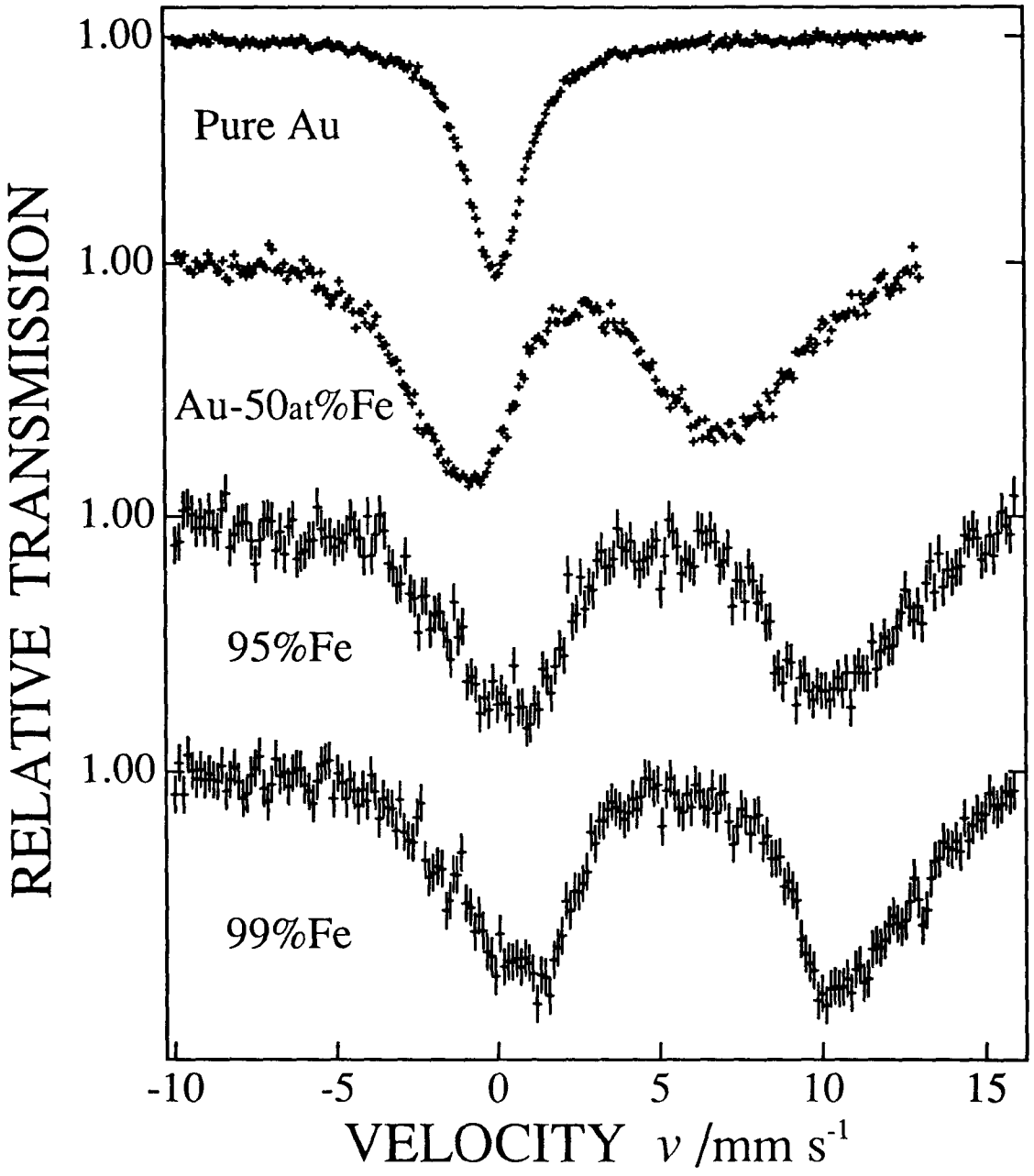

Fig. 3-4 ^{197}Au Mössbauer spectra of AuFe alloys (95at%, 99at%Fe) at 16K.

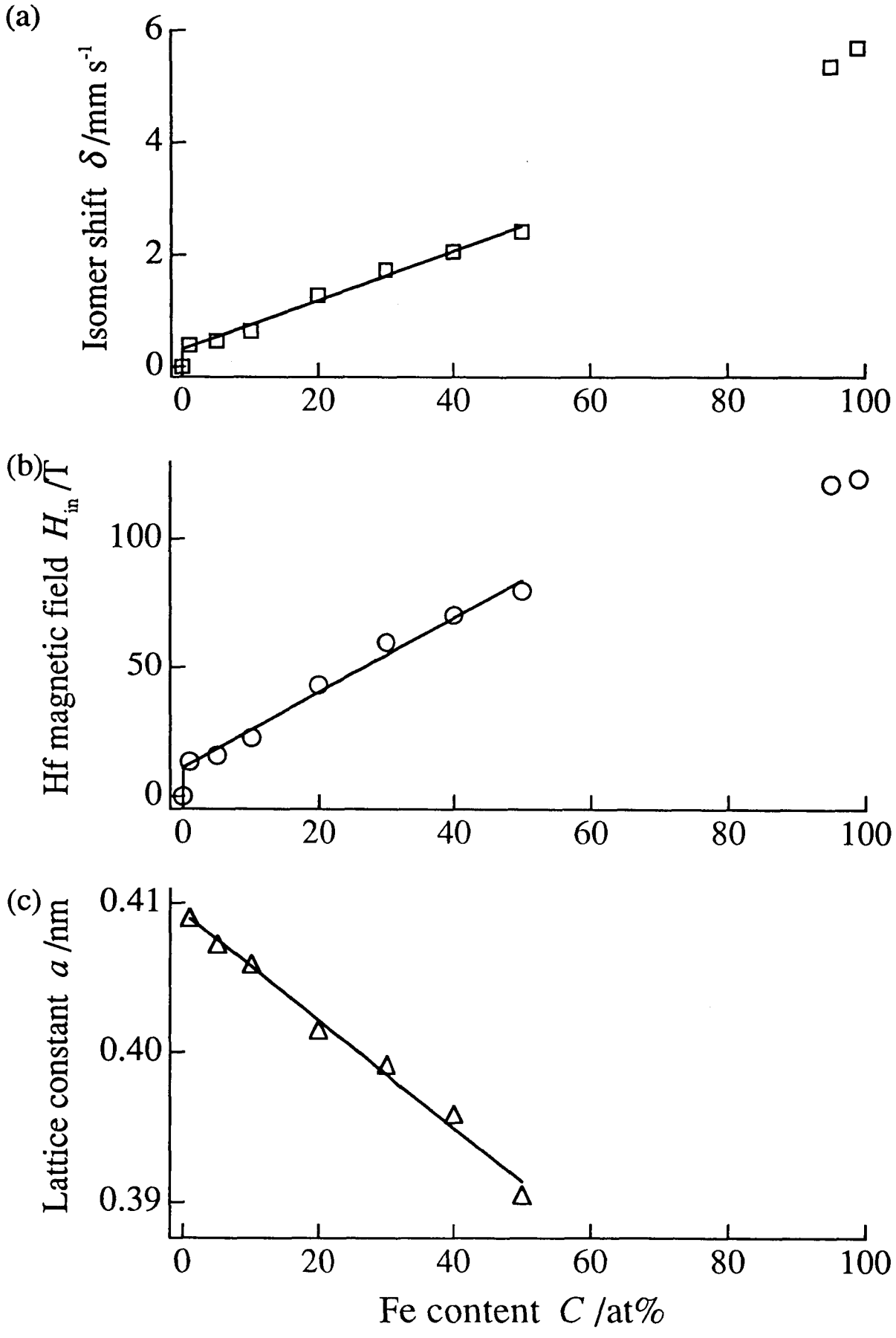

Fig. 3-5 (a) ^{197}Au isomer shifts, (b) hyperfine magnetic field at ^{197}Au nucleus and (c) lattice constants as a function of Fe concentration of Au-Fe alloys.

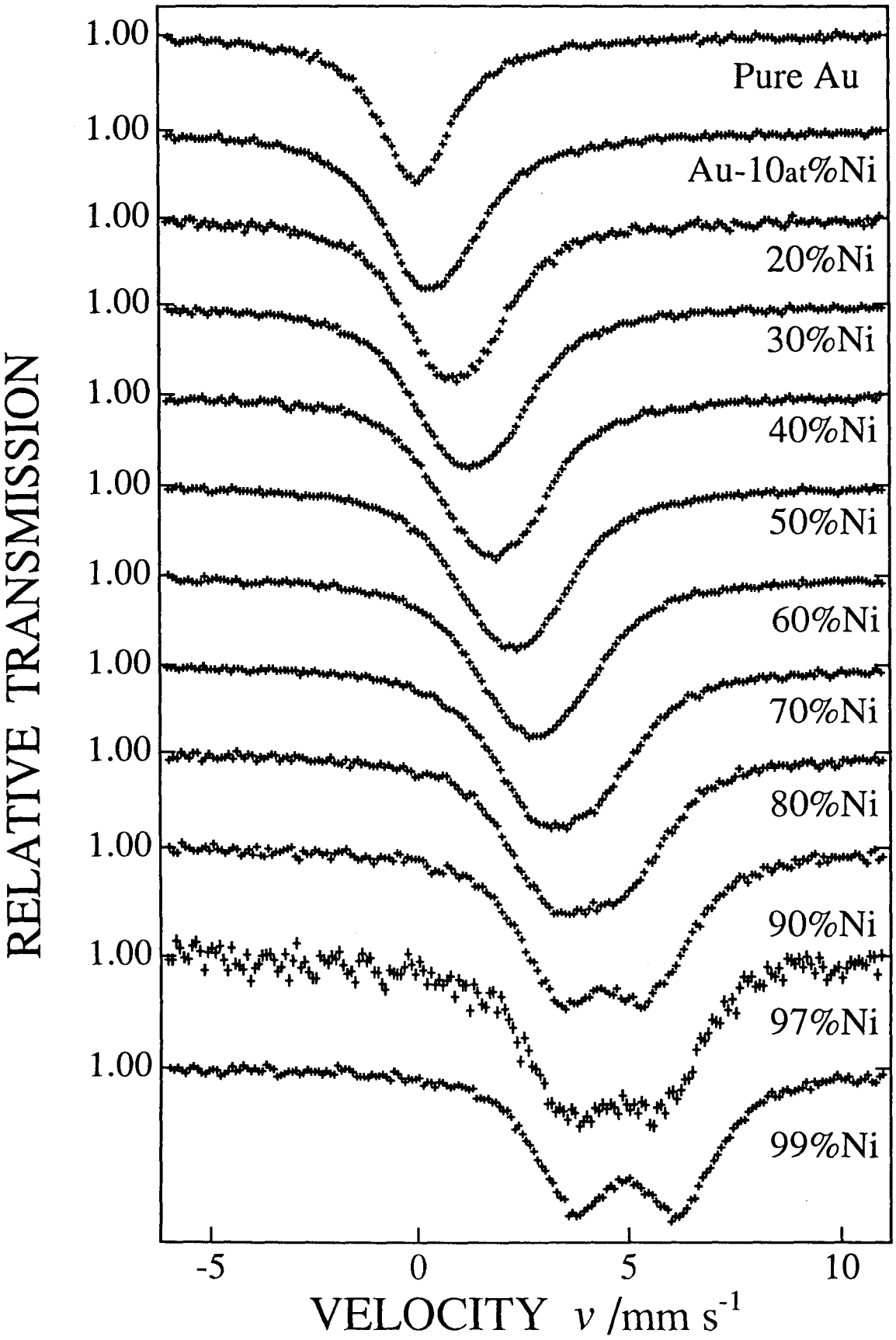

Fig. 3-6 ^{197}Au Mössbauer spectra of AuNi alloys.

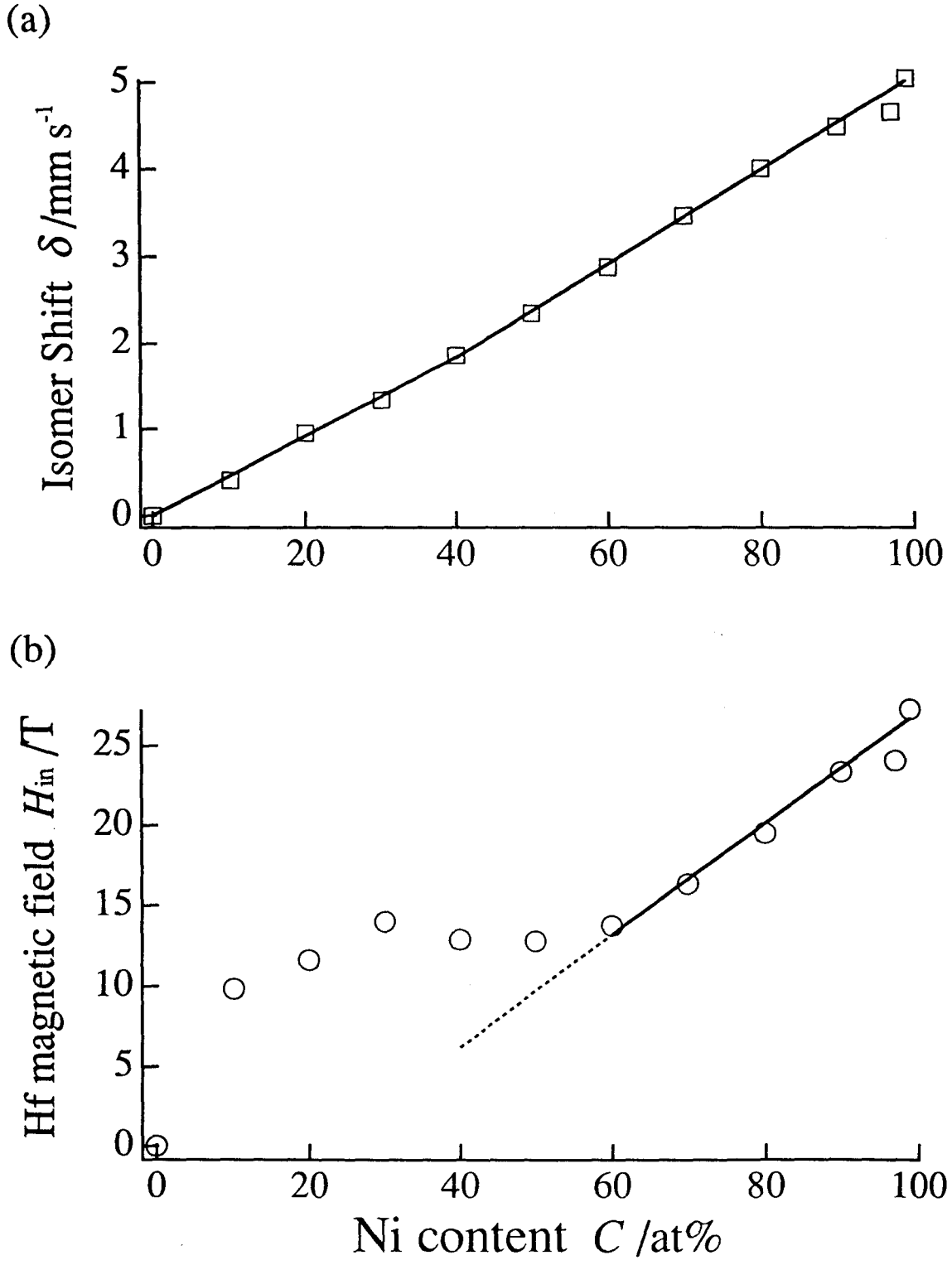

Fig. 3-7 Ni content dependence of (a) isomer shift and (b) hyperfine magnetic field.

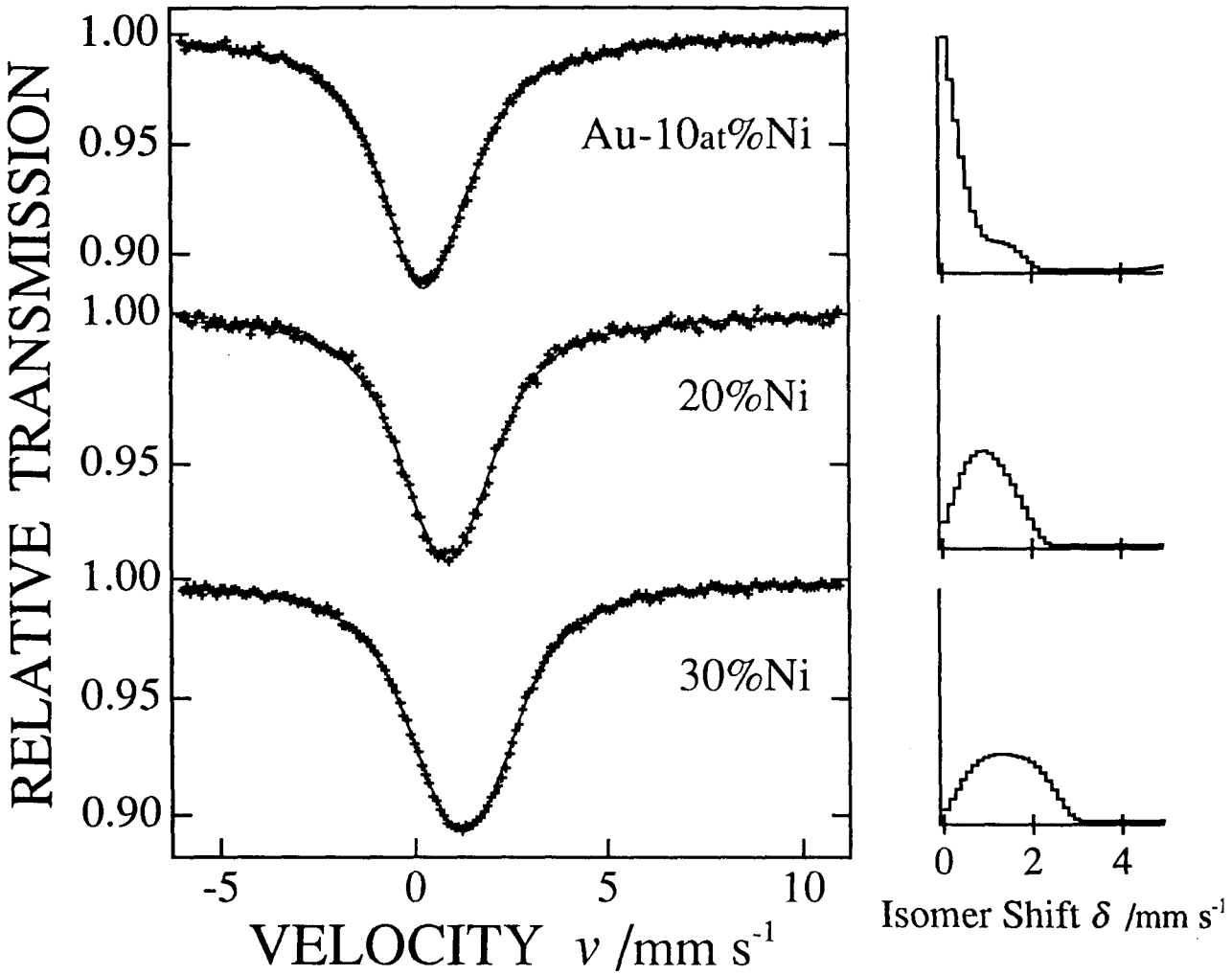

Fig. 3-8 ^{197}Au Mössbauer spectra of AuNi alloy fitted by isomer shift distribution model.

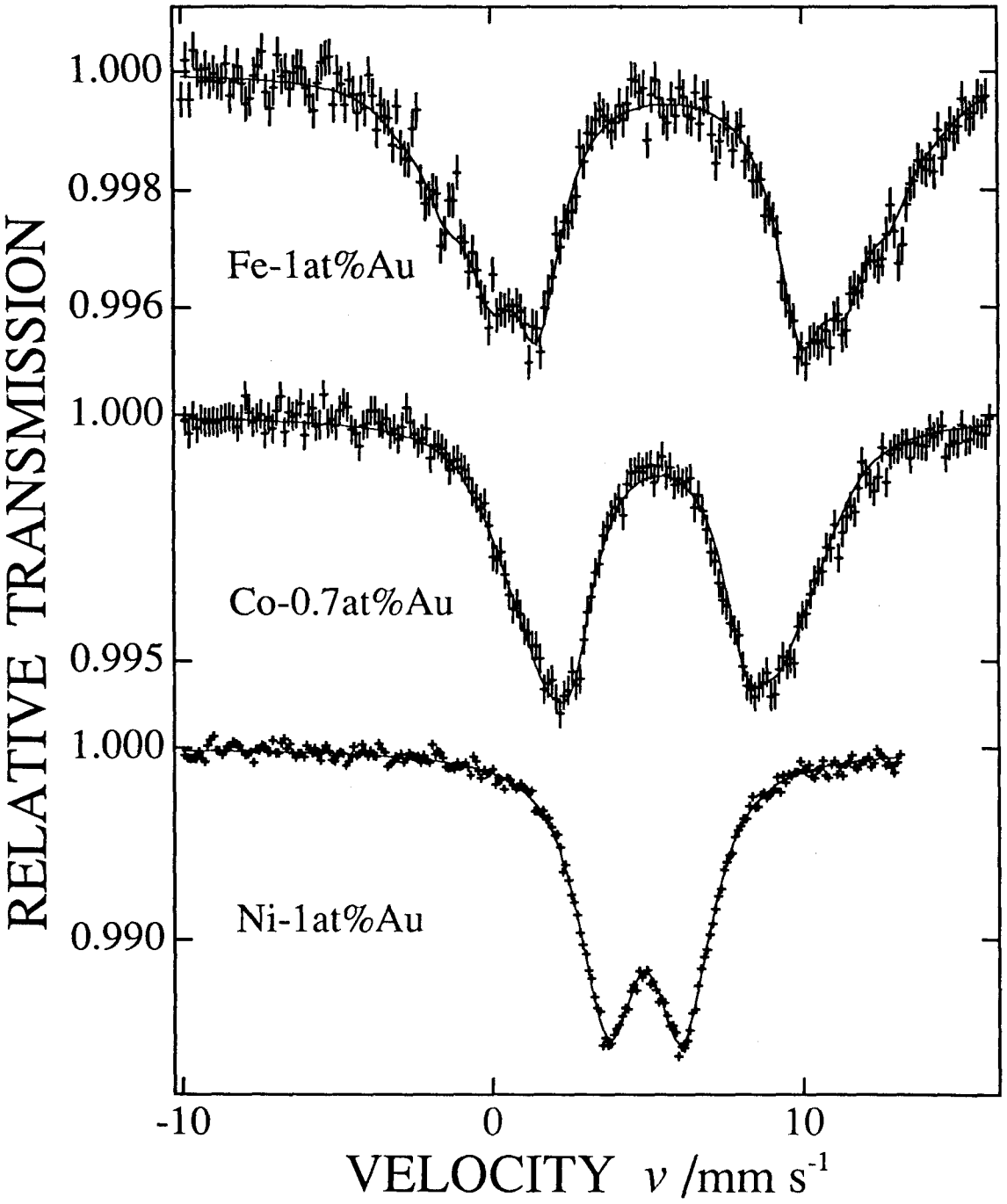

Fig. 3-9 ^{197}Au Mössbauer spectra of Au diluted alloys.

3.2 Magnetic Properties

We performed ^{197}Au Mössbauer measurements to elucidate the magnetic properties of the multilayers consisted of Au and magnetic metals [8, 9]. The construction of the samples are shown in Table 2-1 as the samples for measurement "M". The thickness of the magnetic layers was fixed and the thickness of Au layers was changed.

Figure 3-10 shows ^{197}Au Mössbauer spectra of Au/Fe multilayers obtained at 11 K. These spectra show asymmetrical line-shapes, which suggest the existence of the components having positive isomer shift values. The components having positive isomer shifts show a very small contribution in the spectrum obtained from Au(3.0 nm)/Fe multilayer, and the spectrum from Au(0.5 nm)/Fe multilayer includes huge components which have isomer shifts and also large hyperfine magnetic fields. To analyze these spectra, we assumed as follows. In the first, these spectra are decomposed several components which have having same isomer shifts and same hyperfine magnetic fields. These components come from Au atoms in the multilayers whose Au layers have different thickness. The behavior of an influence from the Fe layers might be assumed not to depend on the Au thickness. In the second, the fitting model include pure Au component, which has zero isomer shift and zero hyperfine magnetic field. Obviously, the spectra of Au(3.0 nm)/Fe and Au(2.0 nm)/Fe multilayers include large zero isomer shift component. In the third, a quadrupole splitting is fixed to be zero. It is common to assume the zero quadrupole splitting for these broad spectra obtained from metallic system. We used the four-partial-component model to fit the spectra of the Au/Fe multilayers. It is the simplest model to satisfy these assumptions.

Figure 3-11 shows results from spectral analyses by four-partial-components model. The solid lines show the fitted lines and the dashed lines show partial components. The four-partial-components model consists of one nonmagnetic component having zero isomer shift and three magnetic components having positive isomer shifts. The nonmagnetic component is due to the unperturbed Au atoms that are isolated from Fe layers. The magnetic components are due to the Au atoms that are strongly perturbed by the ferromagnetic Fe layers. The value of the isomer shifts and the hyperfine magnetic fields are shown in Table 3-1. The spectrum of Au(0.5 nm)/Fe multilayer is completely entirely split by magnetic interaction and the largest hyperfine magnetic field was determined to be 115 T. The magnitude of this value is similar to the value at the ^{197}Au nuclei dissolved into the bulk Fe metals. Figure 3-12 shows ^{57}Fe Mössbauer spectra at 298 K. All spectra show magnetically split sextets even at 298 K and the spectral widths are rather sharp, so that the serious mixing of Fe and Au atoms at the interface does not occur. Thus the hyperfine magnetic field at the ^{197}Au nucleus is due to the interaction between Au atoms and Fe atoms at the interface and is not due to mutual alloying. The detail of the ^{57}Fe Mössbauer spectra of Au/Fe multilayers is discussed later.

The area of the magnetic components decreases with an increase of Au thickness; and are 92% in Au(0.5 nm)/Fe, 74% in Au(1.0 nm)/Fe, 40% in Au(2.0 nm)/Fe, and 28% in Au(3.0 nm)/Fe multilayers, respectively. The spectrum of Au(3.0 nm)/Fe(0.8 nm) multilayer contains 72% nonmagnetic component. We assume that the nonmagnetic component corresponds to the unperturbed Au atoms in the middle of the Au layer and the magnetic components correspond to the perturbed Au atoms existing by the interface between Au and Fe layers. Figure 3-13 shows

schematic drawing of affected Au layers by Fe layers according to above assumption. Expecting the Au(0.5 nm)/Fe multilayer, Au atoms within the 0.4 nm layer from the interface are perturbed magnetically in Au/Fe multilayers. The oscillatory polarization of secondary electrons emitted from Au/Fe bilayers are reported for 1.0 ~ 4.0 nm Au layers [34]. This result shows the oscillatory polarization of conduction electrons in the Au layers. However, results from the present investigation show that the strong magnetic Au atoms exist in the region of only 0.4 nm from the interface between Au and Fe layers. This shows that the conduction electron polarization does not create the large hyperfine magnetic field at ^{197}Au nucleus, but that the perturbation, which is shown in ^{197}Au Mössbauer spectra, is mainly due to hybridization of the electrons of Au and Fe atoms at the interface.

Guo *et al.* reported calculated hyperfine magnetic field of Au atoms in Au/Fe multilayers [35]. The magnitude of the hyperfine magnetic fields are reported to be -81 T for first Au mono-layer from the interface, and 20 T for the second Au mono-layer from the interface in Au(5 ML)/Fe(3 ML) multilayer. The "ML" means "mono-layer". In our experimental results, Fig 3-13, the first Au layer from interface contains the two components that have the largest and the second largest hyperfine magnetic field. The components from first layer are separated into two components. The experimental values of hyperfine magnetic field of these components are 115 T and 70 T. The sign of the hyperfine magnetic field is determined by Mössbauer spectra only under external high magnetic field. Present results show the spectra without external magnetic field and did not determine the sign of the hyperfine magnetic field. The calculated value is between these values. This separation is perhaps caused by the roughness at interface. The second layer

corresponds to the third-largest-hyperfine-field component and the experimental magnitude of the hyperfine magnetic field is 25 T. This value shows good agreement to the calculation.

In the ^{57}Fe Mössbauer spectra shown in Fig. 3-12, the intensities of the second and fifth peaks become larger with an increase of thickness of the Au layers. This experimental result indicates clearly that magnetic anisotropy of the Fe layers changes from parallel in plane to perpendicular with a decrease of Au thickness. This result agrees with the that of the magnetization measurements, which have been discussed in Chapter 2 (Fig. 2-3). Figure 3-14 shows the values of isomer shifts, hyperfine magnetic fields, and quadrupole splitting of ^{57}Fe Mössbauer spectra as a function of thickness of Au layers. The isomer shift and quadrupole splitting do not change with the thickness. However, when the thickness of Au layers is less than 1.0 nm, the hyperfine magnetic fields increase with a decrease of Au thickness. Figure 3-15 shows the ^{57}Fe Mössbauer spectra of Au(0.5 nm)/Fe and Au(2.0 nm)/Fe multilayers at 298 K, 77 K and 11 K. The intensities of the second and fifth peaks do not change with temperature, thus the magneto anisotropy of these multilayers does not depend on temperature. Figure 3-16 shows the temperature dependence of the isomer shift, hyperfine magnetic field and quadrupole splitting. The magnitude of the quadrupole splitting does not depend on temperature. The temperature dependence of the isomer shift is caused by the second order Doppler shift. The magnitude of the hyperfine magnetic field of the Au(2.0 nm)/Fe multilayer decreases with an increase of temperature and its rate is steeper than that of the Au(0.5 nm)/Fe multilayer. This result is interpreted as that the Curie temperature of Au(0.5 nm)/Fe multilayer is higher than that of Au(2.0 nm)/Fe multilayer. Figure 3-17

shows the temperature dependence of magnetization of the Au(0.5 nm)/Fe and Au(2.0 nm)/Fe multilayers [36]. The applied field was 5 T and parallel to film plane. The magnetization was normalized by the values at 5 K. The magnetization of the Au(2.0 nm)/Fe multilayer decreases with an increase of temperature and its rate is larger than that of the Au(0.5 nm)/Fe multilayer, whose behavior is same as the temperature dependence of the hyperfine magnetic field.

Figure 3-18 shows ^{197}Au Mössbauer spectra observed from pure Au foil and Au/*M* (*M* = Fe, Co, Ni) multilayers. The spectra were analyzed by four-partial-components model. The value of the isomer shifts and the hyperfine magnetic fields are shown in Table 3-1. The values of the largest magnetic hyperfine magnetic field are 115 T for Au/Fe, 69 T for Au/Co and 23 T for Au/Ni. Magnitudes of these values are similar to the values at the ^{197}Au nuclei dissolved into bulk Fe, Co (fcc) and Ni metals. Figure 3-18 (a) shows the ^{197}Au Mössbauer spectra observed from Au(2.0 nm)/*M* (*M* = Fe, Co, Ni) multilayer. These spectra include nonmagnetic components 60% for Au/Fe, 63% for Au/Co and 61% for Au/Ni multilayers, respectively. In Fig. 3-18 (b), spectra of Au(1.0 nm)/*M* multilayers, the areas of nonmagnetic components are 29% in Au/Fe and 26% in Au/Ni multilayers, but only 43% in Au/Co multilayers. Figure 3-18 (c) shows ^{197}Au Mössbauer spectra of Au(0.5 nm)/*M* (*M* = Fe, Co, Ni) multilayers. The areas of nonmagnetic components are 7 and 1% in Au/Fe and Au/Ni multilayers, and almost all the Au atoms in the multilayers are strongly perturbed by magnetic layers. On the contrary Au/Co multilayers contain 22% nonmagnetic component. These results suggest that influences of Co layers are weaker than those of Fe and Ni layers. Using same assumption as Au/Fe multilayers, the schematic

drawing of affected Au layers are shown in Fig. 3-19. Au atoms within the 0.4 nm layer from interface are perturbed in Au/Fe and Au/Ni multilayers. In the Au/Co multilayers ferromagnetic Co layers perturb Au atoms within 0.2 ~ 0.3 nm layer from interface.

The oscillatory inter-layer coupling in Co/Au/Co trilayers is reported for the 1.0 ~ 4.0 nm Au layers [37]. These result shows the oscillatory polarization of conduction electrons in Au layers in Au/Co multilayer as Au/Fe multilayer. However, from our results, the strongly magnetic Au atoms exist only near the interface as Au/Fe multilayer. The oscillatory inter-layer coupling in Au/Ni multilayer has not been reported.

Emoto *et al.* reported the hyperfine magnetic field of ^{119}Sn atoms that is inserted middle of Au layers in Au/Co and Au/Fe multilayers and some of the ^{119}Sn Mössbauer spectra are shown in Fig. 3-20 [38, 39]. They reported the existence of hyperfine magnetic field at the middle of Au(2.6 nm) layer in Au/Co multilayers and at middle of Au(4.0 nm) layer in Au/Fe multilayers. However from the ^{197}Au Mössbauer spectra of Au/Co and Au/Fe multilayers we determined that ferromagnetic Co and Fe layers perturb Au atoms within 0.2 ~ 0.4 nm layer from interface. Results from ^{119}Sn Mössbauer spectroscopy are differ from the present investigation in which ^{197}Au Mössbauer spectroscopy is employed. The discrepancy may come from two causes. The first is different sensitivity of Au and Sn probes to the magnetic polarization. ^{119}Sn atoms have large nuclear magnetic dipole moment and show large hyperfine splitting comparing with ^{197}Au nuclei. The second is different of the observation part. ^{197}Au Mössbauer spectra were observed about the whole of Au layers and the sensitivity is not high for the estimation of small hyperfine magnetic field fraction.

They also reported that the hyperfine magnetic field of ^{119}Sn atoms in Au/Co multilayer is larger than that in Au/Fe multilayers when Au layers are thin. The magnitude of hyperfine magnetic field of ^{119}Sn is not proportional to the magnetic moments of the ferromagnetic layers [39]. However that of ^{197}Au is nearly proportional. This discrepancy is possibly caused by a difference of electronic state between Au and Sn, but it is not yet clear.

Table 3-1 Mössbauer parameters of four-partial-components model.

		Subspectrum 1	Subspectrum 2	Subspectrum 3	Subspectrum 4
Au/Fe	I.S. (mms^{-1})	0	0.8	2.2	3.5
	H (T)	0	25	70	115
Au/Co	I.S. (mms^{-1})	0	1.7	3.3	5.0
	H (T)	0	25	51	76
Au/Ni	I.S. (mms^{-1})	0	1.1	2.3	3.6
	H (T)	0	0	15	23

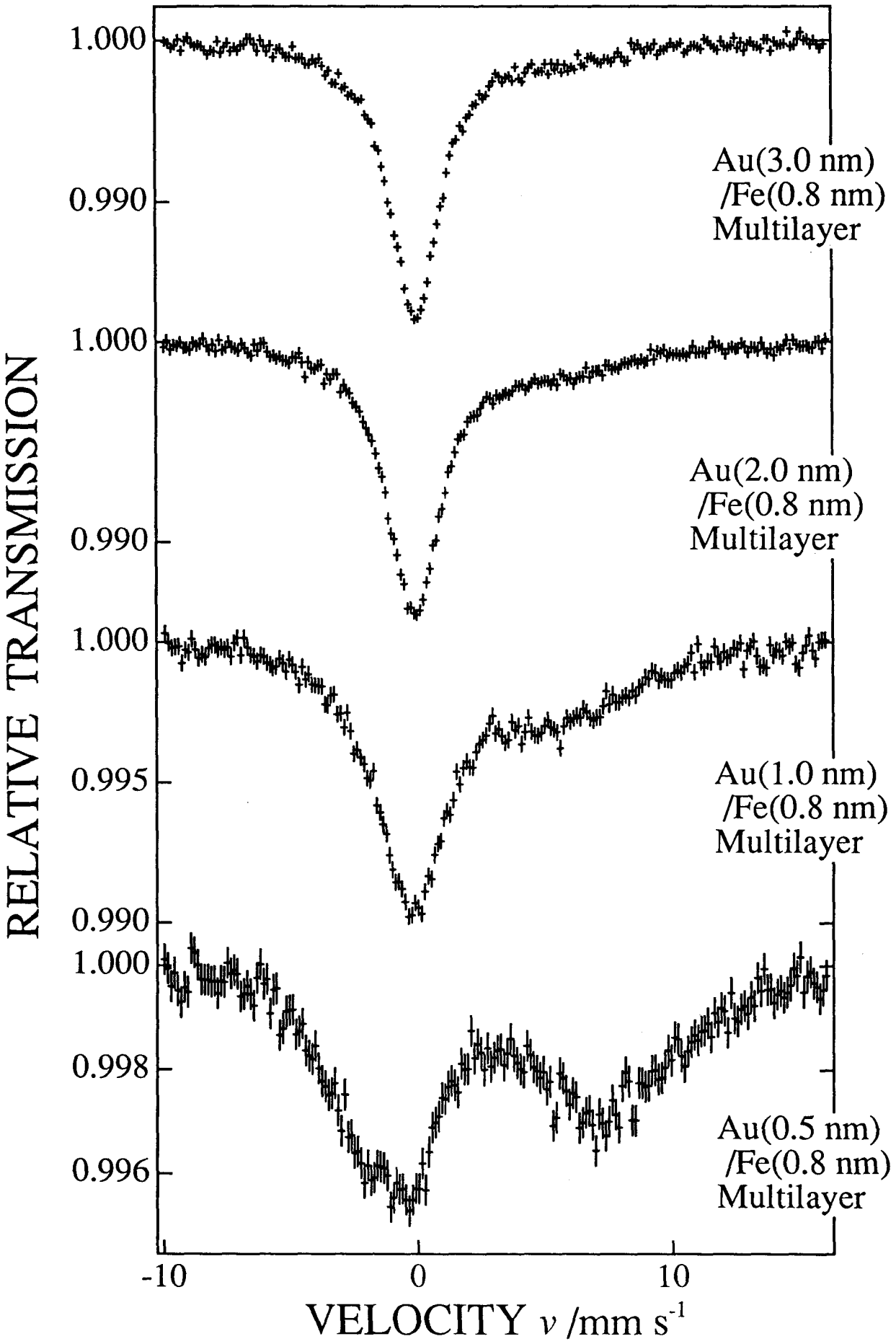

Fig. 3-10 ^{197}Au Mössbauer spectra obtained from Au/Fe multilayers at 11 K.

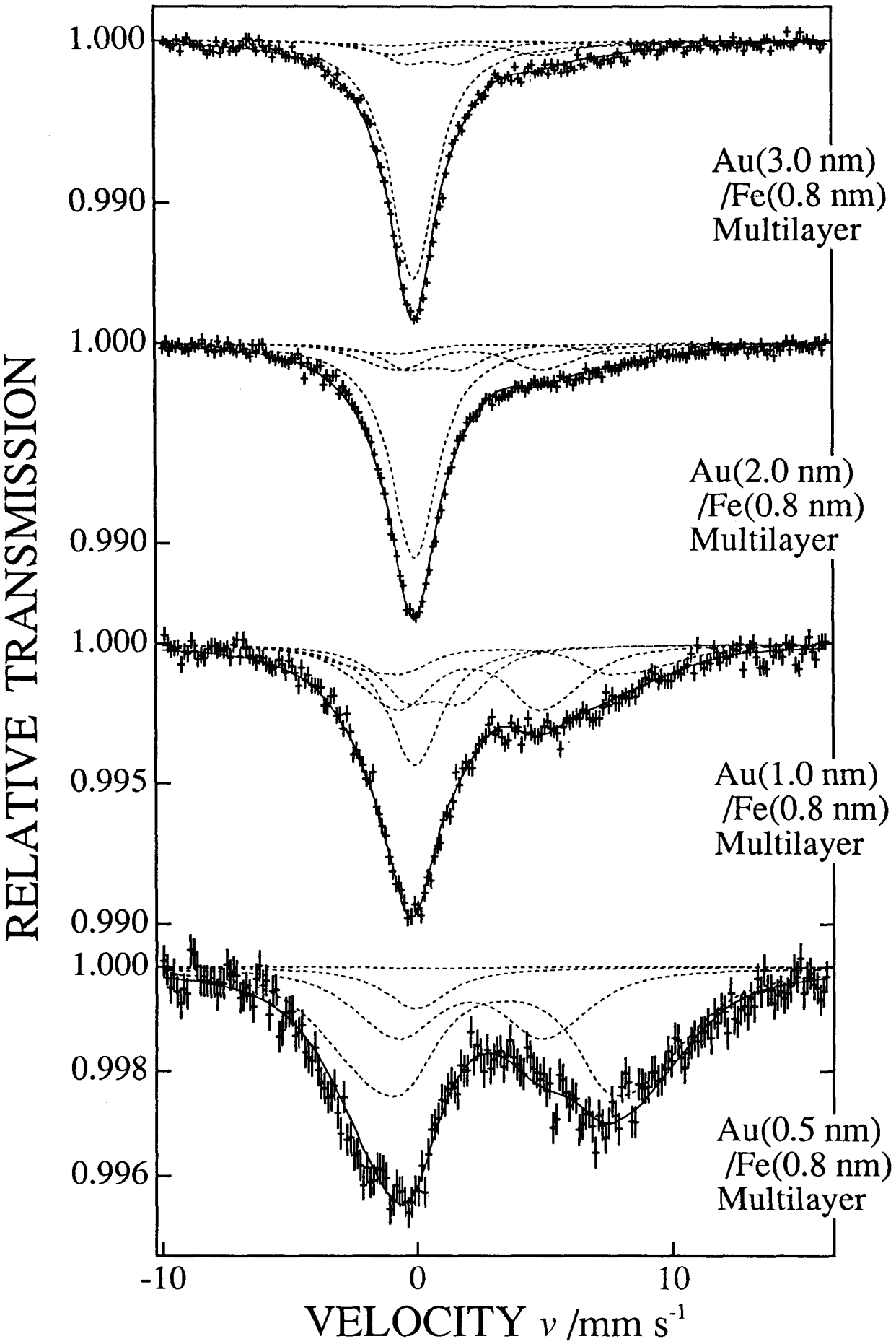

Fig. 3-11 ^{197}Au Mössbauer spectrum obtained from Au/Fe multilayers fitted by the four-partial-components model.

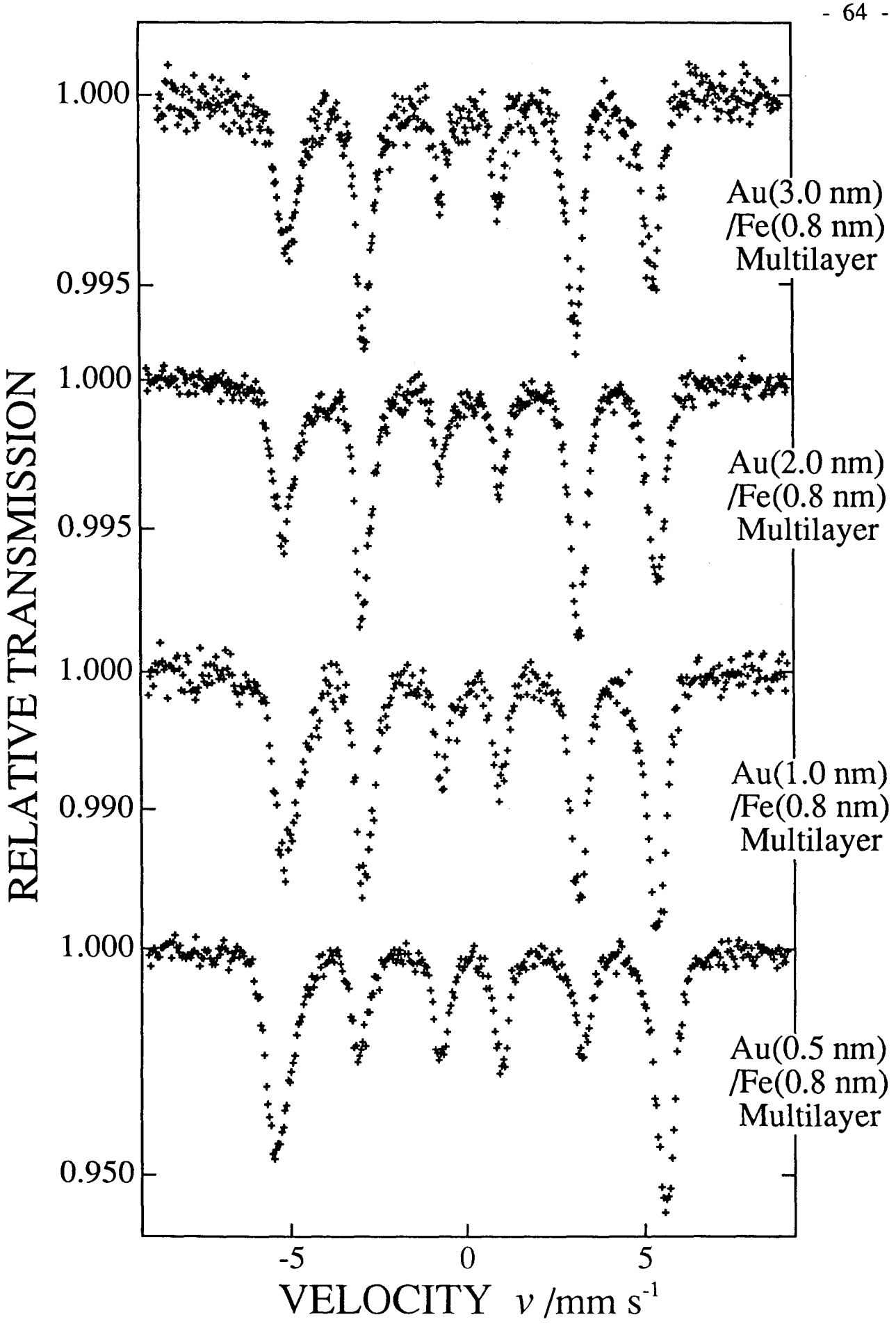

Fig. 3-12 ^{57}Fe Mössbauer spectra of Au/Fe multilayers at 300K.

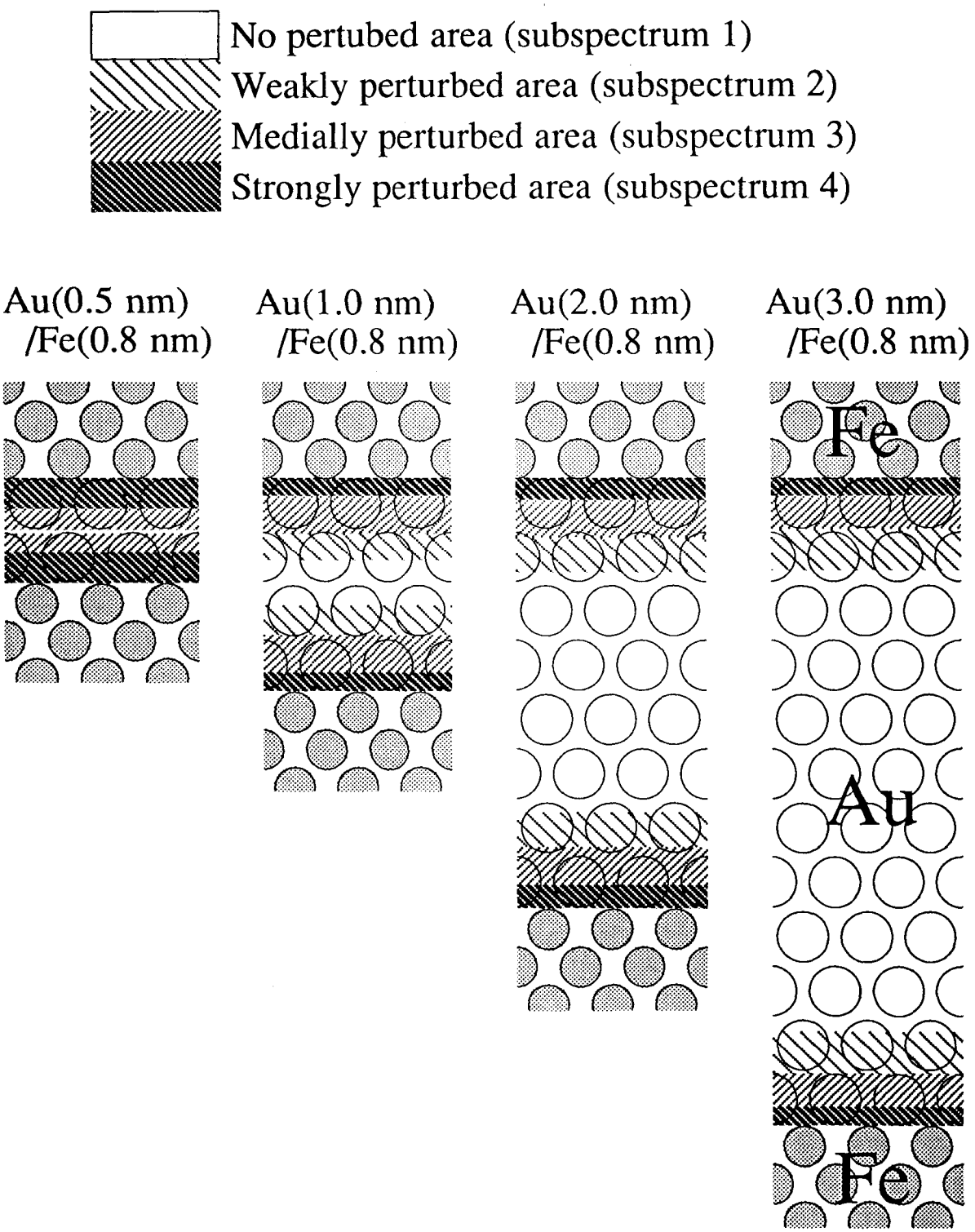

Fig. 3-13 Schematic drawing of the Au layers perturbed by Fe layers.

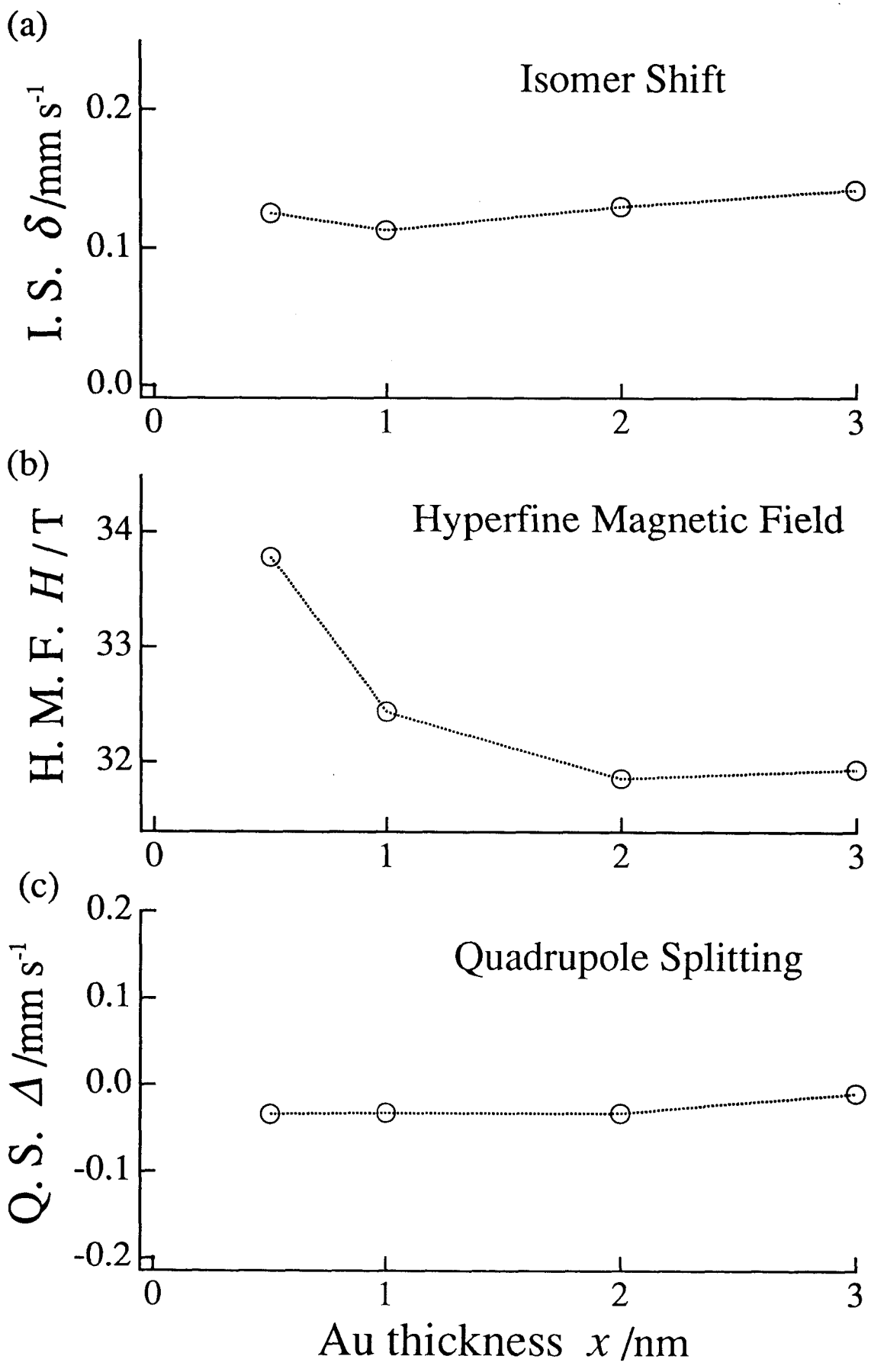

Fig. 3-14 ^{57}Fe (a) isomer shift, (b) hyperfine magnetic field and (c) quadrupole splitting as a function of Au layers thickness of Au(x nm)/Fe(0.8 nm) multilayers at 300K.

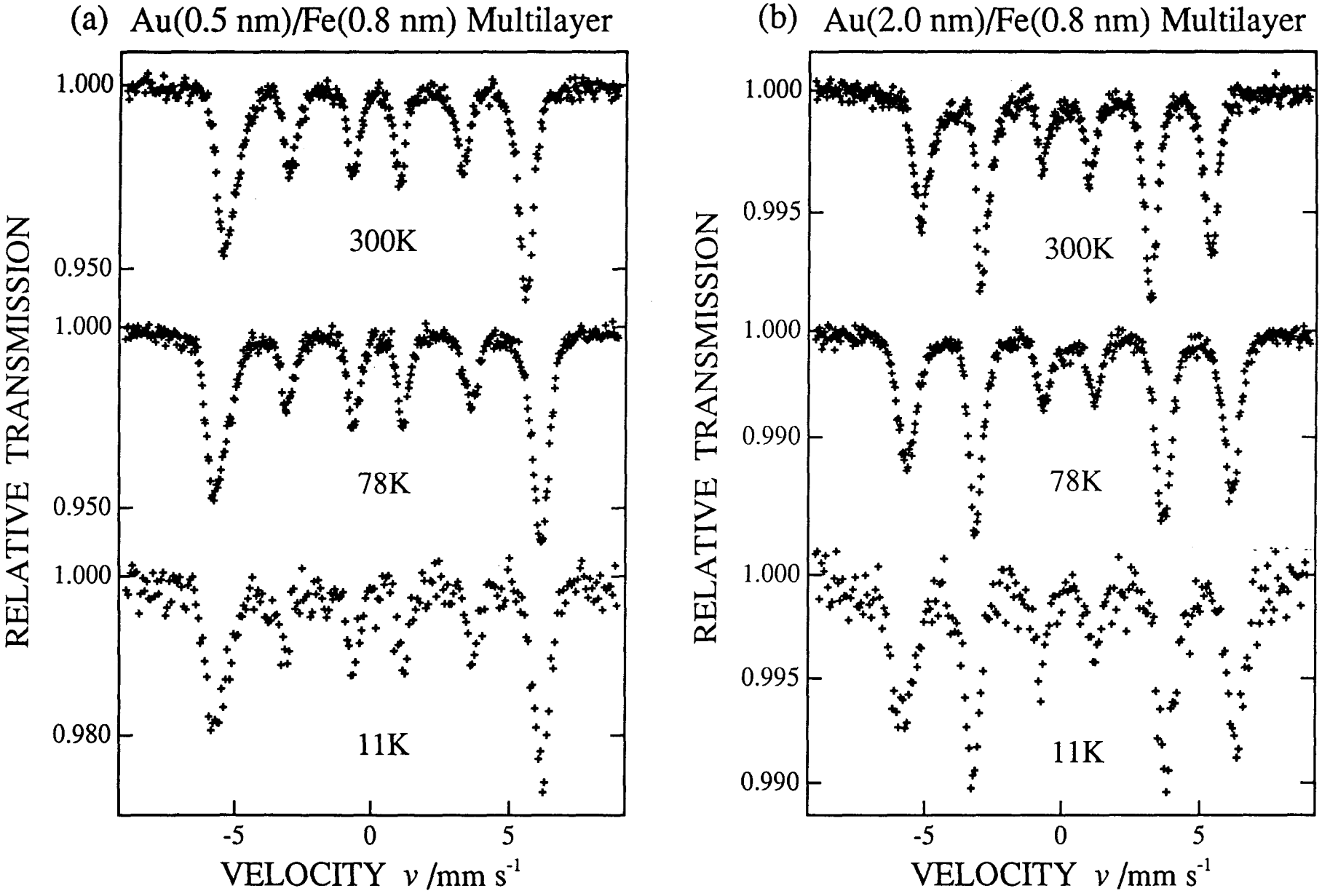

Fig. 3-15 ^{57}Fe Mössbauer spectra of (a) Au(0.5 nm)/Fe(0.8 nm) and (b) Au(2.0 nm)/Fe(0.8 nm) multilayers at 11, 78 and 300K.

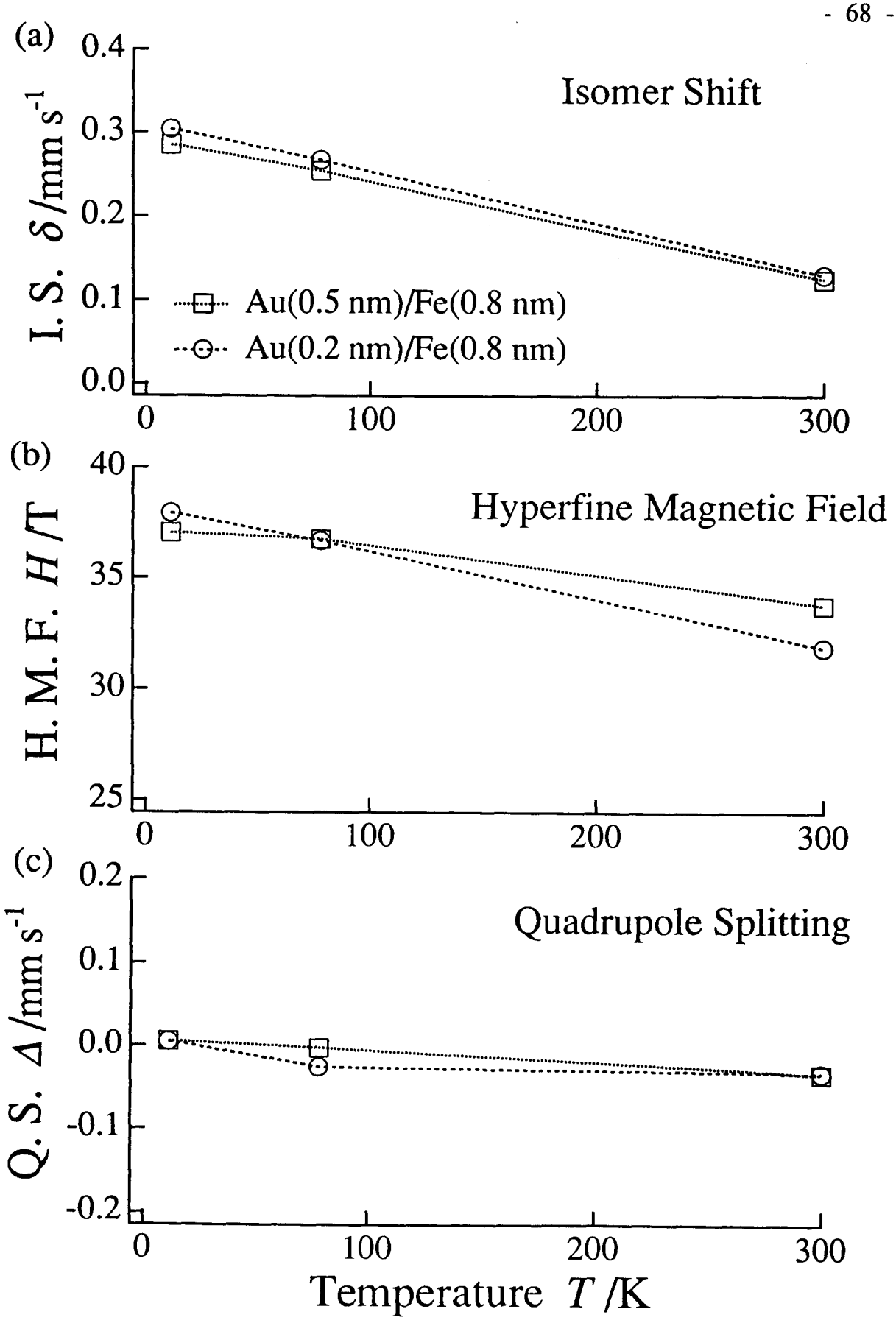

Fig. 3-16 ^{57}Fe (a) isomer shift, (b) hyperfine magnetic field and (c) quadrupole splitting as a function of temperatures of Au(0.5 nm)/Fe(0.8 nm) and Au(2.0 nm)/Fe(0.8 nm) multilayers.

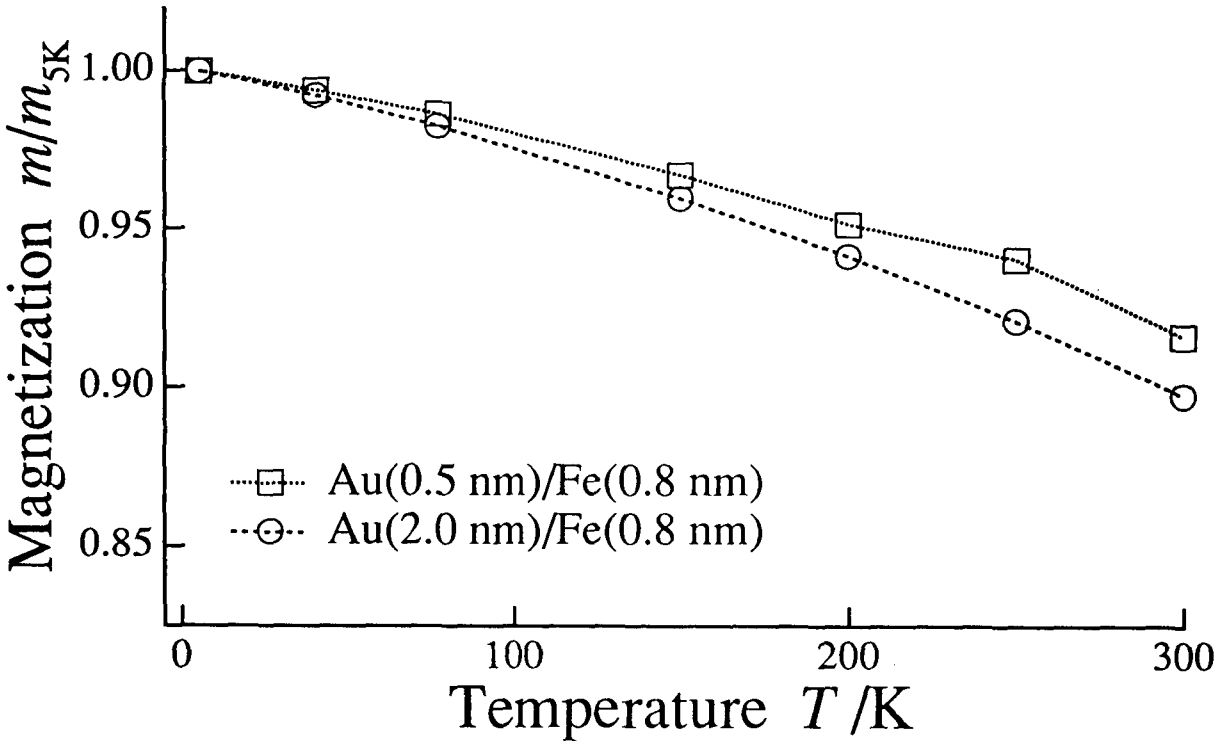

Fig. 3-17 Magnetization as a function of temperatures of Au(0.5 nm)/Fe(0.8 nm) and Au(2.0 nm)/Fe(0.8 nm) multilayers

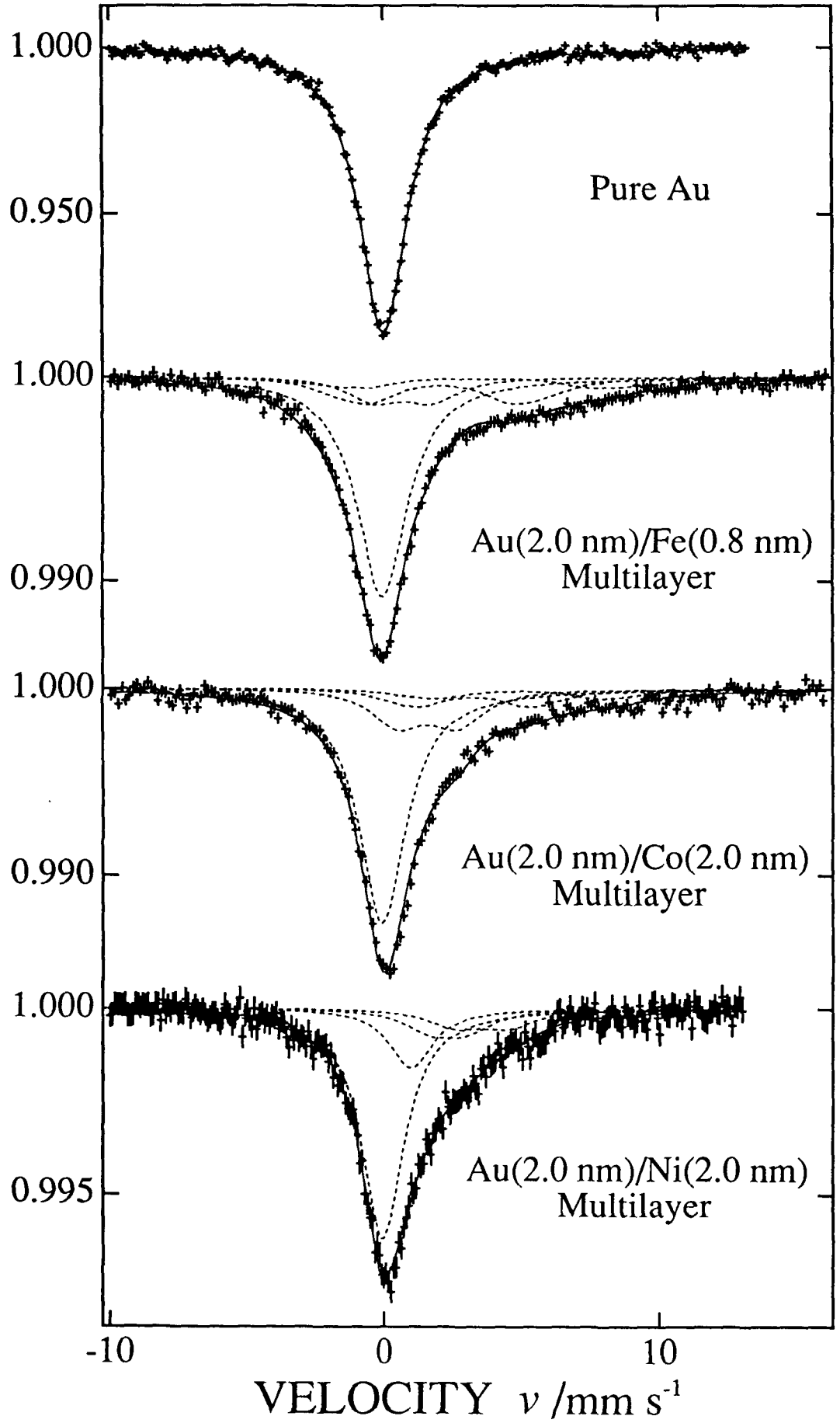

Fig. 3-18 (a) ^{197}Au Mössbauer spectrum oftained from pure Au and Au(2.0 nm)/*M* (*M* = Fe, Co Ni) multilayers.

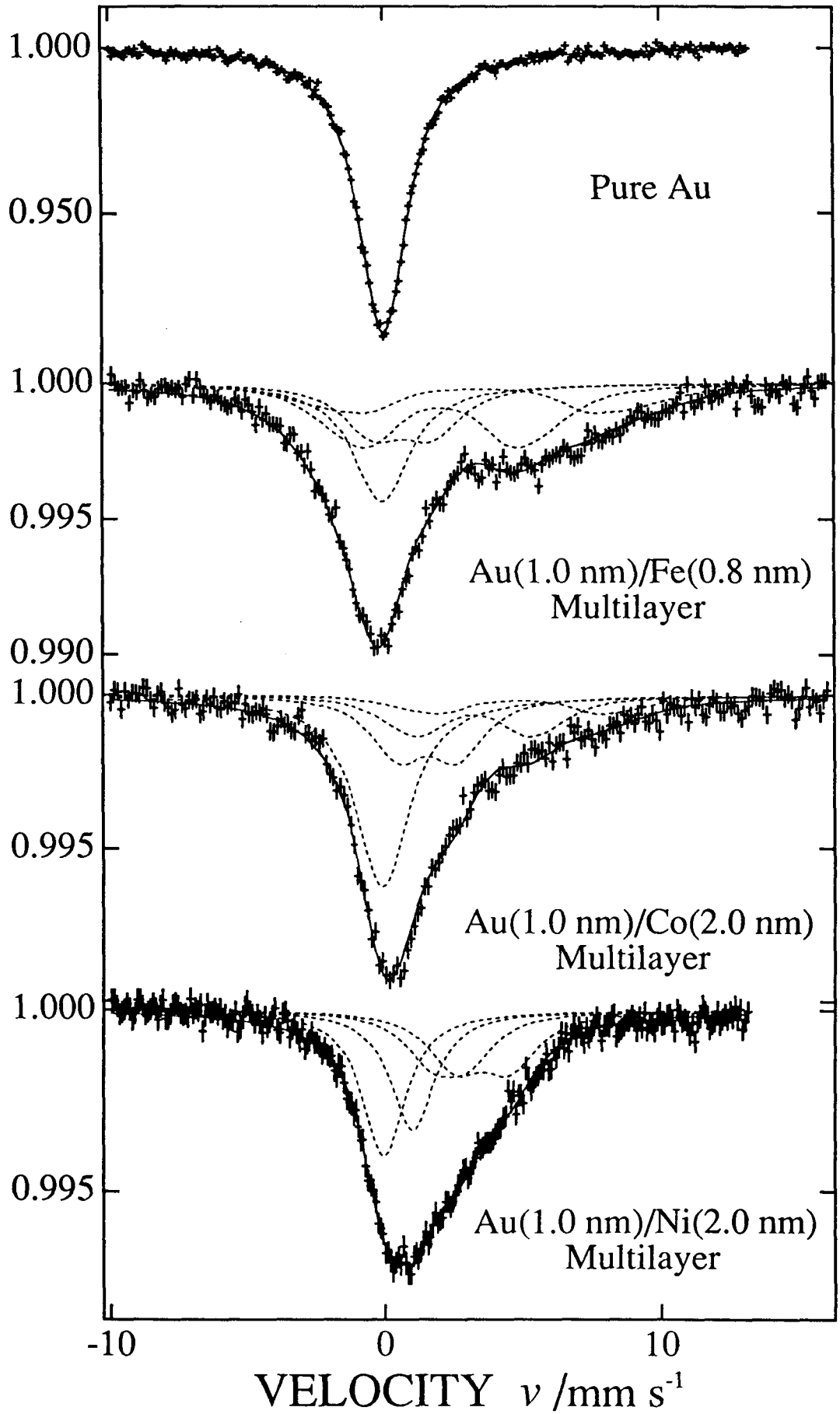

Fig. 3-18 (b) ^{197}Au Mössbauer spectrum oftained from pure Au and Au(1.0 nm)/*M* (*M* = Fe, Co Ni) multilayers.

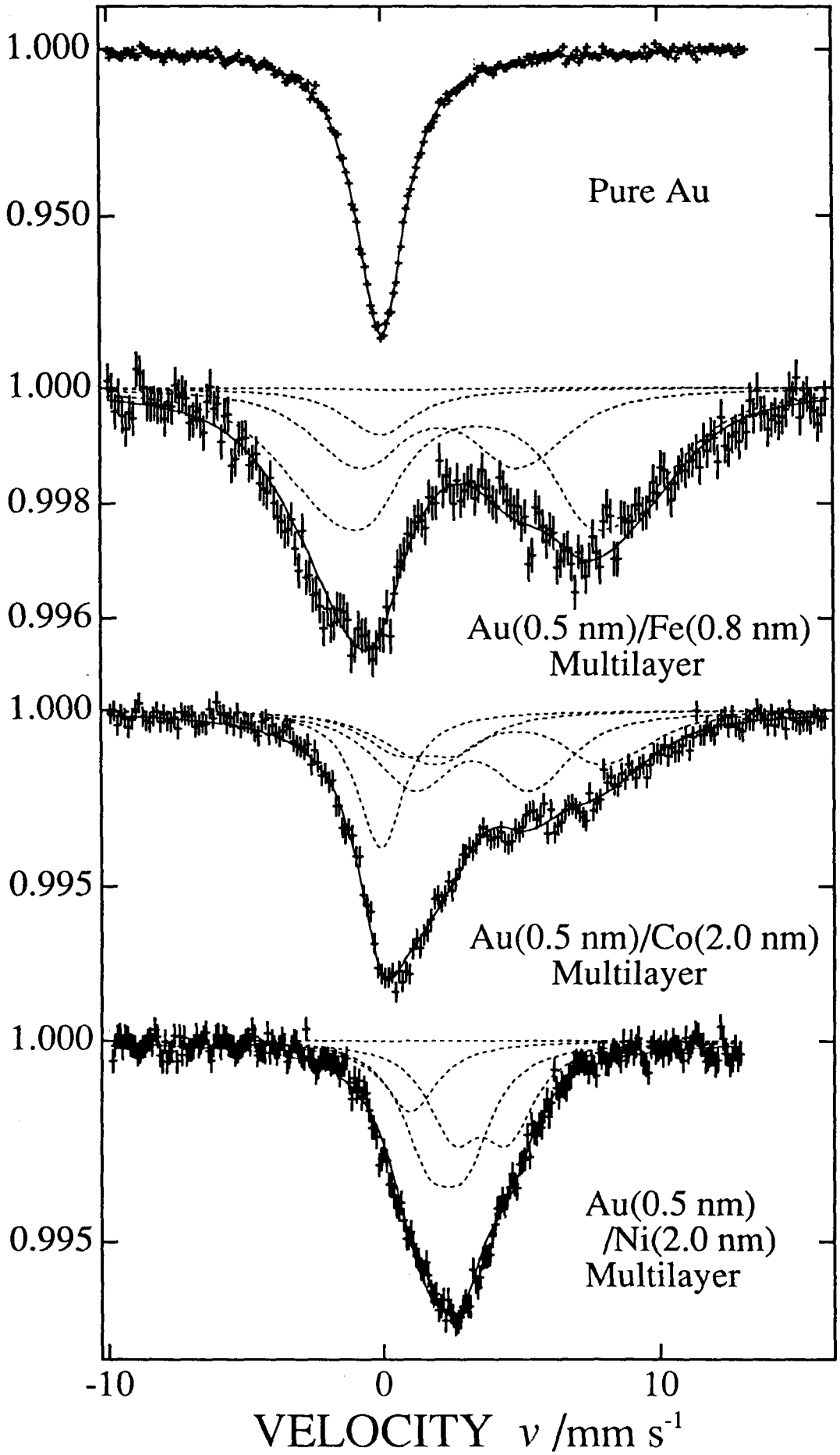

Fig. 3-18 (c) ^{197}Au Mössbauer spectrum oftained from pure Au and Au(0.5 nm)/*M* (*M* = Fe, Co Ni) multilayers.

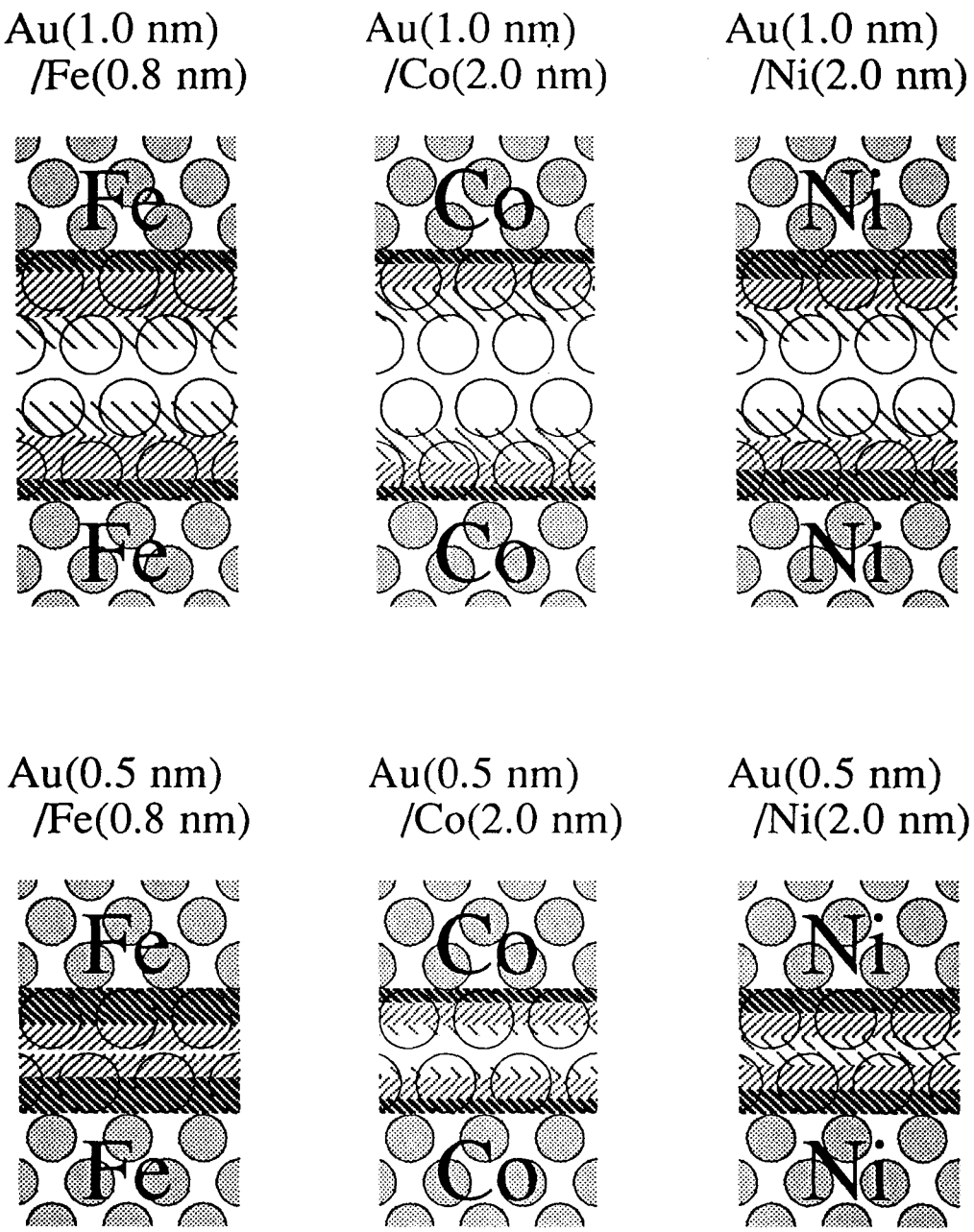

Fig. 3-19 Schematic drawing of the Au layers perturbed by Fe,Co and Ni layers.

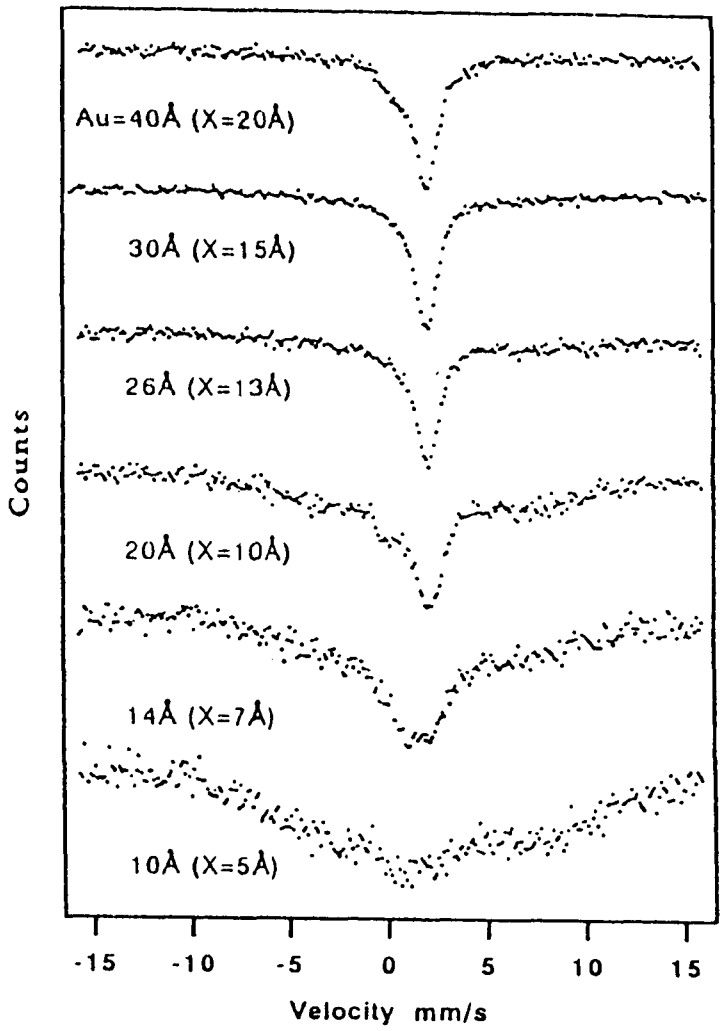

Fig. 3-20 (a) Transmission ^{119}Sn Mössbauer spectra at room temperature. Samples are Co(20 Å)/Au(x Å)/Sn(1.5 Å) /Au(x Å); x = 5, 7, 10, 13, 15, 20 [38].

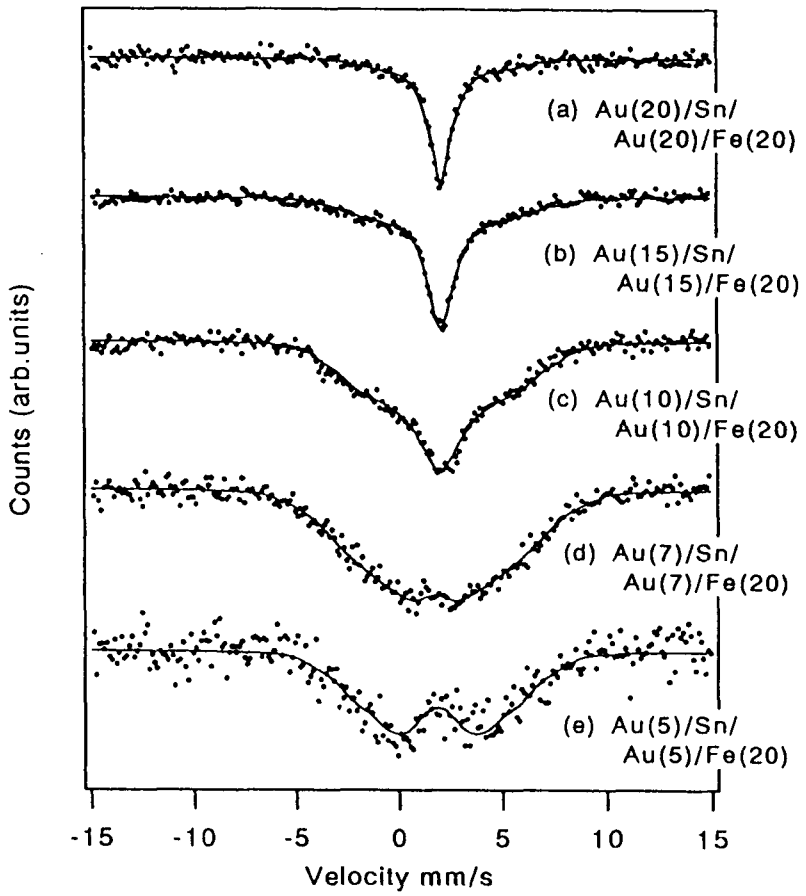

Fig. 3-20 (b) ^{119}Sn Mössbauer spectra at room temperature. Samples are Au(x Å)/Sn(1.5 Å)/Au(x Å)/Fe(20 Å); x = 5, 7, 10, 15, 20 [39].

3.3 Supermodulus Effect

In the present investigation, ^{197}Au Mössbauer measurements have been performed to clarify the vibrational properties of Au layers in Au/Ni, Au/Fe and Au/Co multilayers [10]. Vibrational properties of Au are closely related to its elastic properties. The larger elastic modulus yields the larger second derivative of the two-body atomic potential and might cause the smaller amplitude of the atomic displacement from its equilibrium position at finite temperature. The enhancement of the elastic modulus will cause the smaller magnitude of the mean square displacement of the atom, which can be discussed using the recoil-free fraction of Mössbauer effect.

Usually the recoil-free fraction is measured by the resonant absorption area of the spectrum. The absorption area is proportional to the product of the number of resonant atoms and recoil-free fraction. However the measurement of the absolute quantity of absorption is difficult because the disturbance from non-Mössbauer absorption and emission. Especially in the ^{197}Au Mössbauer measurement, the half-life of the source, ^{197}Pt, is short, so the intensity of γ-ray source decrease in rather short periods. The measurement of the absolute quantity of the absorption is very difficult by the change of background on ^{197}Au Mössbauer measurement. So we measured relative absorption between the multilayer and pure bulk Au whose Debye temperature is known.

The structure of the sample used for this measurement are shown in Table 2-1 as the samples for measurement "E". In all samples, the thickness of Au layers are 1.0 nm. On the Au(1.0 nm)/Ni(1.0 nm) multilayer, we compared the absorption area from multilayer and Au(25 nm) buffer layer. The thickness ratio between Au layers in multilayer

and buffer layer is (1.0 nm × 50) : 25 nm = 2 : 1. Au(1.0 nm)/Ni(2.0 nm) multilayer is a reference sample for a ^{197}Au Mössbauer spectrum of multilayer. Au/Fe and Au/Co multilayers do not have Au buffer layer, so the comparison of the absorption area between multilayer and buffer layer is impossible. We stacked a thin film of pure Au on the multilayer sample. The film is 0.9 μm thickness and prepared by the spattering technique. The seven films were stacked on the multilayer sample, and the multilayer sample stacked about 200 pieces, so Au thickness ratios between the Au layers in the multilayers and the films are (1.0 nm × 70 × 200) : (0.9 μm × 7) = 14.0 μm : 6.3 μm = 69 : 31.

Figure 3-21 shows ^{197}Au Mössbauer spectra obtained from Au(1.0 nm)/Ni(2.0 nm) multilayer without buffer layer at 16 K and Au(1.0 nm)/Ni(1.0 nm) multilayer on 25 nm Au buffer layer at 11, 25, 50 and 75 K. The absorption area decreases with an increase of the temperature. These spectra have been analyzed by following three different least-square-fit models. In the first model the spectrum was assumed to be superposition of four components. This model is the simplest one but gave good results in an analysis of the spectra of multilayers with various layer periods and thickness. This model is used for analysis of magnetic properties as described in previous Section 3.2. The second model assumed the superposition of 8 components and third fit model assumes the continuous distribution of the isomer shift values.

Figure 3-21 shows the result of fitting by the four-partial-components model, the solid lines are results of least square fit and the dotted lines show the partial components. One single line component has a zero isomer shift value to pure Au metal, and the other three components have positive isomer shift. The former component is a contribution

from the Au atoms having identical electronic and magnetic properties to the pure Au bulk metal. The uppermost spectrum in Fig. 3-21 is obtained from Au/Ni multilayer without buffer layer. In this spectrum, the relative intensity of the component having zero isomer shift value is smaller than that of same component observed in the second spectrum from the top in Fig. 3-21 (multilayer with 25 nm Au buffer layer). This result indicates clearly that the pure Au buffer layers contribute to the component having zero isomer shift value.

To a fair degree of accuracy as described in one of previous studies [40], the Mössbauer parameters allow determination of the ratio in recoil-free fraction of two or more components. The area A_i of the absorption lines corresponding to the ith component is proportional to the product of its recoil-free fraction f_i and relative abundance a_i,

$$A_i = k f_i a_i \sum_j L_{ij} \qquad (3.5)$$

where k is a constant determined by geometry, absorber thickness etc., and the sum is over the areas under the Lorenzian absorption lines of the ith component derived from the least-squares-fit to the experimental data. Since atomic ratio of Au in multilayer and buffer layer was always maintained as 2 to 1 by the preparation condition, relative abundance a_{ML}(multilayer) / a_{Au}(Au buffer layer) is nearly equal to 2. Using the relative abundance and the area A_i obtained from least squares fit to the experimental data, we can determine the relative recoil-free fraction f_{ML}(multilayer) / f_{Au}(Au buffer layer) in thin foil approximation.

By the four-component model, area A_i of the component having zero isomer shift was determined to be 29% and 46% for the multilayer samples without and with buffer layer, respectively. Assuming that the

ratio of area A_i of zero-isomer-shift component to the total area in the same for both Au(1.0 nm)/Ni(1.0 nm) and Au(1.0 nm)/Ni(2.0 nm) multilayers, the area A_{Au} from the pure Au buffer layer was determined to be 24% and the contribution from the multilayer A_{ML} was 76%. Since the area A_i depends on the product of number of resonant ^{197}Au nuclei for each component a_i and recoil-free fraction f_i as described by the Eq. (1.30), the ratio between recoil-free fraction of the multilayer, f_{ML}, and of the buffer layer, f_{Au}, should be given by $2 f_{ML} : f_{Au} = 76:24$, assuming equal values of f_i for multilayer components at each temperature.

From this relation the determination of f_{ML} / f_{Au} is straightforward, giving 1.6. This value deviates considerably from unity and indicates a larger recoil-free fraction for multilayers than for bulk Au metal, which means that the mean square displacement of resonant Au atoms in multilayers is quite small compared with that in bulk Au metal. To clarify the above fitting, the temperature dependence of the area ratio of the multilayer to the buffer layer component was measured. The lower four spectra in Fig. 3-21 are obtained from Au(1.0 nm)/Ni(1.0 nm) multilayer stacked on the Au buffer layer (25 nm in thickness) at 11, 25, 50 and 75 K. With temperature increase, the total absorption area decreases rapidly.

Using method mentioned above, the area A_i from the Au buffer layer was determined to be 17, 16 and 9% at 25, 50 and 75 K. Since the second-order Doppler shift is 2×10^{-5} mm/s from 11 K to 75 K and negligibly small, we performed the least squares fit to the data under the constraint of having the same isomer shift values as at 11 K for each component at each temperature. If the multilayer and buffer layer have the same temperature dependence of recoil-free fraction, the area contribution from the multilayer should not depend on temperature.

The decrease in area contribution from the Au buffer layer suggests that the recoil-free fraction of the multilayer is higher than that of bulk Au, which is Au in the buffer layer.

Since the experimental data at each temperature show broad spectra as shown in Fig. 3-21, the determination of A_i contains larger errors and might depend on the fit model. We fitted the experimental data using three different fit models as mentioned above and compared the results obtained. The first model is the four-partial-component model of which results are shown in Fig. 3-22. The second model is the eight-partial-component model that is an improvement of the first model, and results are shown in Fig. 3-23. One component in these two models has zero isomer shift and no hyperfine magnetic field. This component includes absorption of buffer layer, and the area ratio of this component is compared with hat of multilayer without buffer layer, as for the four-component model. The third model is one that takes a distribution of isomer shift [33] into account and results are shown in Fig. 3-24. This model is a histogram method with contains one zero-isomer-shift component and nineteen components that have continuous change in isomer shift values.

Resultant area contributions are shown in Fig. 3-25 as a function of temperature. Area contributions of the multilayer component do not show appreciable dependence on the fit model. In Fig. 3-25 the dotted lines show the temperature dependence of area contribution of multilayer calculated by the Debye model at various Debye temperatures. As shown in Fig. 3-25 the area contribution of multilayer increase with an increase of temperature and does not depend on the fit model. From these experimental results, it is clearly shown that the Debye temperature of multilayers is higher than that of pure Au buffer

layer. Comparing the data and the calculated values, the Debye temperature of this multilayer was found to be 235 ± 20 K that is much higher than that of bulk Au metal (164 K). Present experimental find of larger recoil-free fraction and higher Debye temperature of Au in Au(1.0 nm)/Ni(1.0 nm) multilayer than those of bulk Au metal might originate from the increase of the elastic modulus of Au in this multilayer. This result supportes the existence of the supermodulus effect in the Au(1.0 nm)/Ni(1.0 nm) multilayer.

To compare to this result, we measured the recoil-free fraction of Au/Fe and Au/Co multilayers. On Au/Fe multilayers, supermodulus effect have not been reported, and on Au/Co multilayers, the decrease of Rayleigh sound velocity is reported [41, 42]. All the Au/Fe and Au/Co multilayers that we used for the experiment were deposited on Ag buffer layer, so the comparison of the absorption between multilayer and buffer layer is impossible. We stacked thin pure Au films on the multilayer sample. The Au thickness ratio between the multilayer and the film is 14.0 μm : 6.3 μm = 69 : 31. Figure 3-26 shows the ^{197}Au Mössbauer spectra of Au(1.0 nm)/Fe(0.8 nm) multilayers at 11 K without Au foil and 16, 30 and 60 K with Au foil. These spectra were fitted by four-partial-component model as the Au/Ni multilayer. The shape of the spectra does not change with temperature. The area A_{Au} from Au foil was determined to be 28%, 29% and 25% at 16 K, 30 K and 60 K, previously. These values are not so different from 31% that is the thickness ratio of the Au foil, and the temperature dependence is not so large. These results deny the high Debye temperature of Au layers in the Au/Fe multilayers. Figure 3-27 shows the Au(1.0 nm)/Co(2.0 nm) without Au foil at 11 K and with Au foil at 15 K and 60 K. The shape of the spectra looks changed between 15 K and 60 K, but this is change on

peak width owing to vibration from the refrigerator. In spectrum at 60 K, all peak widths become wider than those of 15 K. However the area ratios of the each component are not so change. The area ratio of pure Au components are 26% and 20% at 15 K and 60K, respectively. This result shows that the Debye temperature of Au layers in the Au/Co multilayer is not so larger than that of pure Au metal, as Au/Fe multilayers.

Figure 3-28 shows the temperature dependence of relative recoil-free fraction, f_{ML}/f_{Au}, of Au/Ni, Au/Fe and Au/Co multilayers from four-partial-components model. The relative recoil-free fraction increases with an increase of the temperature only for Au/Ni multilayers. Debye temperatures of the each multilayer are 235 K in Au/Ni, 175 K in Au/Fe and 185 K in Au/Co multilayers. Only the Au/Ni multilayer shows very high Debye temperature. We consider that the enhancement of elastic modulus does not exist on Au layers in Au/Fe and Au/Co multilayers.

On this Au(1.0 nm)/Ni(1.0 nm) sample, Konishi *et al.* reported the enhancement of the elastic modulus from the X-ray diffraction experiments determined the lattice constant of Au under the external high pressure [6]. They reported that the lattice constant of the Au buffer layer decreased with the increase with the external pressure, but the lattice constant of multilayers (average of Au and Ni) not so decrease, comparing the Au buffer layer. This result shows the enhancement of the elastic modulus in this Au(1.0 nm)/Ni(1.0 nm) multilayer. This result agrees with our result. In other hand, Hillebrands *et al.* [41] and Song *et al.* [42] reported the decrease of the Rayleigh sound velocity in Au/Co multilayer prepared by sputtering technique. This result means the softening of the lattice. This seems to conflict with our result. However there are two different point between

their experiment and our experiment. The first point is the preparation of samples. Their samples were prepared by the sputtering technique and our samples were prepared evaporation technique. The condition of the interface between Au and Ni is different. The second point is the methods of the measurement. They measured the Rayleigh sound velocity. By this method, they measured the elastic modulus of whole of the multilayer. However, we measured only Au layers. If the Co layers become soft, the total elastic modulus of Au/Co multilayer is decrease.

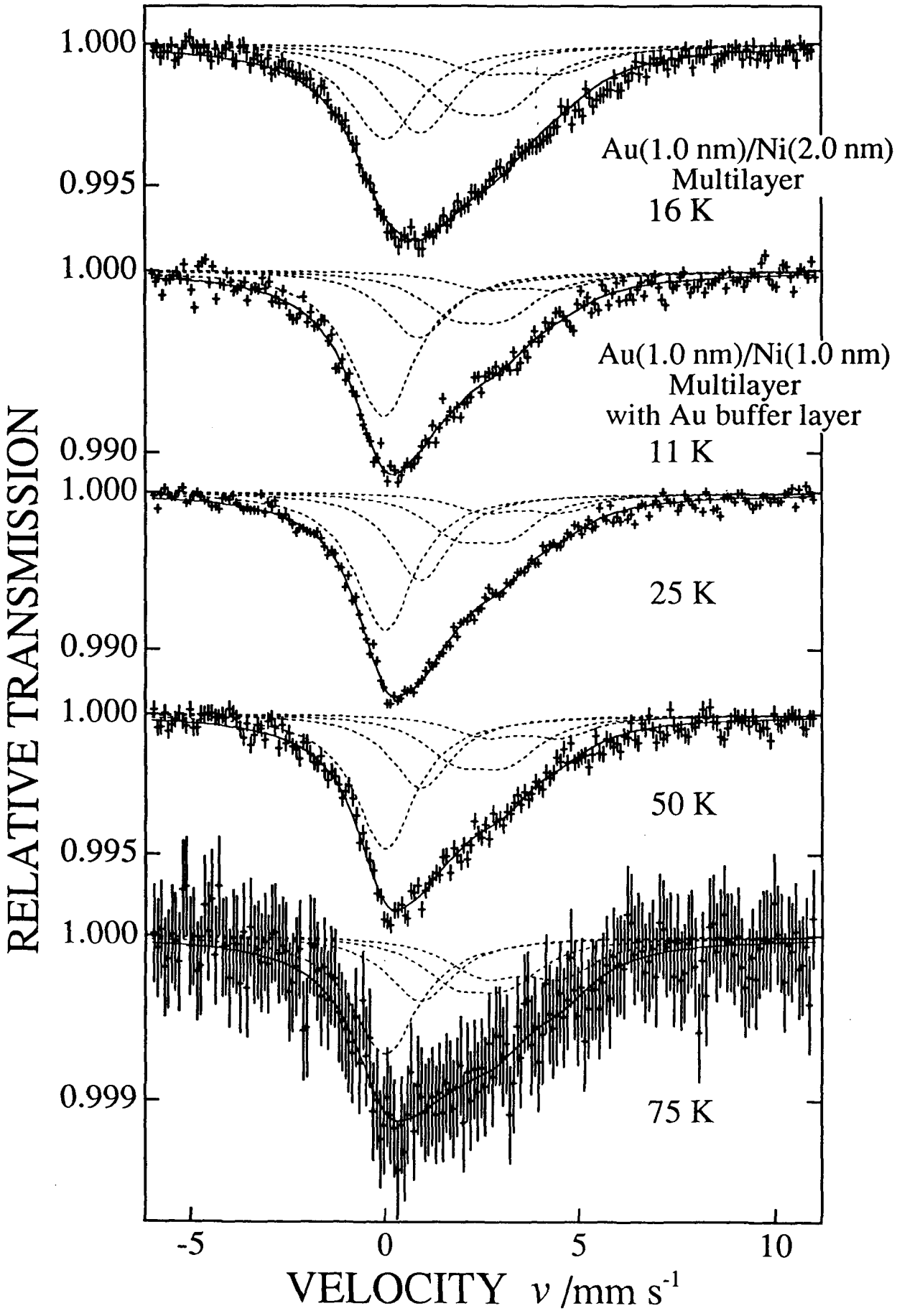

Fig. 3-21 ^{197}Au Mössbauer spectra of Au(1.0 nm)/Ni(2.0 nm) multilayers and Au(1.0 nm)/Ni(1.0 nm) multilayers with bufferlayers at 11,25,50 and 75K fitted by the four components model.

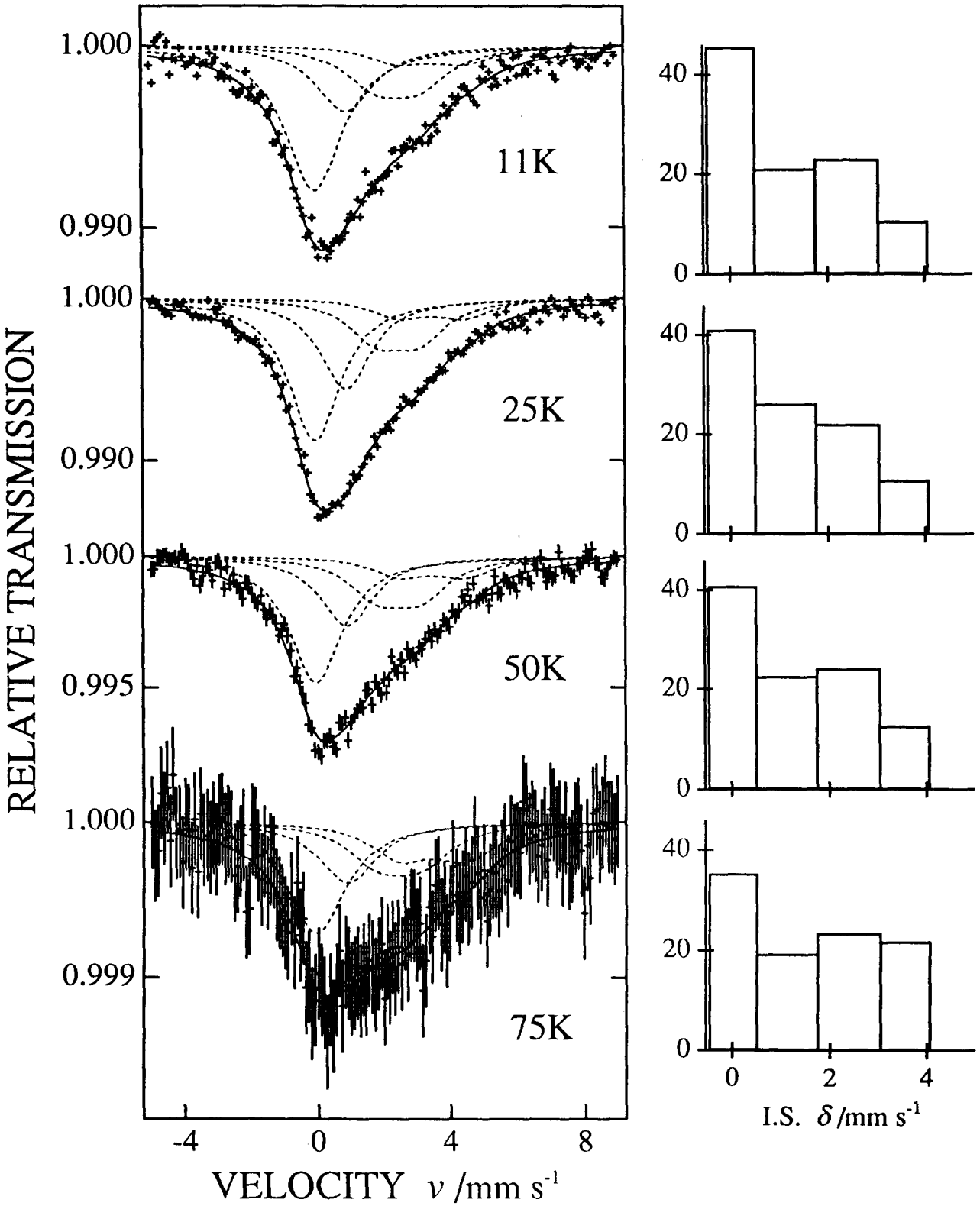

Fig. 3-22 ^{197}Au Mössbauer spectra of Au(1.0 nm)/Ni(1.0 nm) multilayers with buffer layers fitted by the four components model and area ratio of the components.

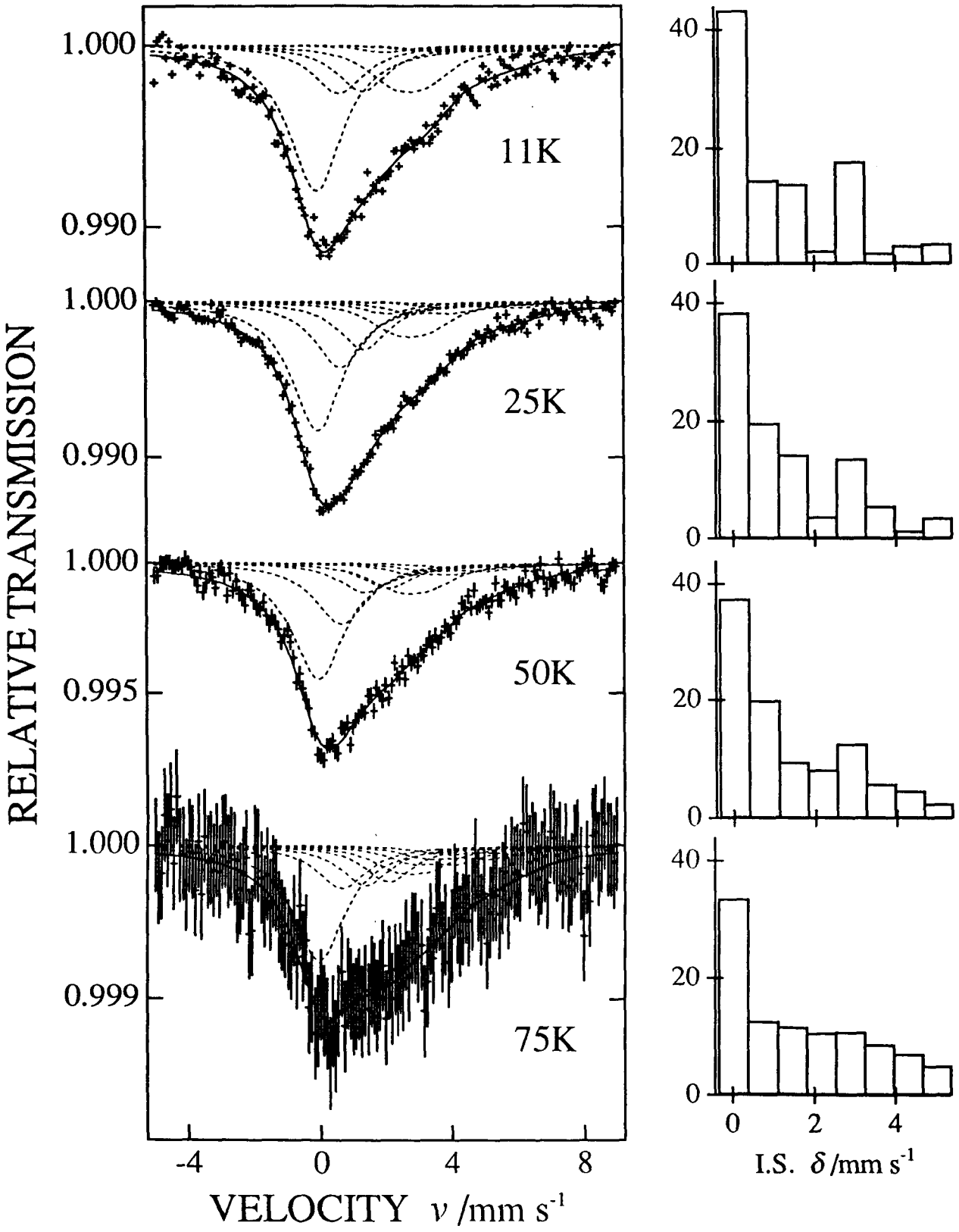

Fig. 3-23 ^{197}Au Mössbauer spectra of Au(1.0 nm)/Ni(1.0 nm) multilayers with buffer layers fitted by the eight components model and area ratio of the components.

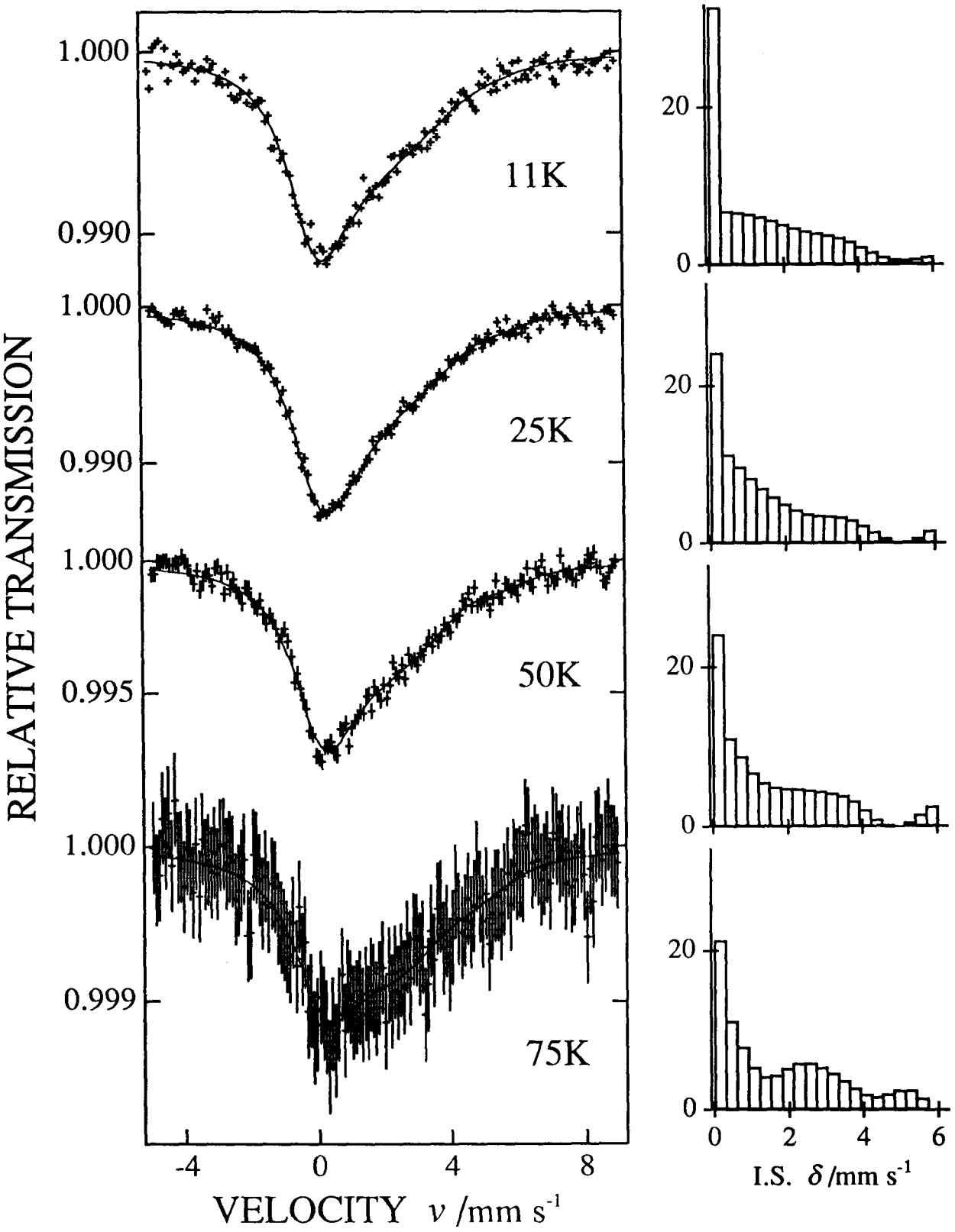

Fig. 3-24 ^{197}Au Mössbauer spectra of Au(1.0 nm)/Ni(1.0 nm) multilayers with buffer layers fitted by the distribution of isomer shift model and area ratio of the components.

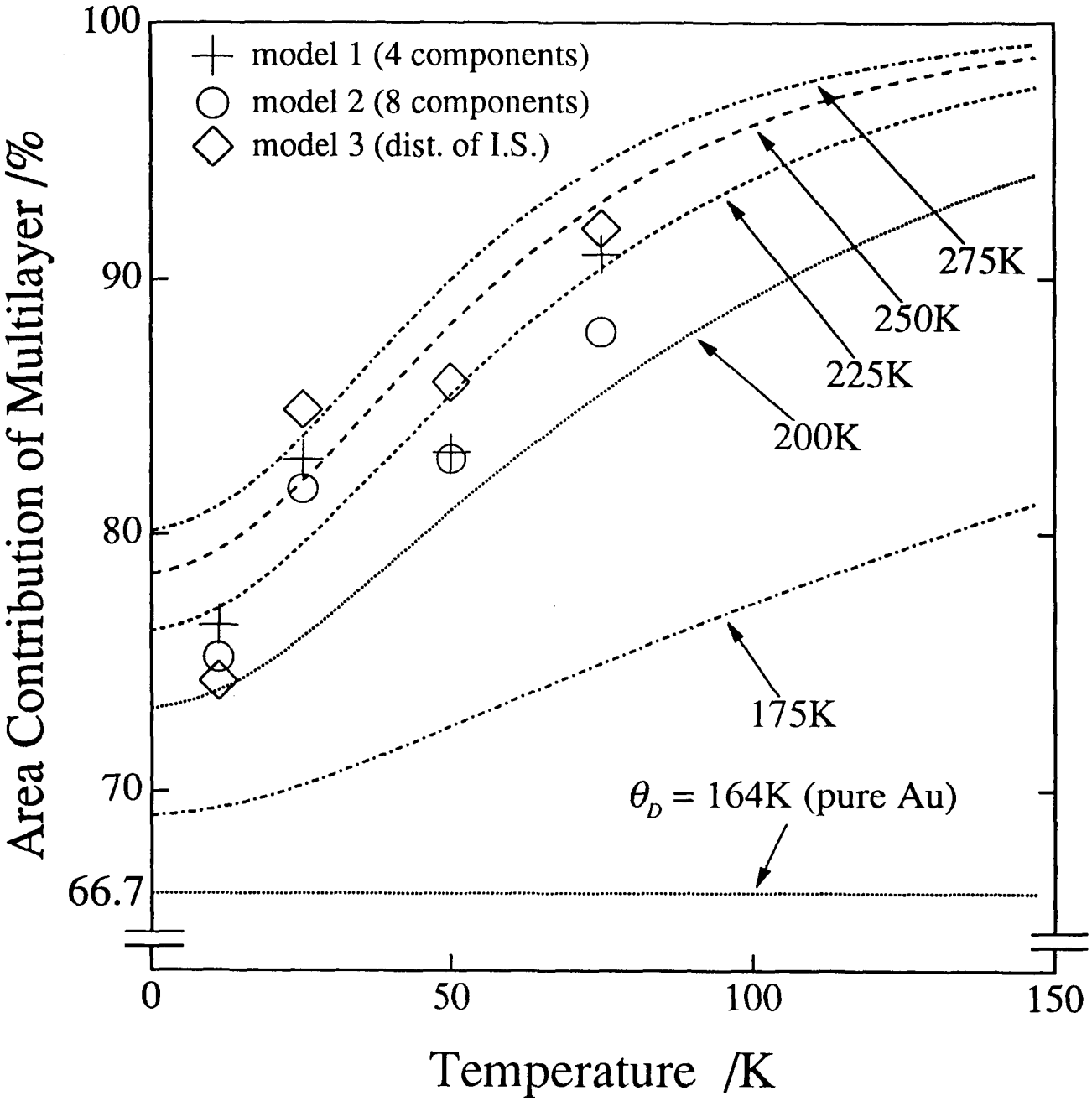

Fig. 3-25 Temperature dependence of the area contribution in ^{197}Au Mössbauer spectra of Au(1.0 nm)/Ni(1.0 nm) multilayers determined by the three models. The dotted lines are calculated by the Debye model with different Debye temperatures.

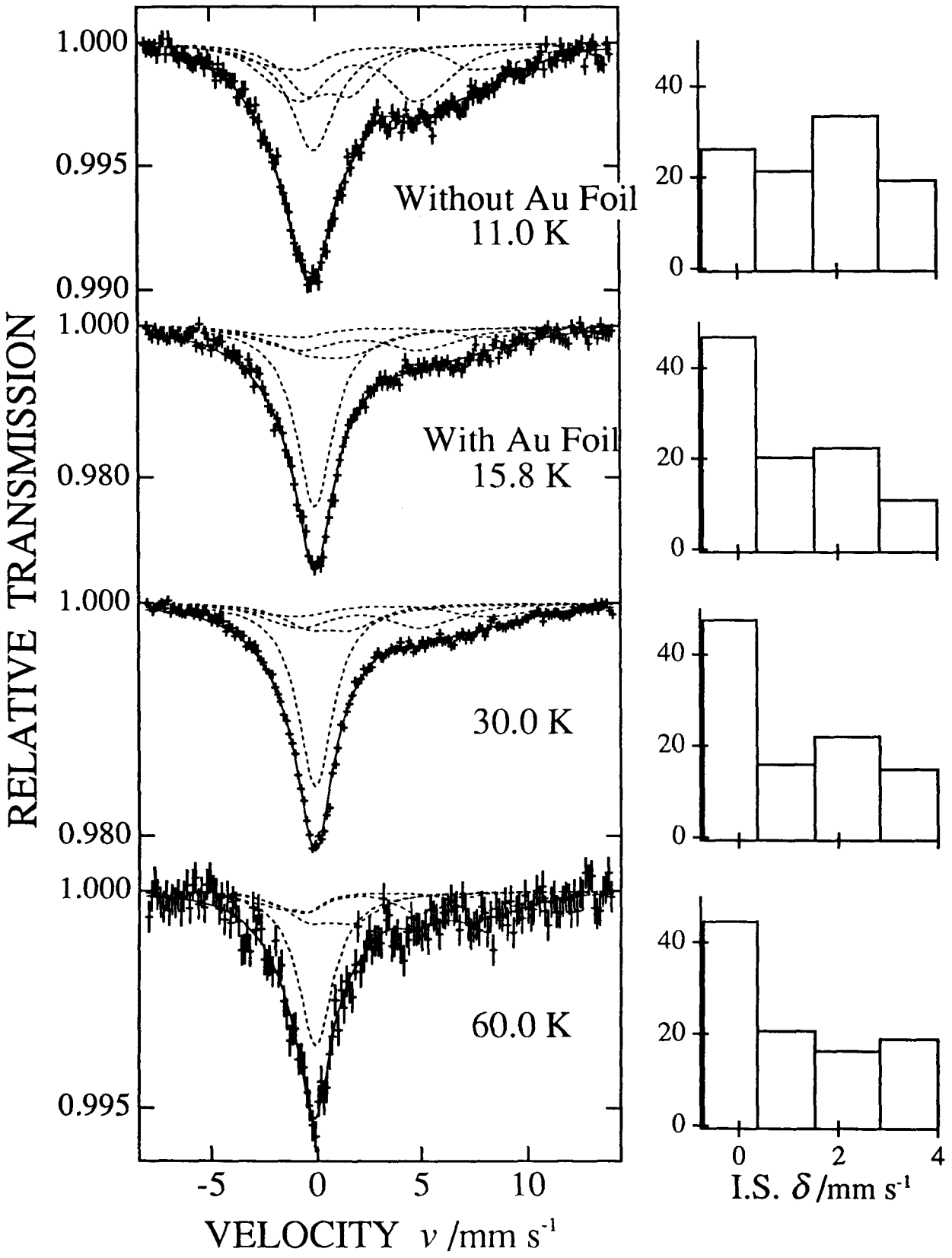

Fig. 3-26 ^{197}Au Mössbauer spectra of Au(1.0 nm)/Fe(0.8 nm) multilayers without and with Au foil fitted by the four components model and area ratio of the components.

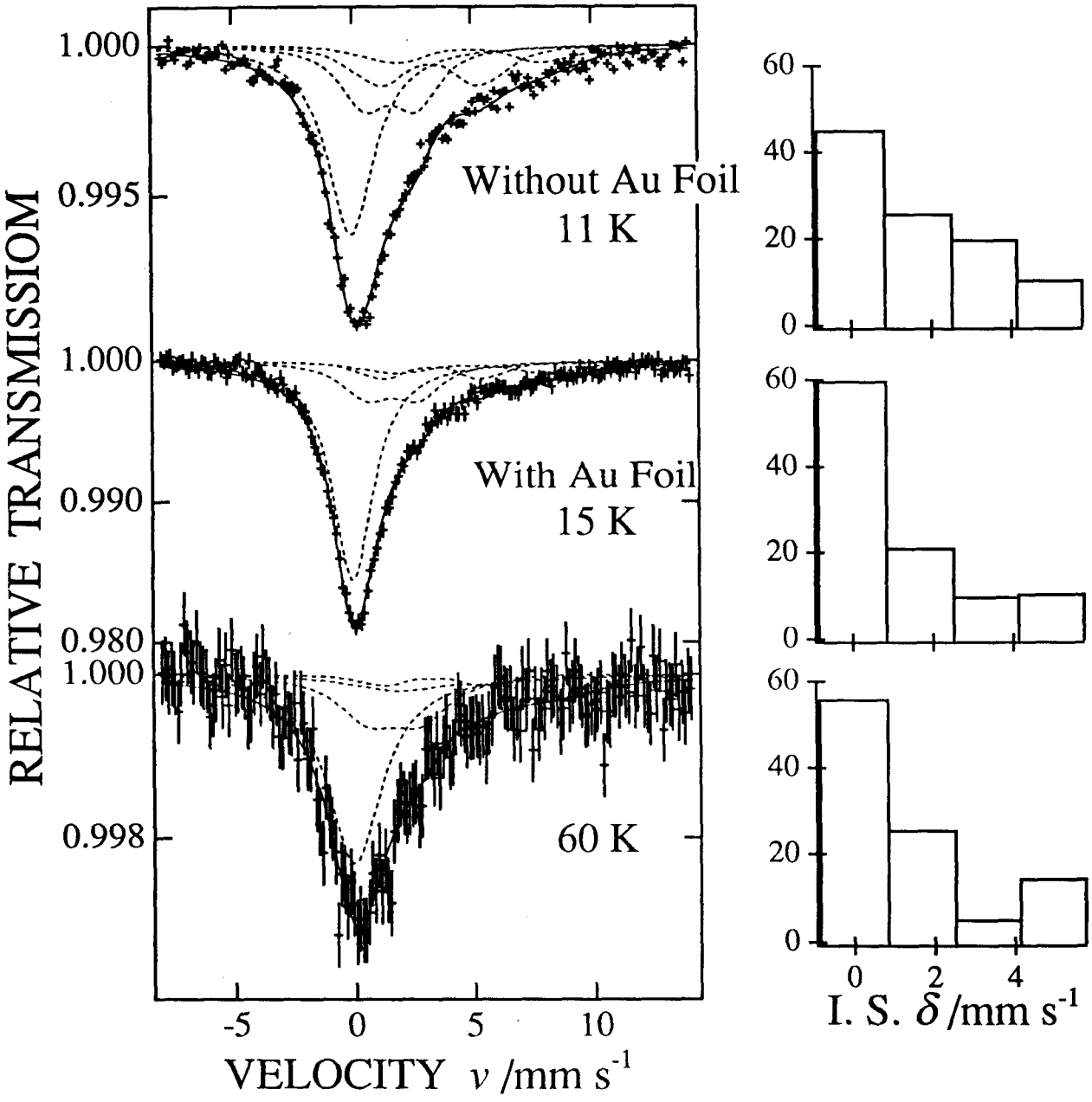

Fig. 3-27 ^{197}Au Mössbauer spectra of Au(1.0 nm)/Co(2.0 nm) multilayers without and with Au foil fitted by the four components model and area ratio of the components.

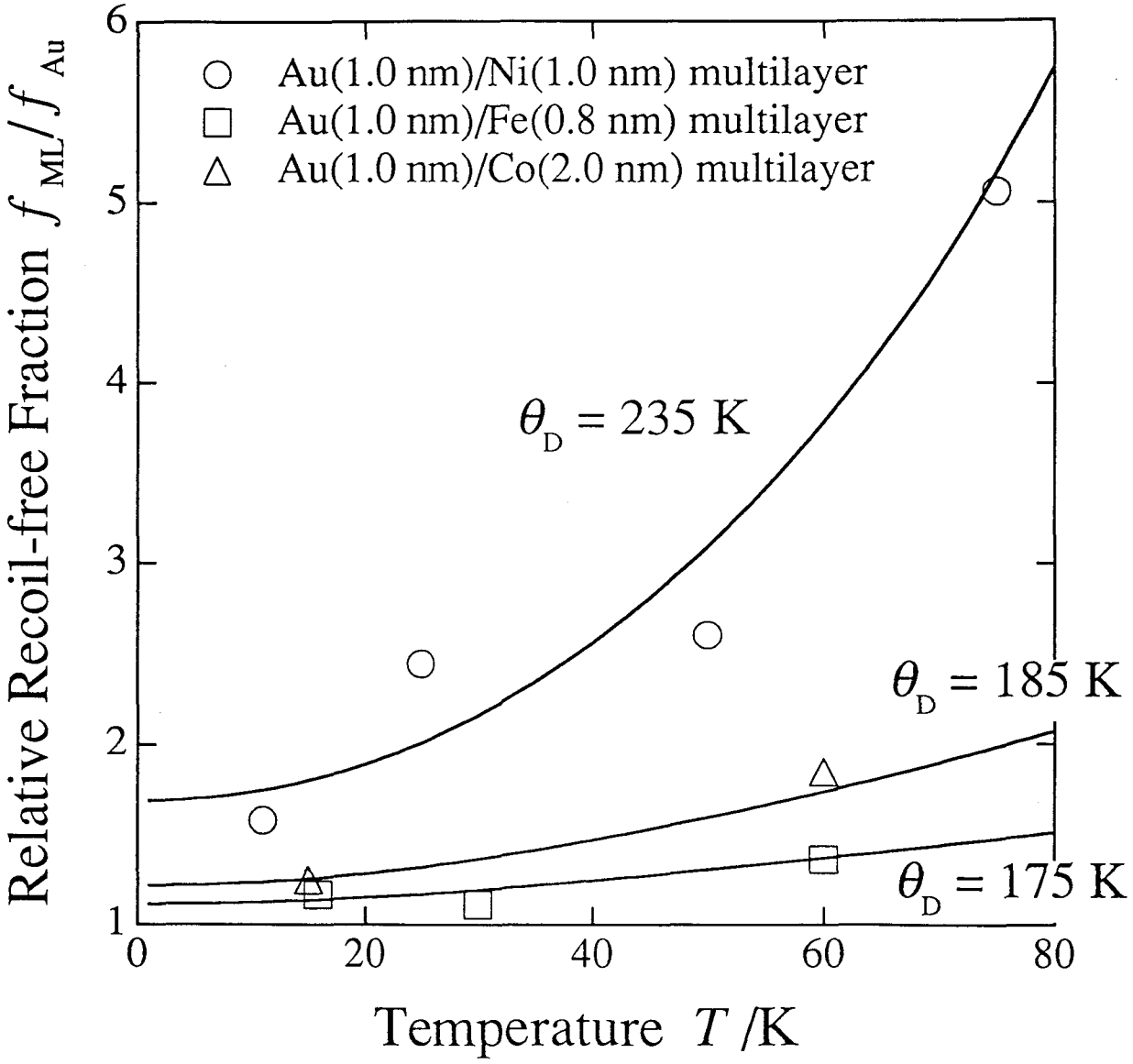

Fig. 3-28 Temperature dependence of the relative recoil-free fraction between pure Au and the multilayers. The lines are calculated by the Debye model.

4. Conclusion

Alloys

The ^{197}Au Mössbauer spectra of Au-Fe (20 ~ 50at.%Fe) alloys show asymmetric shape owing to the distribution of the hyperfine magnetic field and the isomer shift. The ^{197}Au Mössbauer spectra of Au-Fe (0 ~ 50at.%Fe) alloys show positive isomer shifts that increase with an increase of the Fe content. The positive isomer shift means to increase of the charge density at ^{197}Au nuclei. This increase of the charge density is owing to the decrease of atomic volume of Au atoms by the decrease of lattice constant. The magnitudes of hyperfine magnetic field increase linearly with an increase of Fe content.

The ^{197}Au Mössbauer spectra of Au-Ni (0 ~ 99at.%Ni) alloys show positive isomer shift. The isomer shifts increase linearly with an increase of the Ni content and increases with different proportionally constant above 40at.%. The hyperfine magnetic fields increase with an increase of the Ni alloy contents above 60at.%. The alloy specimens below 40at.%Ni show the spectra, which can be analyzed without hyperfine magnetic field. These are due to the loss of the magnetic moments below 40at.%Ni, which is suggested by the rigid band model.

The magnitudes of the hyperfine magnetic fields of Au atoms in alloys that were diluted by Fe, Co and Ni elements are nearly proportional to the magnetic moments of the magnetic metals.

Magnetic Properties

The ^{197}Au Mössbauer spectra of Au/M (M = Fe, Co, Ni) multilayers mainly consist of two components. One component is a nonmagnetic component having zero isomer shift. This component is due to the non-

perturbed Au atoms existing far from the magnetic layer. Another component is the magnetic component, which is due to the strongly perturbed Au atoms by adjacent ferromagnetic layers. The maximum magnitudes of the hyperfine magnetic field in each multilayer are 115 T in Au/Fe, 69 T in Au/Co and 23 T in Au/Ni multilayers. These values are similar to the value at the ^{197}Au nuclei dissolved into bulk Fe, Co (fcc) and Ni metals. From the area ratio of the magnetically split subspectra, it is found that the strongly perturbed Au atoms exist only near the interface between Au and magnetic layers. The affected Au atoms exist 0.2 ~ 0.4 nm from the interface. Similar values have been obtained for all of the multilayers investigations.

In Au/Fe and Au/Co multilayers, the oscillatory inter-layer coupling between the magnetic layers across the Au layers was reported, and the distance of this coupling is 1.0 ~ 4.0 nm. It is much longer than the distance of the affected Au atoms, which shown in ^{197}Au Mössbauer spectra. This results show that the influence from the inter-layer coupling to the ^{197}Au Mössbauer spectra is very small.

Supermodulus Effect

^{197}Au Mössbauer measurements have been performed to clarify the vibrational properties of Au layers in Au/Ni, Au/Fe and Au/Co multilayers. The enhancement of the elastic modulus will cause the smaller magnitude of the mean square displacement of the atom, which is shown as a high Debye temperature and a high recoil-free fraction. The Debye temperature of Au(1.0 nm)/Ni(1.0 nm) multilayer has been determined to be 235 K and this value is higher than that of bulk Au (164 K). This result suggests that the elastic modulus of Au layers in

this multilayer becomes larger. So it is concluded that the supermodulus effect exists in this multilayer. However the Debye temperatures of Au layers in Au(1.0 nm)/Fe(0.8 nm) and Au(1.0 nm)/Co(2.0 nm) multilayers are 175 K and 185 K, and not so different from that of bulk Au. These results deny the existence of the supermodulus effect in the Au layer in Au(1.0 nm)/Fe(0.8 nm) and Au(1.0 nm)/Co(2.0 nm) multilayers.

Acknowledgments

I would like to express my greatest appreciation and gratitude to Professor S. Nasu of Osaka University for his continual encouragement and support in coordinating this thesis. I wish to express my gratitude to Professor T. Shinjo and Mr. T. Emoto of ICR, Kyoto University for preparation and offering of the multilayer specimens. I especially wish to thank Professors Yu. Maeda and Y. Kawase, Dr. M. Seto and Mr. S. Kitao of RRI, Kyoto University for their kind support in ^{197}Au Mössbauer measurement. I would like to thanks to Professor R. Oshima of Osaka Prefecture University and Dr. S. Morimoto of Osaka University for their helpful discussion.

Other thanks are due to all members of Nasu Laboratory for their helpful discussion and continuous encouragement.

References

[1] edited by H. Fujimori, T. Shinjo R. Yamamoto, S. Maekawa and M. Matsui: *Kinzokujinkokoshi (Metallic Multilayer)* (Agune, Tokyo, 1995) [in Japanese].

[2] edited by T. Shinjo and T. Tanaka: Metallic Superlattices (Elsevier, Amsterdam, 1987).

[3] M. N. Baibich, J. M. Broto, A. Fert, F. Nguyen Van Dau, F. Petroff, P. Eitenne, G. Creuzet, A. Friederich and J. Chazelas, Phys. Rev. Lett., **61** (1988) 2472.

[4] W. M. C. Yang, T. Tsakalakos and J. H. Hilliard, J. Appl. Phys., **48** (1977) 876.

[5] T. Shinjo, Hyperfine Int., **90** (1994) 159.

[6] H. Konishi, Y. Fujii, N. Hamaya, H. Kawada, Y. Ohishi, N. Nakayama, L. Wu, H. Dohnomae, T. Shinjo and T. Matsushita, Rev. Sci. Instrum., **63** (1992) 1035.

[7] S. Nasu and Y. Kobayashi, Mat. Res. Soc. Symp. Proc., **384** (1995) 467.

[8] Y. Kobayashi, S. Nasu, T. Emoto and T. Shinjo, J. Magn. Magn. Mater., **156** (1996) 45.

[9] Y. Kobayashi, S. Nasu, T. Emoto and T. Shinjo, Conference Proceeding Vol. 50 "ICAME-95", ed. I. Ortalli (SIF, Bologna, 1996) p. 619.

[10] Y. Kobayashi, S. Nasu and T. Shinjo, J. Phys. Soc. Jpn., **64** (1995) 1076.

[11] K. Wertheim: *Mössbauer Effect Principles and Applications* (Academic, London, 1964).

[12] H. Sano: *Mesubaua Bunkougaku (Mössbauer Spectroscopy)* (Kodansha, Tokyo, 1972) [in Japanese].

[13] N. N. Greenwood and T. C. Gibb: *Mössbauer Spectroscopy* (Chapman and Hall, London, 1971).

[14] R. W. Wood: *Physical Optics* (Macmillan, New York, 1954.

[15] edited by J. G. Stevens and V. E. Stevens: *Mössbauer Effect Data Index 1974* (Plenum Data Company, New York, 1975).

[16] R. L. Mössbauer, Z. Physik, **151** (1958) 124.

[17] edited by C. M. Lederer and V. S. Shirley: Table of Isotopes 7th Edition (John Wiley & Sons, New York, 1978).

[18] V. Matijasevic and M. R. Beasley: Metallic Superlattices (Elsevier, Amsterdam, 1987) p. 187.
[19] P. C. Clapp, edited by T. Tsakalakos: *Modulated Structure Materials* (Martinus Mijhoff Publishers, 1984).
[20] U. Gradmann, J. Magn. Magn. Mater., **54-57** (1986) 733.
[21] H. Itoh, T. Hori, J. Inoue and S. Maekawa, J. Magn. Magn. Mater., **136** (1994) L33.
[22] K. Shintaku, Y. Daitoh and T. Shinjo, Phys. Rev. B, **47** (1993) 14584.
[23] P. Bruno and C. Chappert, Phys. Rev. B, **46** (1992) 261.
[24] B. A. Jones and C. B. Hanna, Phys. Rev. Lett., **71** (1993) 4253.
[25] A. F. Jankowski, J. Appl. Phys., **71** (1992) 1782.
[26] H. Dohnomae, N. Nakayama and T. Shinjo, Materials Transaction JIM, **31** (1990) 615.
[27] C. H. Lee, Hui He, F. Lamelas, W. Vavra, C. Uher and Roy Clarke, Phys. Rev. Lett., **62** (1989) 653.
[28] T. Emoto, unpublished.
[29] Y. Maeda, H. Sakai, M. Katada and H. Negita, Annu. Rep. Res. React. Inst. Kyoto Univ., **6** (1973) 64.
[30] Y. Kobayashi, S. Nasu, T. Emoto and T. Shinjo, Physica B, in press.
[31] H. Takayama: Spin Grass (Maruzen, Tokyo, 1991) [in Japanese].
[32] edited by T. B. Massalski: *Binary Alloy Phase Diagrams* (American Society for Metals, 1986).
[33] R. A. Brand: *Habilitationsschrift* (Duisburg, 1988).
[34] K. Koike, T. Furukawa, G. P. Gameron and Y. Murayama, Phys. Rev. B, **50** (1994) 4816.
[35] G. Y. Guo and H. Ebert, Phys. Rev. B, **53** (1996) 2492.
[36] T. Emoto, unpublished.
[37] J. J. de Vries, W. J. M. de Jonge, M. T. Johnson, J. aan de Stegge and A. Reinders, J. Appl. Phys., **75** (1994) 6440.
[38] T. Emoto, N. Hosoito and T. Shinjo, J. Magn. Magn. Mater., **156** (1996) 47.
[39] T. Emoto, N. Hosoito and T. Shinjo, J. Phys. Soc. Jpn., in press.
[40] M. P. Pasternak, S. Nasu, K. Wada and S. Endo, Phys. Rev. B, **50** (1994) 6446.
[41] B. Hillebrands, P. Krams, K. Spörl and D. Weller, J. Appl. Phys., **69** (1991) 938.
[42] Y. Song, A. Yoshihara, A. Yamaguchi and R. Yamamoto, J. Magn. Magn. Mater., **126** (1993) 203.

List of Publications

(1) S. Nasu, Y. Kobayashi, T. Shibatani, H. Dohnomae, N. Mima and T. Shinjo
"^{197}Au Mössbauer Study of Au/Ni Multilayers"
J. Magn. Magn. Mater., **126** (1993) 221-224.

(2) Y. Kobayashi, S. Nasu, T. Emoto and T. Shinjo
"^{197}Au Mössbauer Study of Au/Ni and Au/Fe Metallic Superlattices"
Hyperfine Int., **94** (1994) 2273-2278.

(3) Y. Kobayashi, S. Nasu and T. Shinjo
"Recoil-Free Fraction of ^{197}Au Mössbauer Resonance in Au(1 nm)/Ni(1 nm) Multilayer"
J. Phys. Soc. Jpn., **64** (1995) 1076-1080.

(4) S. Nasu and Y. Kobayashi
"^{197}Au Mössbauer Study of Au/Fe, Au/Co and Au/Ni Magnetic Multilayers"
Mat. Res. Soc. Symp. Proc., **384** (1995) 467-475.

(5) Y. Kobayashi, S. Nasu, T. Emoto and T. Shinjo
"^{197}Au Mössbauer Study of Au/M (M = Fe, Co, Ni) Multilayers"
J. Magn. Magn. Mater., **156** (1996) 45-46.

(6) Y. Kobayashi, S. Nasu, T. Emoto and T. Shinjo
"^{197}Au and ^{57}Fe Mössbauer Study of Au/Fe Multilayers"
Conference Proceeding Vol. 50 "ICAME-95", ed. I. Ortalli (SIF, Bologna, 1996) p. 619-622.

(7) T. Harami, G. Miyazaki, M. Seto, X. W. Zang, Y. Kobayashi, Y. Yoda, H. Shiwaku, S. Nasu and S. Kikuta
"Inelastic Nuclear Resonant Scattering by Hemoglobin CO at Room Temperature"
Conference Proceeding Vol. 50 "ICAME-95", ed. I. Ortalli (SIF, Bologna, 1996) p. 831-834.

(8) Y. Kobayashi, S. Nasu, T. Emoto and T. Shinjo
"^{197}Au Mössbauer study of Au/TM (TM = Fe, Co, Ni) multilayers and alloys"
Physica B, in press.

(9) Y. Kobayashi, S. Nasu, T. Emoto and T. Shinjo
"^{197}Au Mössbauer Study of Au/TM (TM = Fe, Co, Ni) Multilayers"
Hyperfine Int., in press.